

Forschungszentrum Karlsruhe

Technik und Umwelt

Wissenschaftliche Berichte

FZKA 5954

Development and Validation of a Transition Boiling Model for
the RELAP5/MOD3 Reflood Simulation

V. H. Sanchez-Espinoza, E. Elias*, Ch. Homann, W. Hering, and
D. Struwe

Institut für Reaktorsicherheit
Projekt Nukleare Sicherheitsforschung

*Technion University Haifa, Israel

Forschungszentrum Karlsruhe GmbH, Karlsruhe

1997

Abstract

The heat transfer model of the RELAP5/MOD3.1 (R5M3) code was extensively reviewed and assessed. The most important deficiency of the current version of the code was attributed to its treatment of the transition boiling heat transfer regime. The current transition boiling model significantly underpredicts the liquid heat transfer rate. Since at low quality conditions the liquid boiling component is a major fraction of the total heat transfer, the current model underpredicts the quench temperature and the quenching rate under most conditions relevant to LOCA and degraded core analysis.

Therefore, a new model has been developed and implemented in the R5M3 code for predicting the transition boiling heat transfer. The new model is based on an extension of the phenomenological formulation suggested originally by Chen. It utilizes only local state variables calculated by the R5M3 code and does not require other history parameters, such as quench position or CHF and minimum film boiling temperatures, which are not available at each time step.

A number of separate effect and bundle test experiments are analyzed with the modified code version. The predictions are compared with those obtained by the frozen code version and with available experimental data. Several variables, such as wall temperatures, vapor and liquid velocities, void fraction etc., are examined in order to evaluate the general prediction capability of the code in modeling boil-off and reflood transients. In addition, the current and the modified stand-alone transition boiling models are tested against a large sample of the available data-base on steady-state post dryout heat transfer.

In all cases, the predictions of the modified model fit the measured data better. The temperature curves are physically and conceptually more sound than those predicted by the frozen code version. This is achieved by introducing a more realistic modeling of the transition boiling heat transfer which affects only one subroutine of the R5M3 code.

Entwicklung und Validierung eines Übergangssiedemodells für die
RELAP5/MOD3 Flutsimulation
Zusammenfassung

Die Wärmeübertragung-Flutmodelle des Programmsystems RELAP5/MOD3.1 (R5M3) wurden ausführlich überprüft und bewertet. Dabei hat sich herausgestellt, daß die bisherige Modellierung des Übergangssiedens wesentliche Mängel aufweist. Dazu gehört die starke Unterschätzung der Wärmeübertragungsrates zu der Flüssigkeit, die den grössten Anteil des gesamten Wärmeübergangskoeffizienten im Übergangssieden unter Bedingungen geringen Dampfgehalts ausmacht. Dies führt dazu, daß die Quenchtemperatur und -rate in den meisten Fällen, die für LOCA- und Kernschmelze- Unfallszenarien relevant sind, ebenfalls unterschätzt werden. Es wurde daher ein neues Modell für das Übergangssieden entwickelt, qualifiziert und in der Programmversion R5M3 implementiert. Das Modell erweitert die ursprünglich vom Chen vorgeschlagene phänomenologische Formulierung, welche nur auf vom R5M3 berechneten, lokalen Zustandsparametern basiert. Parameter wie Quenchfrontlage, kritischer Wärmestrom, minimale Filmsiedentemperatur, die nicht in jedem Zeitschritt zur Verfügung stehen, werden nicht gebraucht.

Das erweiterte Übergangssiede-Modell wurde anhand zahlreicher Einzelstab- und Bündelversuchen validiert. Die dabei erzielten Ergebnisse wurden mit denen der ursprünglichen R5M3-Version verglichen. Darüberhinaus wurde das ursprüngliche und das modifizierte Übergangssiedemodell als ein Stand-Alone-Programm gegenüber einer breiten quasi-stationären Daten-Basis validiert.

In allen untersuchten Fällen hat sich gezeigt, daß die Einführung des neuen Modells die Übereinstimmung der berechneten mit den gemessenen Daten erheblich verbessert hat. Die berechneten Temperaturen beschreiben den Flutvorgang in realistischerer und physikalisch sinnvoller Weise als das bisher der Fall war. Die verbesserte Vorhersage des Flutprozesses wurde durch eine mechanistischere Modellierung der Wärmeübertragung im Übergangssiedegebiet erreicht. Die Implementierung dieses Modells im Programmsystem R5M3 erfordert Änderungen in lediglich einem Unterprogramm (pstdnb).

Contents

1	Introduction	1
2	The RELAP5/MOD3 Reflood Model	3
2.1	RELAP5/MOD3 Code Basis	3
2.2	R5M3 Reflood Heat Transfer Models	5
2.3	Reflood Heat Conduction	11
3	Experimental Programs for Code Validation	12
3.1	The FZK Single-Rod Quench Tests	13
3.1.1	Single-Rod QUENCH Rig Description	13
3.1.2	Test Procedure	13
3.1.3	Measurement Uncertainty	17
3.2	The NEPTUN Bundle Tests	18
3.2.1	Test Description and Procedure	18
3.2.2	Measurement Uncertainty	20
3.3	The Validation Matrix	20
4	Test Modeling for Reflood Model Assessment	22
4.1	The FZK Single-Rod Test Rig	22
4.2	The NEPTUN Facility	26
5	Results of Assessmental Calculations with RELAP5/MOD3	26
5.1	FZK Single-Rod	28
5.2	NEPTUN Facility	31
6	Stand-Alone Assessment of the RELAP-Reflood Model	31
6.1	Validation Matrix	31
6.2	Discussion of Results	34
7	Limitations of the Current Transition Boiling Model	37

8	The Suggested Transition Boiling Model	40
8.1	Total Boiling Heat Flux	40
8.2	Liquid Contact Area Fraction	42
8.3	Implementation of the new Transition Boiling Model	43
9	Validation of the New Transition Boiling Model	44
9.1	Stand-Alone Validation	44
9.2	Validation within RELAP5/MOD3.1-FZK	45
9.2.1	Discussion of Results: FZK Single-Rod Tests: Specimen filled with <i>ZrO₂</i>	45
9.2.2	Discussion of Results: FZK Single-Rod Tests: Empty Specimen . . .	59
9.2.3	Discussion of Results: NEPTUN Tests	63
10	Parametric Studies	71
11	Run Statistics and Code Performance	74
12	General Conclusions and Recommendations	80
13	References	82

List of Figures

1	Flow Regime Maps of the Constitutive Relations in R5M3	4
2	Qualitative Representation of the Boiling Curve used in RELAP5/MOD3.1	5
3	Arrangement of the Single Rod Quench Tests at FZK	14
4	Rod QUENCH Rig: Cross Section and Temperature Measurement	15
5	FZK Single-Rod Quench Test Conduction	16
6	Cross Section of the NEPTUN Heater Rod	19
7	Cross Section of the NEPTUN Bundle	21
8	Axial and Radial Nodalization of the Single-Rod Quench Test Rig	25
9	Nodalization Scheme of the NEPTUN Test Section	27
10	Comparison of the Original R5M3 Predictions with the Measured Temperatures in the FZK Single-Rod Test No. T02106	29
11	R5M3 Predictions of a. Surface Heat Flux and Critical Heat Flux, and b. Surface HTC in the FZK Single-Rod Test No. T02106	30
12	Measured and Predicted Clad Outside Temperatures and Steam Coolant Temperature for the Steam-Cooled FZK Single-Rod Test No.T16046	32
13	Measured and Predicted Clad Temperature in the NEPTUN Test 3056	33
14	Measured vs Stand-Alone R5M3 Model Predictions of Transition Boiling Data	35
15	Stand-Alone R5M3 Model Prediction of Run 5251 in Bennett et al. (1967)	36
16	Heat Flux versus Wall Temperature predicted by RELAP5/MOD3 for $G = 20kg/sm^2$, $p = 0.10MPa$ and saturated conditions	38
17	Schematic description of the Suggested Transition Boiling Model	41
18	Comparison with Data of a Stand-Alone Formulation of the New Transition Boiling Model	46
19	Stand-Alone New Model Prediction of Run in Bennett et al. (1967)	47
20	Measured and Predicted Temperatures in the FZK Single-Rod Test No. T16106	49
21	Measured and Predicted Clad Temperatures in the FZK Single-Rod Test No. T31085	50
22	Measured and Predicted Clad Temperatures in the FZK Single-Rod Test No. T24066	51

23	Predicted Heat Flux Parameters at the Mid-Section FZK Single-Rod Test No. T16106	52
24	Comparison of Current and Modified R5M3 Predicted Boiling Curves in the FZK Single-Rod Test No. T16106	53
25	Predicted Flow Parameters in the FZK Single-Rod Test No. T16106	55
26	Measured and Predicted Clad and Pellet Temperatures in the FZK Single-Rod Test No. T02106	56
27	Measured and Predicted Clad Temperatures in the FZK Single-Rod Test No. T21066	57
28	Measured and Predicted Clad Temperatures in the FZK Single-Rod Test No. T24085	58
29	Measured and Predicted Clad Temperatures in the FZK Single-Rod Test No. ITE20115	60
30	Measured and Predicted Clad Temperatures in the FZK Single-Rod Test No. ITE22115	61
31	Measured and Predicted Clad Temperatures in the FZK Single-Rod Test No. ITE29115	62
32	Measured and Predicted Clad Temperatures and Void Fraction in the NEPTUN Test 5036	64
33	Predicted Heat Transfer Parameters in the NEPTUN Test 5036	65
34	Measured and Predicted Clad Temperatures in the NEPTUN Test 5050	67
35	Predicted Heat Transfer Parameters, 0.746 m Elevation in the NEPTUN Test 5050	68
36	Predicted Heat Transfer Parameters, 0.978 m Elevation in the NEPTUN Test 5050	69
37	Predicted Heat Transfer Parameters, 1.21 m Elevation in the NEPTUN Test 5050	70
38	Effect of Gap Conductance on Quench Velocity in the FZK Single-Rod Test No. T16106	72
39	Gap Temperature Curves in the FZK Single-Rod Test No. T16106	73
40	Temperature Difference Across the Gap at Different Heights in the FZK Single-Rod Test No. T16106	74
41	Gap Width Behavior During Reflooding in the FZK Single-Rod Test No. T16106	75

42	Code Performance: Rod Test No. T16106	76
43	Code Performance: NEPTUN Test 5036	78
44	Code Performance: NEPTUN Test 5036	79

List of Tables

1	Comparison of predicted and measured temperature difference for cooldown tests	18
2	NEPTUN measurement errors and scattering of the data	22
3	Test matrix for the validation of the R5M3-reflood model	23
4	Test Matrix for Stand-Alone Validation of R5M3-Reflood Model	33
5	Comparison of RELAP5 and the Original Chen Model for Transition Boiling Heat Transfer	39
6	Comparison of the Original and Modified Chen Model for Transition Boiling Heat Transfer	44

Nomenclature¹

Latin Letters

C_p	$[\frac{J}{kgK}]$	heat capacity at constant pressure
D	$[m]$	Diameter
D_e	$[m]$	Hydraulic diameter
f_l		Fraction of wetted wall surface
G	$[kg/m^2 s]$	Mass flux
Gr		Grashof number
h	$[\frac{W}{m^2K}]$	Heat transfer coefficient
H	$[\frac{J}{kg}]$	Specific enthalpy
H_{fg}	$[\frac{J}{kg}]$	Specific latent heat of evaporation
k	$[\frac{W}{mK}]$	Heat conductivity
L_m	$[m]$	Mean path length
n		Droplet number density
p	$[Pa]$	Pressure
p_r		Reduced pressure
Pr		Prandtl number
q''	$[\frac{W}{m^2}]$	Heat flux
Re		Reynolds number
T	$[K]$	Temperature
v	$[\frac{m}{s}]$	Velocity
X_{tt}		Martinelli flow parameter
g	$[\frac{N}{kg^2}]$	Gravitational constant
M		Multiplier
We		Weber number
r	$[m]$	Surface roughness

¹Variables and Symbols not included here are explained there where they appear first.

Greek Symbols

α		Void fraction
ϵ		Emissivity
λ	$[m]$	Characteristic wave length
μ	$[\frac{N \cdot s}{m^2}]$	Dynamic viscosity
ρ	$[\frac{kg}{m^3}]$	Density
σ	$[\frac{N}{m}]$	Surface tension
Ω		Mole fraction
ℓ		Accommodation coefficient
φ	$[\frac{kg}{Mol}]$	Molecular weight

Subscripts

a	Absorption
c	Conduction
C	Cladding
CHF	Critical heat flux
e	Equivalent
F	Fuel
FB	Film boiling
g	Vapor
gap	Gap
i	Index
l	Liquid
mac	Macroscopic
mic	Microscopic
nc	Number of circumferential segments
NB	Nucleate boiling
pg	Constant pressure-gas phase
pl	Constant pressure-liquid phase
q	Quench
r	Radiation
s	Saturation
stf	Stratified
tot	Total
TB	Transition boiling
TP	Two-phase
w	Wall
web	Weber

Abbreviations

AMM	Accident Management Measures
CAMP	Code Assessment and Maintenance Program
CHF	Critical Heat Flux
CORA	Out-of-pile-Bundle test facility, FZK
CSNI	Committee on the Safety of Nuclear Installations
DBA	Design Basis Accident
DNB	Departure from Nucleate Boiling
EPR	European Pressurized Water Reactor
ECC	Emergency Core Cooling
FZK	Forschungszentrum Karlsruhe, Germany
HTC	Heat Transfer Coefficient
ICAP	International Code Assessment and Applications Program
IMF	Institute of Material Research, FZK
INEL	Idaho National Engineering Laboratory, USA
LOCA	Loss of Coolant Accident
LOFT	Loss of Fluid Test Facility, INEL
LWR	Light Water Reactor
MFB	Minimum Film Boiling
NPP	Nuclear Power Plant
NEPTUN	Thermalhydraulic test facility, PSI
PBF	Power Burst Facility, USA
PSI	Paul Scherrer Institute, Switzerland
PWR	Pressurized Water Reactor
RELAP	Reactor Excursion and Leak Analysis Program
RPV	Reactor Pressure Vessel
R5M3	RELAP5/MOD3
SCDAP	Severe Core Damage Analysis Package
S/R5	Coupled Version of SCDAP and RELAP5/MOD3
LP	Low pressure
FP	Fission Products
SFD	Sever Fuel Damage
TC	Thermocouple

1 Introduction

An important accident management measure (AMM) for controlling severe accidents in Light Water Reactors (LWRs) consists of core quenching by the injection of cold water into the overheated, partially oxidized or even severely degraded core. The fuel temperature at the time of water injection may be larger than the rewetting temperature, which is the highest temperature at which a direct contact is possible between the coolant and a heated surface. A complicated flow and heat transfer pattern, known as post dryout two-phase flow, exists under such conditions, characterized by the formation of a wet patch on the hot surface which eventually develops into a moving quench front. The rate of quenching depends on the heat transfer regimes along the heated surface. At high surface temperatures corresponding to film boiling, the quench proceeds rather slowly as the liquid is separated from the surface by a continuous vapor blanket. As the cladding temperature is decreased to the minimum heat flux temperature (sometimes called Leidenfrost or quench temperature), a transition boiling regime is encountered where the intermittent wetting of the surface begins and the heat transfer rate increases with decreasing surface temperature. At a surface temperature corresponding to critical heat flux, most of the surface becomes available for wetting and intense nucleate boiling ensues, causing the fuel cladding to cool rapidly until the liquid saturation temperature is reached, below which the fuel cladding is cooled by single-phase liquid convection.

Since this quenching process plays an important role in defining the consequences of a severe accident, full characterization of the core conditions during the accident requires a detailed consideration of the coupled phenomena of heat and mass transfer in the coolant channel and on the clad surface together with reliable modeling of possible chemical and material phenomena.

The thermal, hydraulic and chemical phenomena taking place during quenching of degraded fuel bundles by water were recently considered by the Committee on the Safety of Nuclear Installations (CSNI) to be poorly understood and unsatisfactorily modeled by severe accident codes [17]. For instance, analysis of the TMI-2 accident [29] and several bundle experiments such as LOFT LP-FP-2, PBS SFD-ST and CORA [17] have established that quenching of a degraded core may enhance the clad oxidation process, increase hydrogen production and in turn, significantly increase the fuel rod temperatures. These trends are not always predicted by the major transient reactor codes. Moreover, in some cases even the surface temperature history during the preheating and quenching of nonoxidized fuel rods are not always predicted in the desired accuracy [20], [39]. Therefore, several experimental programs have been initiated to complement the present state of knowledge on degraded core quench. In parallel, under the International Code Assessment and Applications Program (ICAP) and the Code Assessment and Maintenance Program (CAMP) [14], there is an international effort to review, assess and improve the

treatment of the quenching process in the major reactor transient analysis code systems.

The code review process is typically based on utilizing data from separate-effect and integral test experiments for validating either individual physical models in the codes or their integral behavior. The reflood model in R5M3 [22] has been recently assessed by Analytis [1], [2]. It was shown that the predicting capability of the code could be improved by introducing two different heat transfer packages to account individually for reflood and general heat transfer conditions. A similar approach is used also in other codes such as RELAP5/MOD2 (R5M2) [23] as well as in the codes ATHLET [4], [5] and REFLA/TRAC [33] which use correlations to predict the quench front velocity. Nevertheless, it should be recognized that the need to rely on empirical correlations or to assume a special reflood heat transfer package stems mainly from the current lack of understanding of the physical processes controlling the reflooding phenomena and from inadequate modeling of the boiling curve near the quench front. Therefore further effort must be spent in order to arrive at a unified heat transfer model suitable for boil-off, reflood and non-reflood heat transfer calculations at low and high initial surface temperatures.

A large amount of heat transfer data on quenching of fuel rods at relatively low initial temperatures is currently available [32], [30], [36],[37],[34], [27], [26], [41], [8], [45], [31], [43]. This information which was mainly generated for developing a reliable heat transfer model for LOCA analysis, may also be relevant for degraded core analysis. Many of the theoretical and experimental studies on the heat and mass transfer mechanisms during top and bottom reflooding have been reviewed by Yadigaroglu [48], Yadigaroglu et al. [50], Elias & Yadigaroglu [13], Collier [12] and Olek [38]. Recently, data on high temperature quenching become available upon completion of several programs on degraded core quenching, [17], [20]. The main difference between the low and high temperature quenching data is that in the latter case the post dryout heat transfer region extends over a longer section along the heated surface and, thus, becomes an important mechanism for cooling the cladding prior to complete quenching. Therefore, improved modeling of the film and transition boiling heat transfer regimes is essential for accurate degraded core analysis at high initial surface temperatures. It must also be recognized that at elevated core temperatures the thermal behavior of the fuel rods strongly affects the rate of clad oxidation. Thus the prediction of the core conditions in that case calls for accurate modeling of both the heat transfer and the chemical problems.

The main objective of the present study is to develop and assess a unified heat transfer model which can be applied for both reflood and general heat transfer computations. In order to effectively benefit from the extensive testing and validation of the Chen transition boiling model [11] , the present study extends the original Chen formulation to improve its prediction capability for low pressures and low qualities. A stand-alone version of the new model was validated against measured transition boiling data over a wide range of

temperatures and pressures. This modified heat transfer model was implemented in the R5M3 code and further tested by comparing its predictions with data obtained in the FZK single rod test program [19] and in the PSI-NEPTUN bundle experiments [39]. In this report, the limitations of the current R5M3 heat transfer model are listed and discussed and a full description of the new transition boiling model is provided.

2 The RELAP5/MOD3 Reflood Model

2.1 RELAP5/MOD3 Code Basis

The R5M3 is being developed at the Idaho National Engineering Laboratory (INEL), for the analysis of both operational and accidental situations (transients and LOCAs) in LWRs within the range of Design Basis Accidents (DBA) [22], [24]. The coupling of R5M3 with the core meltdown code SCDAP, being developed by INEL [22], allows the prediction of the main phenomena of core meltdown accident scenarios (beyond DBA) that take place within the reactor pressure vessel (RPV). In the coupled version SCDAP/RELAP5/MOD3 (S/R5) the quench thermohydraulics are mainly modeled in the R5M3 part.

The code R5M3 uses a one-dimensional, non-homogeneous and non-equilibrium thermodynamic two-fluid approach. Accordingly, a six-equations formulation is used to represent the phasic continuity, momentum and energy conservation equations. The two-phase two-component model accounts for the presence of a non-condensable (hydrogen, helium, air, etc.) component in the gas phase and for the presence of boron in the liquid phase.

A set of constitutive relations is included to close and solve the system of equations, whereby the unknown terms (exchange terms and virtual mass term) in the conservation equations are defined as functions of the state variables. Since the closure laws depend on the flow or heat transfer regime, modern codes like R5M3 update the closure relationships at each time step according to the prevailing flow regime [49]. Figure 1 lists the different flow regime maps considered in R5M3. In these maps different sets of criteria are used to define the various regime boundaries [22], [24].

Since this work concentrates on the analysis of reflood situations in vertical pipes and bundles, the emphasis is focused mainly on the vertical flow map and wall heat transfer mechanisms (see Fig. 1). Relevant parameters are void fraction, wall conditions (wetted or unwetted), mass flux, pipe dimensions, and wall superheating [22], [24].

In DBA and beyond DBA scenarios the reflood quenching process covers over a wide range of flow and heat transfer regimes for certain times both single phase (vapor, liquid) and two phase (film, transition, and nucleate boiling) flow and heat transfer mechanisms.

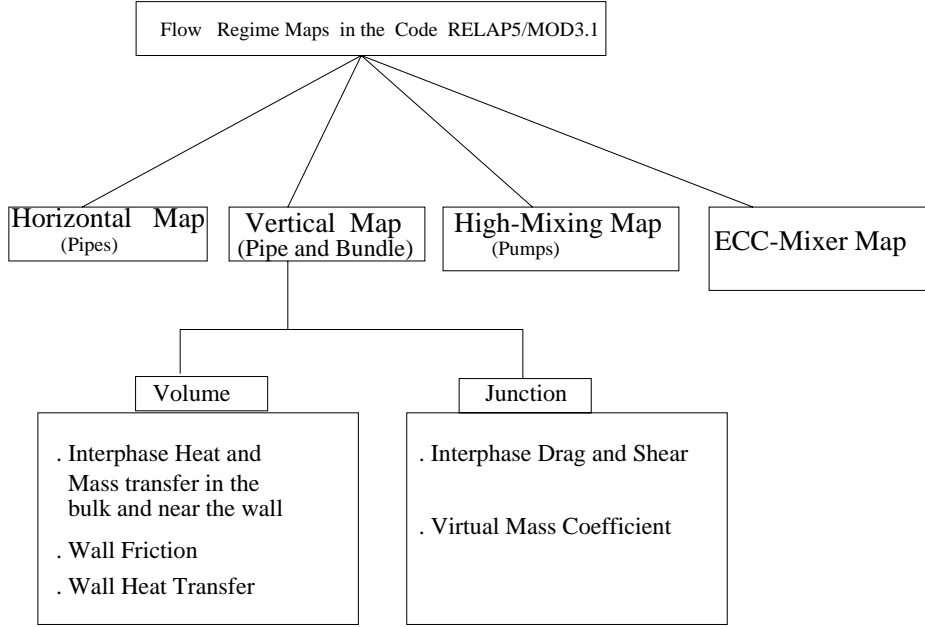


Figure 1: Flow Regime Maps of the Constitutive Relations in R5M3

These heat transfer modes for both reflood and non-reflood conditions are described in R5M3 in terms of a unique boiling curve which is shown in Fig. 2.

Generally, the total wall heat flux (q''_{tot}) is given as:

$$q''_{tot} = h_g (T_w - T_g) + h_l (T_w - T_l) \quad (1)$$

where h is HTC, T is temperature and the subscripts l , g and w refer to the liquid, vapor and wall, respectively. The liquid reference temperature, T_l , is typically taken as the saturation temperature, T_s .

The total HTC is the sum of both h_g and h_l . R5M3 utilizes an energy partitioning logic to determine the heat transfer coefficients and the rate of vapor production, \dot{w} , for each heat transfer mode [22]. Detailed description of the heat transfer models is given in subsection 2.2

The selection logic used in subroutine *htrc1* for defining the boundaries of the pre- and post-CHF modes that are of interest in reflood situations is given below in terms of the wall superheat:

- **Post-CHF**

$$75 \text{ K} < \Delta T_s \leq 600 \text{ K} \begin{cases} \text{if } q''_{FB} > q''_{TB} & \text{then film boiling} \\ \text{if } q''_{FB} \leq q''_{TB} & \text{then transition boiling} \end{cases}$$

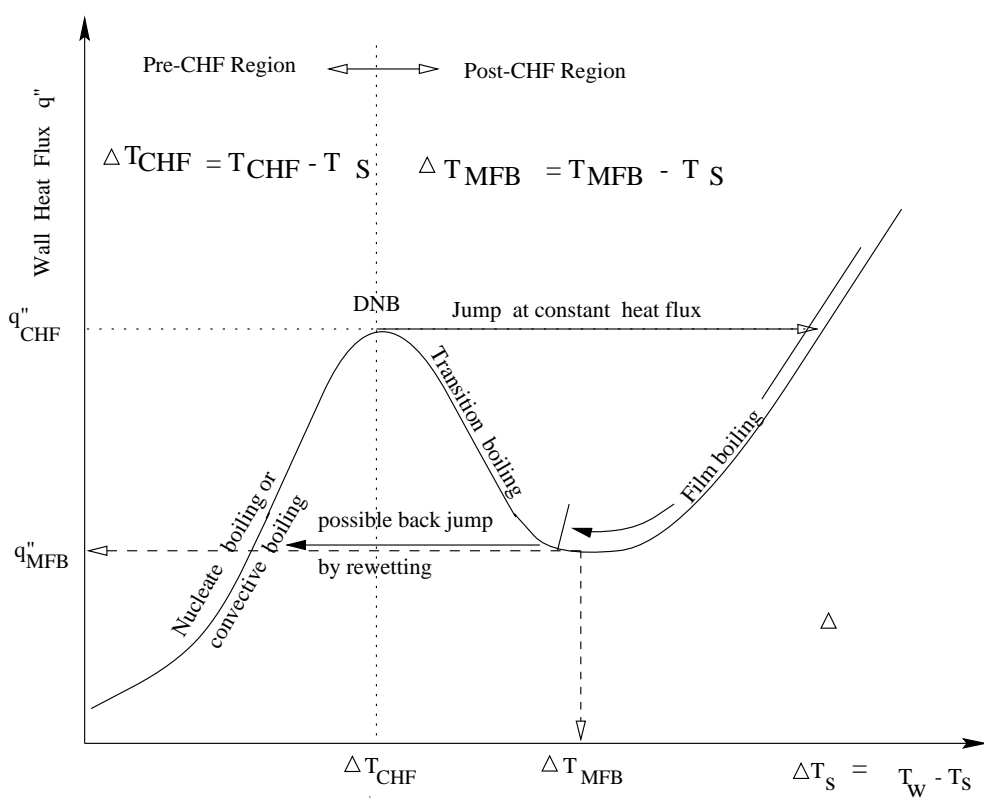


Figure 2: Qualitative Representation of the Boiling Curve used in RELAP5/MOD3.1

if $\Delta T_s > 600 K$ then film boiling is assumed.

• **Pre-CHF**

$$\Delta T_s \leq 75 K \begin{cases} \text{if } q''_{NB} > q''_{CHF} & \text{then transition boiling} \\ \text{if } q''_{NB} \leq q''_{CHF} & \text{then nucleate boiling} \end{cases}$$

where the subscripts FB, TB and NB denote film, transition and nucleate boiling, respectively. Note that the R5M3-approach does not require specific models for the temperature at the CHF, T_{CHF} and the minimum film boiling temperature, T_{MFB} , (see Fig. 2) to model the transition from one heat transfer mode to the other.

The description of the reflow process requires the modeling of both the thermally-hydraulic mechanisms and the heat conduction process within the solid structure. While the reflow thermalhydraulics are embedded in the general wall heat transfer models, R5M3 uses a two dimensional heat conduction approach with a “Fine-Mesh-Rezoning” method only for the reflow structures in order to represent the physics of the process (see subsection 2.3, page 11).

2.2 R5M3 Reflood Heat Transfer Models

During quenching the hot surface passes from an essentially dry state to full contact with liquid [17]. This is done through a series of heat transfer modes ranging from free-

or forced–convection cooling by steam, dispersed–flow film boiling, inverted annular film boiling, transition boiling, nucleate boiling, and finally single–phase convection to liquid. Corresponding to the boiling curve, the quenching process involves a shift from a film boiling heat transfer mode through transition boiling to a nucleate boiling regime. The code R5M3 has no special heat transfer reflow model. The description of the wall–to–fluid heat transfer in reflow situations is modeled within the general heat transfer logic. The most important reflow–relevant correlations used in R5M3 for vertical channels are briefly described below.

•Nucleate boiling

In the nucleate boiling regime heat is transferred mostly to the liquid ($h_g = 0$).

The liquid HTC, h_l , is derived from Chen [10] as a sum of two terms:

$$h_{NB} = h_l = h_{mic} + h_{mac} \quad (2)$$

where h_{mic} and h_{mac} represent microscopic and macroscopic convection terms defined as:

$$h_{mic} = 0.00122 \frac{k_l^{0.79} C_{pl}^{0.45} \rho_l^{0.49}}{\sigma^{0.5} \mu_l^{0.29} (H_{fg} \rho_g)^{0.24}} \Delta T_s^{0.24} p^{0.75} S_l \quad (3)$$

$$h_{mac} = 0.023 \frac{k_l}{D_e} Pr_l^{0.4} Re_l^{0.8} F \quad (4)$$

The suppression factor, S_l , is defined as:

$$S_l = \begin{cases} (1 + 0.12 Re_{TP}^{1.14})^{-1} & : Re_{TP} \leq 32.5 \\ (1 + 0.42 Re_{TP}^{0.78})^{-1} & : 32.5 \leq Re_{TP} \leq 70 \\ 0.0797 & : Re_{TP} \geq 70 \end{cases}$$

with the Reynolds number for the two–phase region, Re_{TP} , defined as:

$$Re_{TP} = \min \left\{ 70, \left[\frac{v_l \rho_l \alpha_l D_e}{\mu_l} \right] F^{1.25} 10^{-4} \right\} \quad (5)$$

The Reynolds factor, F , is correlated as a function of the Martinelli flow parameter, X_{tt} :

$$F = \begin{cases} 1.0 & : X_{tt}^{-1} \leq 0.10 \\ 2.35 (X_{tt}^{-1} + 0.213)^{0.736} & : X_{tt}^{-1} \geq 0.10 \end{cases} \quad (6)$$

$$X_{tt}^{-1} = \min \left(100, \left[\frac{\alpha_g \rho_g v_g}{(1 - \alpha_g) \rho_l v_l} \right]^{0.9} \left[\frac{\rho_l}{\rho_g} \right]^{0.5} \left[\frac{\mu_g}{\mu_l} \right]^{0.1} \right) \quad (7)$$

• **Transition boiling**

As stated above the formulation is based on (but is not completely identical to) the Chen model [11]. Differences with the original work of Chen are discussed in section 7. The total transition boiling wall heat flux is modeled as a weighted sum of two components corresponding to vapor convection and liquid boiling, respectively:

$$q_{TB}'' = (1 - f_l M_{stf}) q_g'' M_\alpha + f_l M_{stf} q_l'' \quad (8)$$

The wall-to-vapor HTC used to calculate q_g'' in eq. (8) is the largest value determined by the correlations for single phase convection in laminar, turbulent or laminar natural convection. In R5M3 the liquid heat flux, q_l'' , is taken as the critical heat flux, q_{CHF}'' , calculated by a look-up table (Groeneveld approach [16]).

The multiplier for stratified flow, M_{stf} , and the void fraction multiplier, M_α , in eq. (8) are correction factors applied to smooth the transition to stratified flow regime and to avoid heat transfer to vapor at low void fractions. Thus M_α is defined as follows:

$$M_\alpha = \begin{cases} 1.0 & : \alpha > 0.5 \\ \text{linear ramp} & : 0.0 < \alpha < 0.5 \\ 0.0 & : \alpha = 0.0 \end{cases}$$

The fraction of wetted wall surface, f_l , in eq. (8) is determined as:

$$f_l = \exp[-\sqrt{1.8a'(\alpha)g'(G) \min(15, \sqrt{\Delta T_s})}] \quad (9)$$

where $a'(\alpha)$ and $g'(G)$ are functions of the void fraction, α_g , and mass flux, G , defined by:

$$a'(\alpha) = \frac{0.05}{1 - \alpha_g^{40}} + 0.075\alpha_g \quad (10)$$

with $\alpha_g \leq 0.999$, and

$$g'(G) = \max(g'_1, g'_2) \quad (11)$$

with

$$g'_1 = 2.4 - \frac{G}{135.6} \quad (12)$$

and

$$g'_2 = 0.2 \frac{G}{135.6} \quad (13)$$

The transition boiling HTC to the liquid, h_l , is then calculated by:

$$h_l = \frac{f_l q_{CHF}''}{\Delta T_s}. \quad (14)$$

The vapor convective heat flux, q_g'' , is given by the relation

$$q_g'' = h_g (T_w - T_g). \quad (15)$$

The convective heat transfer coefficient to the gas h_g is determined by the Dittus Boelter correlation. T_w and T_g are the surface and superheated vapor temperatures, respectively.

The main differences between the original Chen model and the transition boiling model implemented in the frozen R5M3 version is exposed in the Section 7.

•Film boiling

Film boiling may occur during several flow patterns, namely inverted annular flow, slug flow and dispersed flow. In R5M3 [22] both conduction and convection to the vapor film and to the liquid (droplets) as well as radiation to the liquid (continuous blanket or dispersed mixture of droplets and vapor) are taken into account in the calculation of the total heat transfer coefficient. Convection between the vapor film and the liquid is included in the interfacial heat transfer model.

In general the total heat flux, q_{FB}'' , due to film boiling is given by:

$$q_{FB}'' = q_{FB,g}'' + q_{FB,l}'' \quad (16)$$

The first term in eq. (16) is the heat flux to the vapor, calculated in R5M3 by using a suitable single-phase heat transfer coefficient. The heat flux to the liquid, $q_{FB,l}''$, is a sum of the Sun's radiation model [44] and of the modified Bromley's conduction heat flux model [24], [21]:

$$q_{FB,l}'' = q_{FB,r}'' + q_{FB,c}'' \quad (17)$$

The liquid HTC due to conduction, $h_{l,c}$, is expressed by the modified Bromley-Pomeranz correlation [24] as follows:

$$h_{l,c} = 0.62 \left[\frac{g \rho_g k_g^2 (\rho_l - \rho_g) H'_{lg} C_{pg}}{L Pr_g \Delta T_s} \right]^{0.25} M_\alpha \quad (18)$$

The enthalpy factor, H'_{lg} , includes the energy absorbed by the superheated vapor surrounding the tube as:

$$H'_{lg} = H_{lg} + 0.5C_{pg} (T_w - T_s). \quad (19)$$

The parameter L in eq. (18) is expressed by the minimum critical wave length as:

$$L = 2 \pi \left(\frac{\sigma}{g (\rho_l - \rho_g)} \right)^{0.5} \quad (20)$$

where σ is the liquid surface tension and g is the earth gravitation constant.

The void fraction factor, M_α , is given by the relation:

$$M_\alpha = \begin{cases} 1.0 & : \alpha \leq 0.2 \\ spline & : 0.2 < \alpha < 0.999 \\ 0 & : \alpha = 0.999 \end{cases}$$

The property C_{pg} is evaluated at T_g while ρ_g , μ_g , and k_g are evaluated at the film temperature ($T_{film} = \frac{T_w + T_g}{2}$).

The radiation term in eq. (21) describes the radiation energy transfer between a wall and a mixture of vapor–liquid–droplet. The radiation heat flux is expressed by:

$$q''_{FB,r} = F' B (T_w^4 - T_s^4) \quad (21)$$

where F' is a gray–body factor and B is the Stefan–Boltzmann constant ($B = 5.678 \times 10^{-8} \frac{W}{m^2 K^4}$).

The corresponding HTC, $h_{l,r}$, is given as:

$$h_{l,r} = \frac{q''_{FB,r}}{T_w - T_s} = F' B (T_w + T_s)(T_w^2 + T_s^2) \quad (22)$$

The gray–body factor, F' , depends on the emissivities, ϵ_g and ϵ_f , and absorption coefficients, a_g and a_f , of vapor and liquid. It is defined as follows:

$$F' = \frac{1}{[\zeta_2(1 + \frac{\zeta_3}{\zeta_1} + \frac{\zeta_3}{\zeta_2})]}. \quad (23)$$

The factors ζ_1 , ζ_2 and ζ_3 in eq. (23) are given by the relations:

$$\zeta_1 = \frac{(1 - \epsilon_g)}{[\epsilon_g(1 - \epsilon_g\epsilon_l)]} \quad (24)$$

$$\zeta_2 = \frac{(1 - \epsilon_l)}{[\epsilon_l(1 - \epsilon_g\epsilon_l)]} \quad (25)$$

$$\zeta_3 = 0.111 + \frac{1}{(1 - \epsilon_g \epsilon_l)}. \quad (26)$$

The emissivities, ϵ_g and ϵ_l , are given as:

$$\epsilon_g = 1 - \exp(-a_g L_m) \quad (27)$$

$$\epsilon_l = 1 - \exp(-a_l L_m) \quad (28)$$

where L_m is the mean path length of the medium between the structures in radiation exchange. In R5M3 the following assumptions are made:

- $\epsilon_g = 0.02$,
- $L_m = 0.9D_e$, and
- $\epsilon_l = \min(1 - \exp(-0.9D_e a_l), 0.75)$

The liquid absorption coefficient, a_l , is approximated in [22] as:

$$a_l = 1.11 \alpha_l / d. \quad (29)$$

where d is the droplet diameter.

The maximum liquid cylinder diameter, d_{max} , which may be formed in a tube with diameter D , assuming that all the available liquid forms a cylinder in the center of the tube, is given by:

$$d_{max} = D \alpha_l^{0.5} \quad (30)$$

On the other hand, the average droplet diameter, d_{web} , based on a Weber number criterion of 7.5 for the post-CHF, is calculated in R5M3 as:

$$d_{web} = \frac{We \sigma}{\rho_g \max((v_g - v_l)^2, 0.005)}. \quad (31)$$

Consequently the droplet diameter, d , is determined in R5M3 from the relation:

$$d = \min(d_{web}, d_{max}). \quad (32)$$

2.3 Reflood Heat Conduction

As mentioned in earlier sections the reflood process must be described by both (axial and radial) heat conduction within the heat structure and heat transfer mechanisms at the wall–fluid interface. In reflood situations a two–dimensional heat conduction equation is solved only for the reflood–structures. Additionally a fine–mesh rezoning scheme at the quench front position is activated. By this way the axial node, where the quench front is located, is subdivided into smaller meshes depending of the prevailing heat–transfer conditions. According to a set of predefined rules, the number of fine nodes is doubled or halved automatically by the code during the calculation, in order to adequately describe the physical processes of the quench phenomena. This is necessary because some parameters like heat flux and heat transfer coefficient are changing dramatically within very narrow regions, of the order of milimeters, whereas the mesh size normally used is typically 10-20 cm [22].

If the reflood–structure is a typical fuel rod, R5M3 takes into account a two–dimensional heat conduction within the pellets and the cladding. The heat transfer over the gap is also modeled in R5M3 considering not only the gas conductance in the gap but also the radiation exchange between the pellet and the cladding [22]. According to [22] the total effective gap conductivity, $h_{tot,gap}$, is given as:

$$h_{tot,gap} = h_{gap} + h_r \quad (33)$$

where h_{gap} is the gas gap conductivity and h_r is the radiation contribution.

The conductance through the gas in the gap is given by:

$$h_{gap} = \frac{k_g}{N} \sum_{nc=1}^N \frac{1}{[t_{nc} + 3.2(r_F + r_C) + (\eta_1 + \eta_2)]} \quad (34)$$

where:

- nc number of the circumferential segment,
- N total number of circumferential segments (=8),
- k_g thermal conductivity of the gas,
- t_{nc} width of gap at the midpoint of the n-th circumferential segment,
- r_F surface roughness of the fuel,
- r_C surface roughness of the cladding, and
- η_1, η_2 temperature jump distance terms for fuel and cladding.

These terms are defined as follows:

$$\eta_1 + \eta_2 = \frac{0.024688 k_g T_g^{0.5}}{[P_g \sum \Omega_i \ell_i \varphi_i^{-0.5}]} \quad (35)$$

where:

- P_g gas pressure,
- T_g gas temperature in gap,
- Ω_i mole fraction of i-th gas component,
- ℓ_i accomodation coefficient, and
- φ_i molecular weight.

The constant 0.024688 in eq. 35 has the following units $[(J \text{ kmol K})^{0.5}]$.

The radiation part h_r is expressed as:

$$h_r = B \frac{1}{\left[\frac{1}{\epsilon_F} + \left(\frac{R_F}{R_C}\right) \left(\frac{1}{\epsilon_C} - 1\right)\right]} (T_F^2 + T_C^2)(T_F + T_C) \quad (36)$$

where:

- T_F outer pellet temperature,
- T_C inner cladding temperature,
- R_F outer pellet radius, and
- R_C inner cladding radius.

The gap conductance model of R5M3 is also able to consider different gases filling the gap, for example He, Ar, Kr, Xe, N, H, and O, as well as the cladding deformation (ballooning) for the calculation of the effective gap conductivity. The proper modeling of the gap in codes like R5M3 is important for a correct prediction of quench front movement, as will be shown in the following sections.

It must also be mentioned that the axial and radial heat removal of highly oxidized and overheated fuel rods becomes more complicated due to changes in material composition and geometry during the course of severe accidents. The appearance of an oxide layer (ZrO_2) due to cladding oxidation changes dramatically the axial and radial heat conduction, which in turn influence the quench front progression, because the heat conductivity of ZrO_2 is almost ten times lower than that of metallic Zircaloy. This oxide layer is also very porous and wavy, which also may alter the flow conditions (turbulence, nucleation, etc.) near the wall.

3 Experimental Programs for Code Validation

Two experimental programs, the FZK single-rod program [35], [19] and the NEPTUN tests [39], were considered for the validation of the reflood model in R5M3. Both programs are relevant for degraded core reflooding. The single-rod tests are being conducted at FZK while the NEPTUN test program was performed at PSI. The two experiments are briefly described in this section.

3.1 The FZK Single-Rod Quench Tests

A series of separate-effect tests were carried out on Zircaloy PWR fuel rod cladding segments at the Institute of Material Research (IMF) of the FZK. The main objective of the tests is to study the generation of new metallic surfaces by cracking and fragmentation during quenching at high temperatures [35], [19]. Different test series were performed with unoxidized and preoxidized cladding segments (empty or filled with ZrO_2 pellets), where the temperature at the onset of quenching varied from 1273 K to 1873 K.

3.1.1 Single-Rod QUENCH Rig Description

Figure 3 shows the test arrangement. It consists of a small scale specimen enclosed in a quartz tube and heated by an induction coil. The outer diameter of the rod specimen is the same of a PWR fuel rod and the cladding thickness is 0.725 mm. The specimen is 150 mm long. In some of the tests the specimen contained ZrO_2 -pellets of 9 mm diameter, leaving 150 μm annular gap.

As seen in Fig. 3 the quartz tube allows the observation of two-phase phenomena during the quench phase (vapor generation, splashing of droplets, collapsed liquid level movement, etc.). Fast video photographs were taken for each test. Relevant parameters of the single-rod quench tests including the rod specimen cross section with the location of the thermocouples are shown in Figure 4.

The temperature measurement during the whole test period (preheating and quench phases) were made by the use of different thermocouples depending on the test conditions. For water quenching tests without pre-oxidation, thermocouples welded on a rhenium foil were used (spot welded). For water quenching tests with pre-oxidation, the thermocouples were fixed by a ~ 2 mm Zircaloy ring. In several of the tests, the temperature were measured not only at different axial positions on the outer clad surface but also in different radial positions (see Fig. 4a and 4b). In the quench tests with the cladding segments filled with ZrO_2 -pellets the thermocouples were positioned axially along the segments and radially over the fuel rod simulator. The radial temperature measurement at the level of 0.075 m consisted of three thermocouples. The first shielded thermocouple was located in the center of the ZrO_2 pellet. The second one was located in the gap between the ZrO_2 pellet and the cladding (in a groove on the pellet touching the cladding inner surface) and the last one spot welded on the outer cladding surface.

3.1.2 Test Procedure

Figure 5 depicts a typical temperature curve for the pre-quench and quench phase. The specimen is first heated in an argon (tests with no pre-oxidation) or in an argon/oxygen

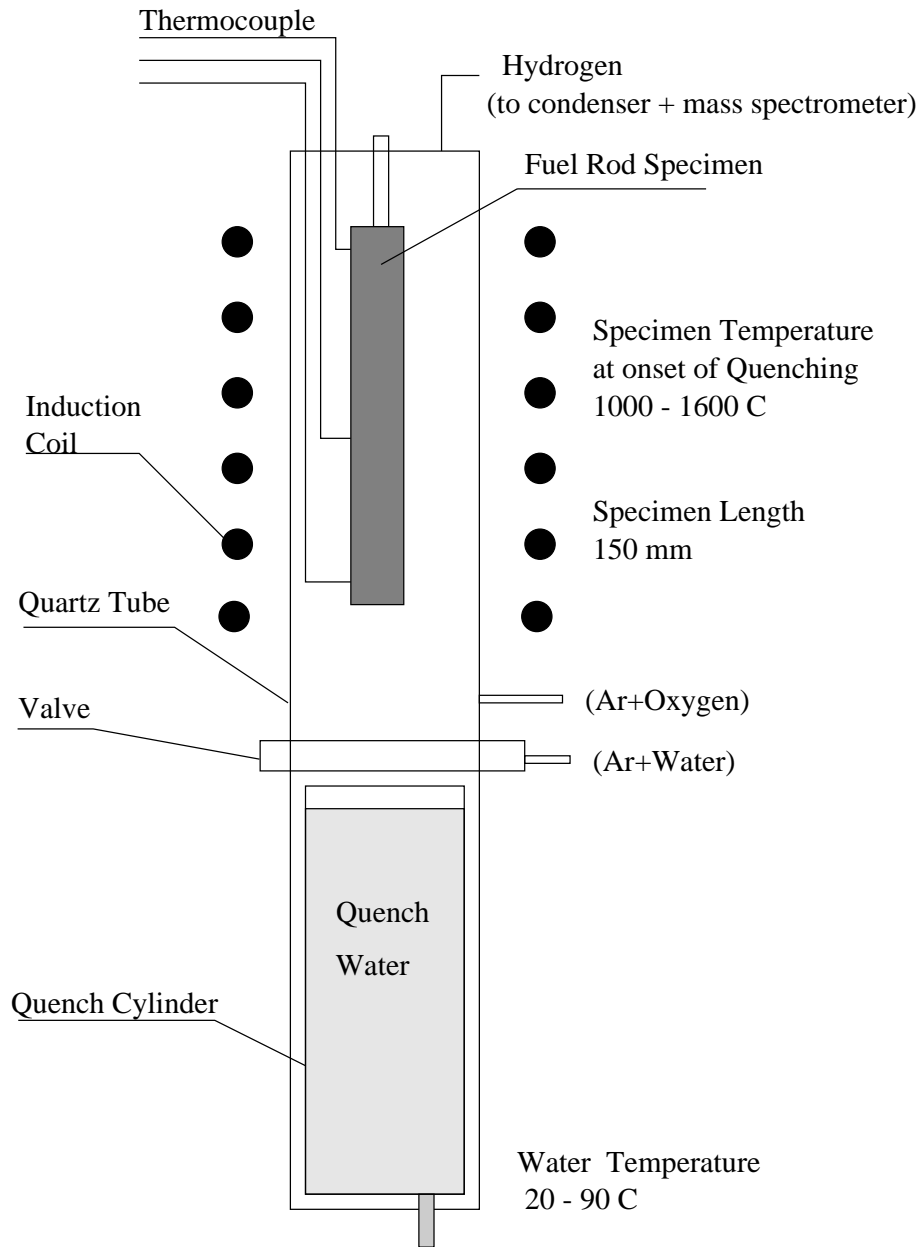


Figure 3: Arrangement of the Single Rod Quench Tests at FZK

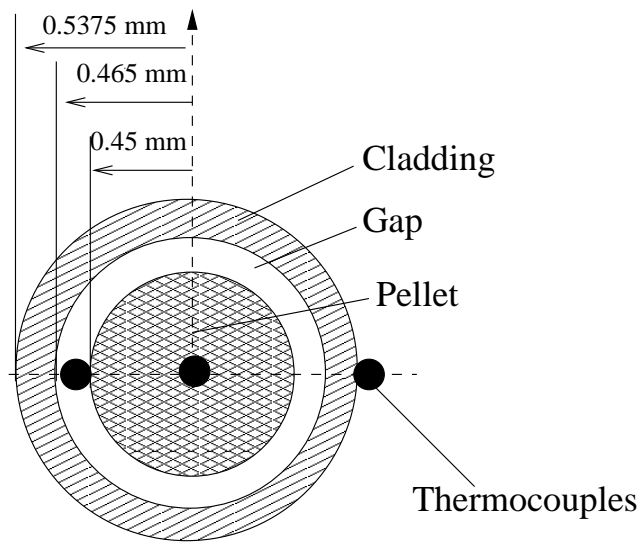
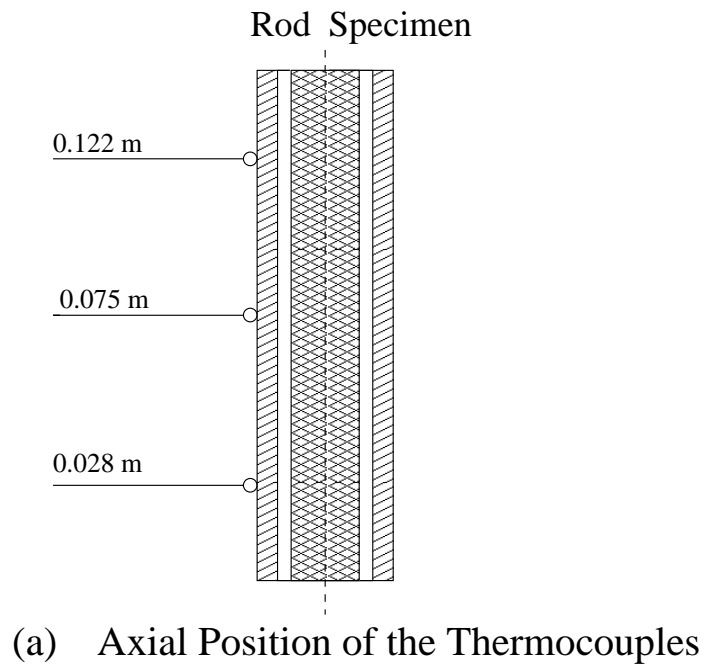


Figure 4: Rod QUENCH Rig: Cross Section and Temperature Measurement

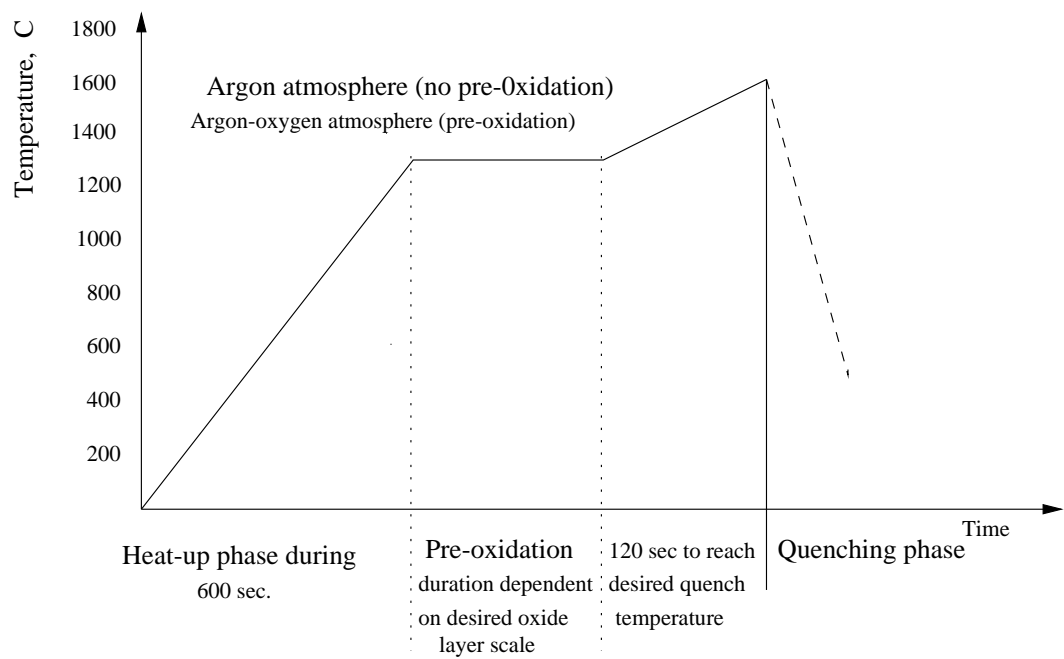


Figure 5: FZK Single-Rod Quench Test Conduction

atmosphere (tests with pre-oxidation) by an induction coil until a predefined temperature is reached. Quenching is then initiated by raising a water filled quartz cylinder with a constant velocity of 0.015 m/sec or by flowing of saturated steam from the bottom of the heated cladding segment. Under that procedure the quench cylinder reaches the top of the specimen within 10 seconds, much before a quench front is established at the bottom of the test section. The induction coil is positioned outside the quartz cylinder (see Fig. 3). The unoxidized specimen is heated during the first 10 min in an argon atmosphere (constant argon flow rate of 40 l/h) until a desired nominal quench temperature, T_0 , is reached at the mid-elevation. The temperature at onset of quenching is kept constant for additional two minutes, before starting the quench phase. The quench phase begins when the quench cylinder touches the lower end of the specimen. At this time the heating is terminated. During the quenching phase, subcooled water is injected from the bottom by moving the quench cylinder upwards at a constant velocity [18], [35] and [19]. From the tests performed with unoxidized empty tubes, only the tests listed in Table 3 were selected for code validation. In these tests three thermocouples were positioned axially along the cladding segment and one thermocouple was fixed on the inside cladding surface at a height of 0.075 m. All tests were performed under atmospheric pressure conditions.

3.1.3 Measurement Uncertainty

The behavior of the rod specimens during the pre-quench and quench phase at the QUENCH rig is determined by measurement of the temperature (at the cladding surface, in the gap and at the pellet centerline) as well as of the hydrogen generated during the tests. Additional metallographic examinations follow after each test to determine oxidation scale, cracks formation, etc. In the case of quenching of unoxidized rod specimens spot welded thermocouples (bare-wire type) at the cladding outer surface were used in the majority of both empty and filled rod specimens. In the gap between pellet and cladding and at the cladding inner surface different methods of thermocouple attachment were used at FZK [35] as follow:

- sleeved thermocouple, in a groove on the outside of the pellet, wedged between the pellet and the clad inner surface.
- sleeved thermocouple, pressed against the inner clad surface by a disk.
- spot-welding of the thin foil, to which the thermocouple (bare-wire type) is attached, to the inner clad surface.

The influence of thermocouple attachment methods on the temperature measurement during the quench tests at the QUENCH rig was investigated by AEA Technology [15] using a finite element heat transfer code aiming to identify the possible cause of measurement errors.

A large number of possible sources of error are mentioned in [15] for the different thermocouple attachment methods in the case of water quenched tests. The most common error sources are:

- fin effects
- added mass
- added surface area
- surface conditions
- thermal contact (air gap)
- enhanced boiling
- false junction

- effectiveness of thermocouple thermal contact
- disk/clad heat transfer
- thermocouple response
- pellet/clad temperature difference
- pellet tube gap offset

A comparison of measured clad temperature using different thermocouple types indicate that the boiling at the clad surface of the thermocouple position is being affected by the presence of the thermocouple and its attachment mechanism. Therefore Fry et al. [15] conclude that the presence of the thermocouple on the outside of the Zircaloy clad can significantly affect the heat loss from the specimen surface, and hence its temperature history. These effects of thermocouple attachment upon the boiling heat transfer will dominate any other error sources of thermocouple error. An error quantification produced by the different attachment methods for water quenched tests with the TAU finite element heat transfer code has not been done at the present. In [15] only an error quantification for the cool-down tests using different model assumptions were made. The Table 1 shows typical ranges of temperature differences predicted by the TAU models for the different attachment methods in comparison with the measured temperature differences. Of course, larger temperature differences are expected for water quenching tests.

Table 1: Comparison of predicted and measured temperature difference for cooldown tests

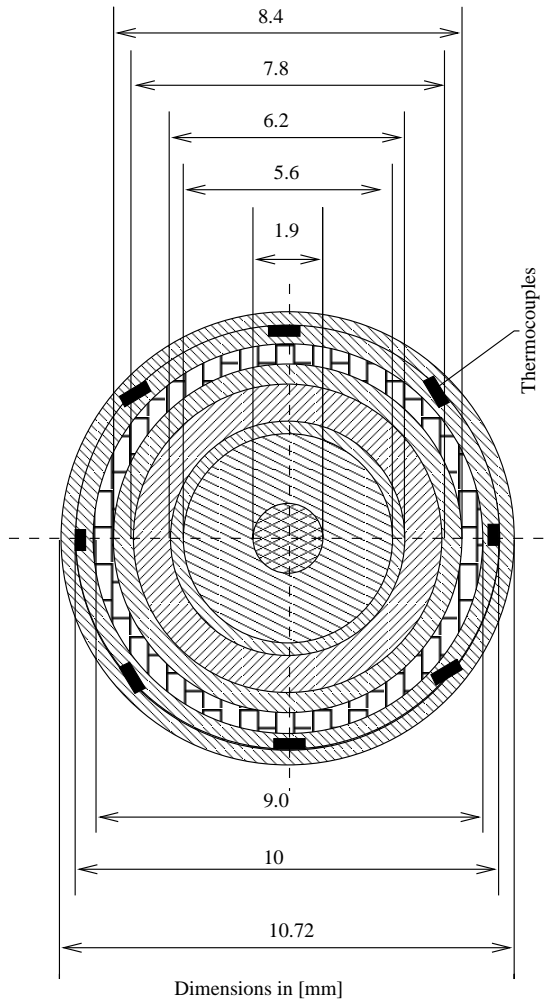
Thermocouple Attachment	Measured	TAU Predictions
Outside Spot-welded	-11 K (assumed)	-11 to -16 K
Inside Spot-welded	+14 to + 28 K	+1 to +14 K
Inside pressed	+23 to +56 K	+15 to + 49 K

3.2 The NEPTUN Bundle Tests

3.2.1 Test Description and Procedure

The NEPTUN test facility was designed to study reflooding in bundle geometries [42]. It consists of 33 electrically heated rods and four guide-tubes. The layout and dimensions of the heater rods are shown in Fig. 6.

The outer dimensions of the rods are similar to those of a PWR fuel rods except being half length in size (1.68 m heated length, 10.7 mm outer diameter and 1.33 pitch



-  Kanthal ((alloy of Fe, Cr, Al and Co))
-  Boron
-  Inconel 60
-  Copper
-  Al₂O₃

Figure 6: Cross Section of the NEPTUN Heater Rod

to diameter ratio). The complete bundle is placed in an insulated octagonal housing. A cosine shape axial power profile with a peaking factor of 1.58 is used. Five spacer grids are used axially at equal distances along the fuel assembly. The tests (5036 and 5050) were carried out under the pressure of 0.41 MPa. The rod power amounted to 2.45 kW.

Rod cladding temperatures, fluid temperatures and differential pressures are measured at eight levels. The lower measurement level is located 50 mm above the beginning of the heated zone. The other measurement points are distributed at equal axial distances (232 mm) along the rods. Each heater rod is instrumented with four to eight thermocouples, placed inside the cladding at the eight measurement levels. The five central heater rods are additionally supplied with external thermocouples (see Figure 7). Furthermore the flooding rate, exhaust steam flow rate, water carry over, absolute pressures and heating power are measured. The void fractions and the collapsed liquid level are deduced from the measured absolute pressure and the pressure difference. The pressure in the upper plenum of the test section is held constant during the experiments by a pressure control system.

The NEPTUN facility consists, in general, of an inlet water supply system, a test section and an exit section. During the initial test period, the test section is kept in a saturated steam environment at a defined experimental pressure. The power in the heater rods is then switched on and the heater rod temperatures start to increase. A short time before the cladding temperatures reach the desired value, the test section is quenched from below with water at given temperature. The power at the bundle is held constant throughout the experiment.

3.2.2 Measurement Uncertainty

A discussion of errors made by measurements of quench-relevant parameters is given in [39]. In that reference there is no detailed quantification of the measurement accuracy in the NEPTUN test facility, so that the errors of the measured data were mostly estimated [39]. The Table 2 summarizes the estimated measurement errors and scattering of the test data of seven NEPTUN tests [39].

3.3 The Validation Matrix

For the assessment of the R5M3-reflood model, different Single Rod Quench tests without pre-oxidation were selected. The test matrix includes quenching by water of empty and filled tube segments. In addition, one test is selected in which the specimen is cooled by steam flow. Although this last case is not a true quenching test, it provides essential data for analyzing the measurement uncertainties. Moreover steam quenching is representative for the flow conditions in the upper part of the bundle (Table 3).

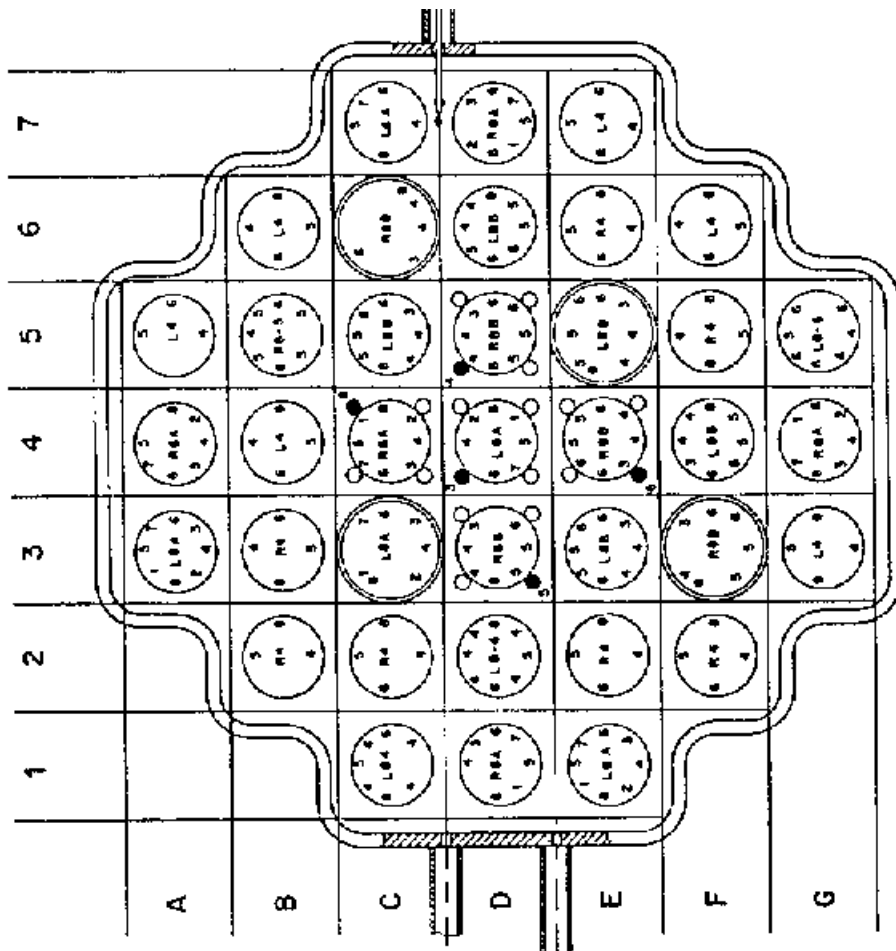


Figure 7: Cross Section of the NEPTUN Bundle

Table 2: NEPTUN measurement errors and scattering of the data

Quantity	Probable error	Largest scattering
Flooding water mass flow	± 5.3	
Flooding water temperature	$\pm 0.5^\circ C$	
Test section pressure	± 0.03 bar	
Collapsed water level	± 4 cm	
Void fractions	± 0.04	
Rod clad temperature between all rods without external thermocouples	$\pm 5^\circ C$	$48^\circ C$, exp. 5050 $90^\circ C$, exp. 5036
Quench times between all rods without external thermocouples at measurement level 4 and 5	$\pm 1.2s$	$2.5s$, exp. 5050 $14.2s$, exp. 5036

Two NEPTUN tests (No. 5036 and 5050) were selected for the validation effort. The first is a low inlet velocity test which has been used formerly as a base case in the assessment of the R5M2 code [39] and the R5M3 code [2]. The second represents a high inlet velocity case (Table 3).

4 Test Modeling for Reflood Model Assessment

The numerical models applied to represent experiment setup and test procedure for the calculation with the code R5M3 are described here. The results of assessmental calculations related to the reflood model are discussed in the next subsections 4.1 and 4.2.

4.1 The FZK Single-Rod Test Rig

In modeling the test system and procedure it is recognized that the main quench phenomena take place within the quench cylinder which, upon reaching predetermined initial conditions, is pushed upwards at a constant velocity of 0.015 m/s. The movement of the quench cylinder is modeled by specifying a constant inlet velocity of water at the bottom of the coolant channel.

Radiation losses from the test section to the environment are initially high, mainly because of the high initial temperature level. The inner and outer quartz cylinders are

Table 3: Test matrix for the validation of the R5M3-reflood model

Test	T_0/T_{sub} (K)	Specimen Type	TC Type	TC Fixation	v_{in} (cm/s)
FZK Separate-Effect Tests					
ITE20115	1273/363	empty	radial	spot welded	1.5
ITE22115	1673/363	empty	radial	spot welded	1.5
ITE29115	1866/363	empty	radial	spot welded	1.5
T24085	1475/363	filled	axial	spot welded	1.5
T02106	1520/363	filled	radial	spot welded	1.5
T21066	1673/363	filled	axial	spot welded	1.5
T31085	1873/363	filled	axial	spot welded	1.5
T24066	1873/363	filled	axial	spot welded	1.5
T16106	1873/363	filled	radial	spot welded	1.5
PSI NEPTUN Experiments					
5036	1030/411	Heater rod	axial	inside clad	1.5
5050	1140/411	Heater rod	axial	inside clad	15

almost transparent to radiation. However, when quenching begins, the specimen temperature decreases within a few seconds to temperatures below 1000 K, the radiation losses to the environment do not strongly influence the quench front progression and the accompanying changes of heat transfer mode from film to transition and from transition to nucleate boiling which typically occur at lower values of ΔT_s . The radiation exchange option of R5M3 was activated in the simulation throughout the transient in order to simulate primarily the radiation exchange between the hot specimen and the mixture of droplets and vapor that is present in the channel during film boiling.

The argon flowing through the annular gap around the quench cylinder and the outer quartz cylinder does not play an important role in the quench process. Therefore, it was neglected in the simulation. As in the experiment where tests are carried out at atmospheric pressure, a constant outlet pressure of 0.1 MPa was used in the simulation.

Figure 8 shows the nodalization scheme for the R5M3 simulation of the FZK separate-effect quench tests.

The time-dependent volumes (Tmdpvol) and junctions in Figure 8 are used to represent the initial and boundary conditions at the inlet and outlet of the test section (temperature, mass flux rates, pressure). The branch elements represent the fluid conditions below and above the test section (“Pipe Element”). The quartz cylinder is represented

as a pipe element with 15 internal volumes, where the initial thermalhydraulic conditions (pressure, temperature, mass flux rate, quality etc.) of the fluid channel are fixed. The rod specimen (filled or empty) and the quartz cylinder are modeled as heat structure. The first heat structure represents the rod specimen considering its material composition. This structure is coupled by convective boundary conditions with the fluid channel. It also allows for the specification of the initial distribution of the specimen temperature. The second heat structure is coupled by convective boundary conditions with the fluid channel on one side and with a constant temperature (representing the environment temperature) on the other side. This heat structure is required to represent the heat sink and to activate the radiation exchange model of the R5M3 code, taking into account the radiation absorption by the steam and droplet flow in the channel. The thickness of this outer tube was found to have no effect on the results.

Figure 8(b) shows the radial nodalization of the test specimen. The cladding is subdivided into three rings. More nodes may be necessary to model oxidized clad because of the large difference between the thermal properties of oxidized and non oxidized material. The ZrO_2 pellet (when it exists) is modeled as a single node since the radial temperature variations are typically small.

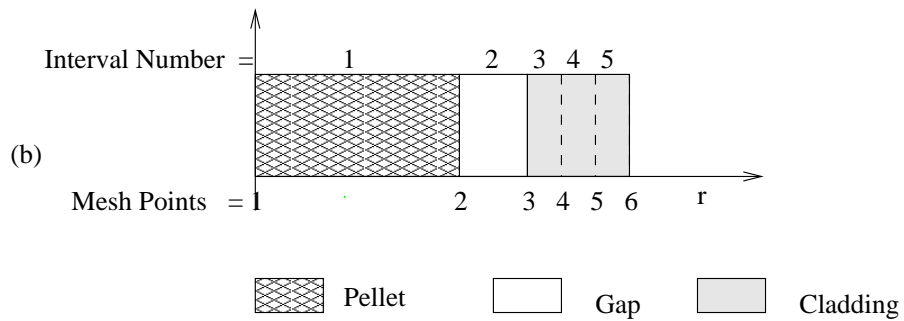
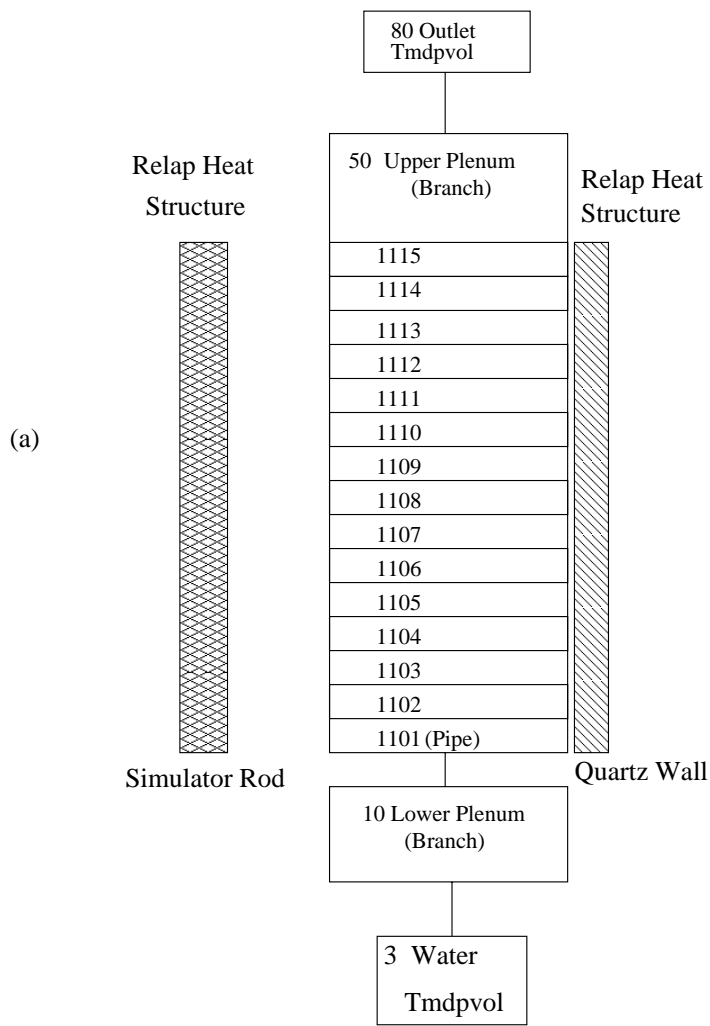


Figure 8: Axial and Radial Nodalization of the Single-Rod Quench Test Rig

4.2 The NEPTUN Facility

The model used to describe the NEPTUN facility is shown in Fig. 9. It is identical to the scheme used formerly in the assessment of the R5M3 code at PSI [2]. The model consists of a pipe component to represent the fluid volumes in the test section. The heater rod is divided into nine radial layers to accurately simulate the radial temperature distribution and material composition.

The inlet water system is simulated by a time-dependent volume connected to the coolant channel by a time-dependent junction. The upper plenum is represented by a time-dependent volume with constant pressure, connected to the upper end of the channel by a single junction. Guide tubes and housing were neglected in the calculation since they have only small effects on the flooding behavior of the bundle [39].

The effect of different nodalizations on the R5M2 code predictions was studied in [39], using 10, 18 and 32 volumes for the bundle for a given number of fine mesh nodes in the heat conduction elements. It was found that in the high flooding rate experiment (test number 5050) the effect of the nodalization on the cladding temperatures is small. In the low flooding rate experiment (test number 5036) the effect of the number of nodes on the results was not systematic. The present calculations were performed with 18 volume elements in the coolant channel and 16 fine mesh points per heat slab as recommended in [39].

5 Results of Assessmental Calculations with RELAP5/MOD3

Using the nodalization scheme mentioned above, base case calculations were carried out with the code version RELAP5/MOD3.1 (R5M3) for the QUENCH rig tests. These calculations started with a steady state calculation to check for input errors and to reach quasi steady state conditions before the initiation of transient calculation. The aim of the transient calculations (pre-quenching phase) was to meet the specimen temperature at onset of quenching for each test. Then calculation of the quenching phase followed.

In the case of the NEPTUN tests, we adopted the same base case as in [39]. Therefore a repetition of this work is not necessary in this place.

Since temperatures are the only data measured in the test program of FZK, the present analysis will be based primarily on the predicted temperatures. In addition, other calculated parameters will be shown to enhance the physical understanding of the results.

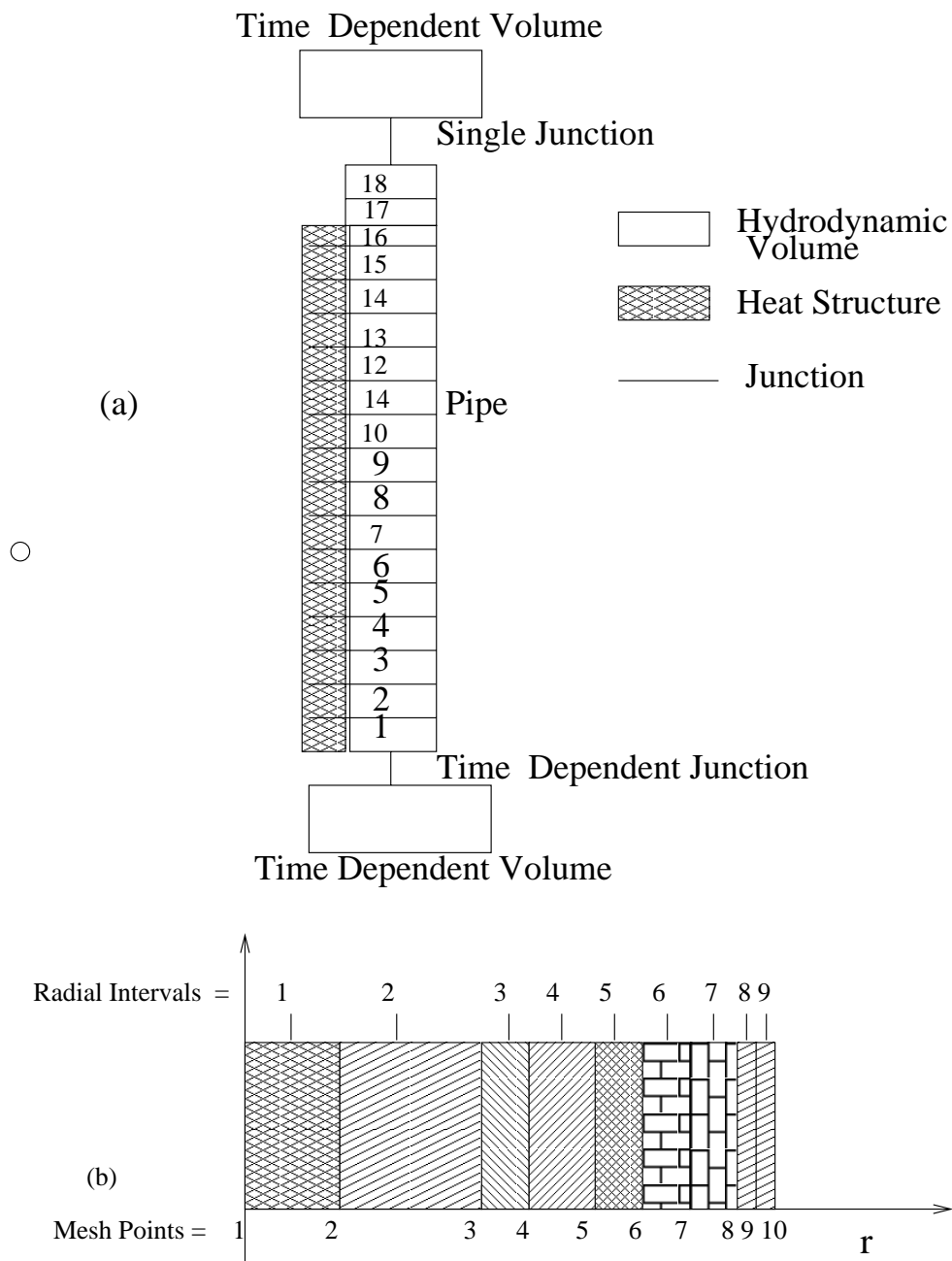


Figure 9: Nodalization Scheme of the NEPTUN Test Section

5.1 FZK Single-Rod

A typical sample of rod temperature histories at various radial locations in the middle of the specimen is shown in Fig. 10. The preheating process lasting for 720 seconds was also simulated by R5M3 but is not shown.

In all the curves of Fig. 10, the temperature changes gradually at the early phase of the transient due to early cooling by steam, two-phase mixture produced mainly at the lower part of the coolant channel and due to radiation. At a certain time, each curve exhibits a ‘knee’ shape when the temperature drops sharply to almost a steady value corresponding to the local fluid temperature. This marks the rewetting of the measured point along the test rod. During a period of few seconds around this knee, the rod experiences dramatic changes of the heat transfer mode from film boiling through transition and nucleate boiling to single phase to liquid (see Figure 11).

The quench temperature, T_q , corresponding to the knee point can be defined as in Barnea et al. [6] at the intersection between the tangent line to the temperature–time curve at the point where its slope is the largest, with the tangent to the curve before quenching. The quench temperature marks the onset of rapid surface cooling caused by an enhanced heat transfer rate without complete liquid–solid contact. The measured T_q at the inner and outer sides of the cladding are about 800 and 700 K respectively. The corresponding predicted T_q are significantly lower (about 720 and 600 K respectively). The quench temperature, T_q , corresponds roughly to the minimum film boiling temperature, T_{MFB} , at which the film boiling and transition boiling heat fluxes become equal. The systematic underprediction of T_q depicted in Fig. 10*b, c* indicates, therefore, an underprediction of the transition boiling heat transfer. This is further demonstrated in Fig. 11 which shows the predicted heat flux, critical heat flux and heat transfer coefficient at the mid-level of the specimen’s outer surface. The rewetting process is shown to be accompanied by a sudden increase in the heat flux as the heat transfer mode changes from film boiling to the more intense boiling mechanisms characteristic to the transition and nucleate boiling regimes. However, the predicted peak heat flux in Fig. 11*a* is very low relative to the local critical heat flux. This is a direct result of the transition boiling model used in R5M3 as described in eq. (9).

The measured clad outside temperature prior to quenching is shown to be lower than the calculated (see Fig. 10*c*). This is assumed to be caused by local measurement errors: the size of the thermocouple and of its welded bead is of the order of the thickness of the thermal boundary layer developing along the specimen. The layer is smaller at the bottom of the specimen. The rhenium foil acts as a cooling fin and the thermocouple is to a larger extent exposed to water droplet in the vapor film surrounding the cladding. The same effect is encountered in the case of steam cooling tests. For this case, the Fig. 12 exhibits a comparison between predicted and measured surface temperature at three different

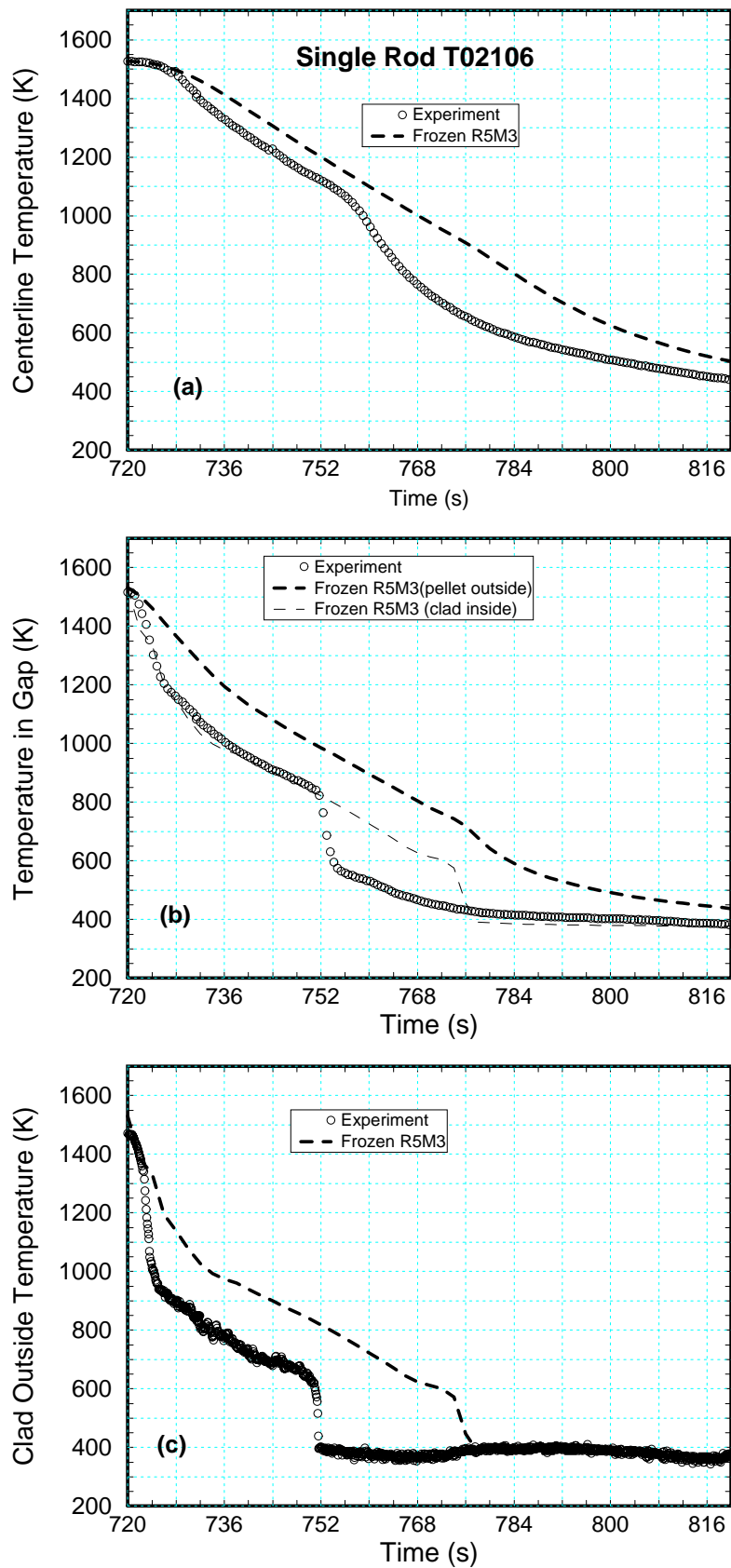


Figure 10: Comparison of the Original R5M3 Predictions with the Measured Temperatures in the FZK Single-Rod Test No. T02106

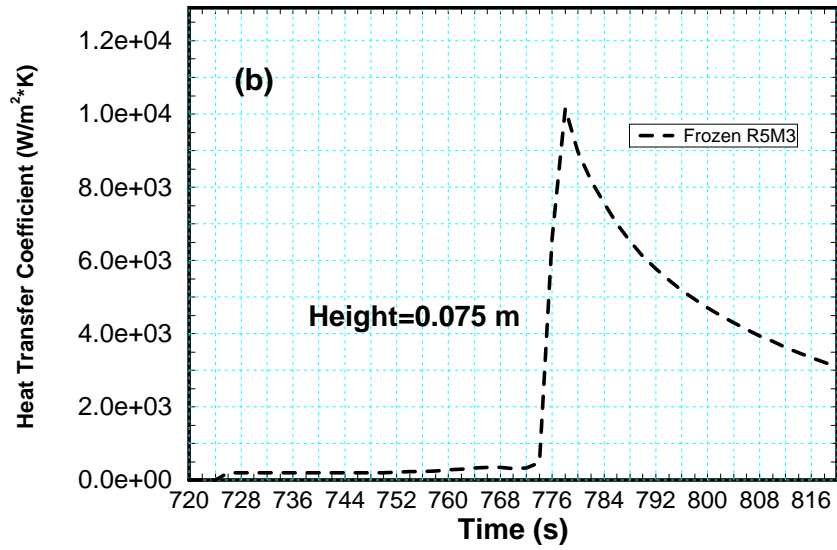
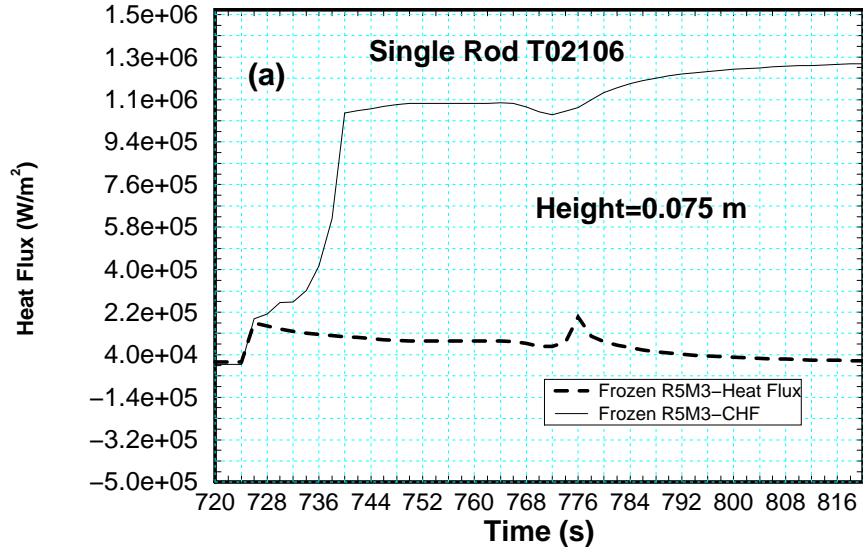


Figure 11: R5M3 Predictions of a. Surface Heat Flux and Critical Heat Flux, and b. Surface HTC in the FZK Single-Rod Test No. T02106

levels along the specimen. In all cases the measured temperatures are lower than the calculated surface temperature and their measured values correspond to an intermediate values between the surface temperature and the steam coolant temperature.

The predicted clad inner surface temperature prior to quenching (part *b* in Fig. 10) is generally in good agreement with the measured data. It should be recognized that the measured inner surface temperature may be overestimated because of the finite size of the inner thermocouple which makes it sensitive to possible radiation and convection heat transfer from the ZrO_2 pellets. Therefore, it is expected that the measured gap temperature will lay between the predicted inner clad temperature and outer pellet temperature.

5.2 NEPTUN Facility

The results obtained with the frozen version R5M3 for the test 5036 are the same as predicted in [43]. Figure 13 shows a comparison between measured and predicted cladding temperature. As can be seen in Figure 13 the predicted temperature does not show the typical 'knee'-point of a rewetting process. The initial cladding temperature during the first 35 s coincides very well with the measured one. Hereafter the code predicts a higher heat transfer coefficient that leads to an earlier 'turn-around'-point and to faster cladding temperature decrease compared with the measured data. Hence both the quench time and the quench temperature are missed. This also indicates that the modeling of the post-CHF heat transfer mechanisms in the frozen version of R5M3 is not correct.

6 Stand-Alone Assessment of the RELAP-Reflow Model

In order to assess the original transition boiling model implemented in R5M3 as part of the reflow model, a stand-alone program of this model was coded outside the RELAP-code and validated against steady-state experimental data. In particular, steady-state data measured in a heat flux controlled mode, [9], and in temperature controlled mode, [47], [28], were considered for the validation of the stand-alone model.

6.1 Validation Matrix

The Table 4 gives the test data used for model validation.

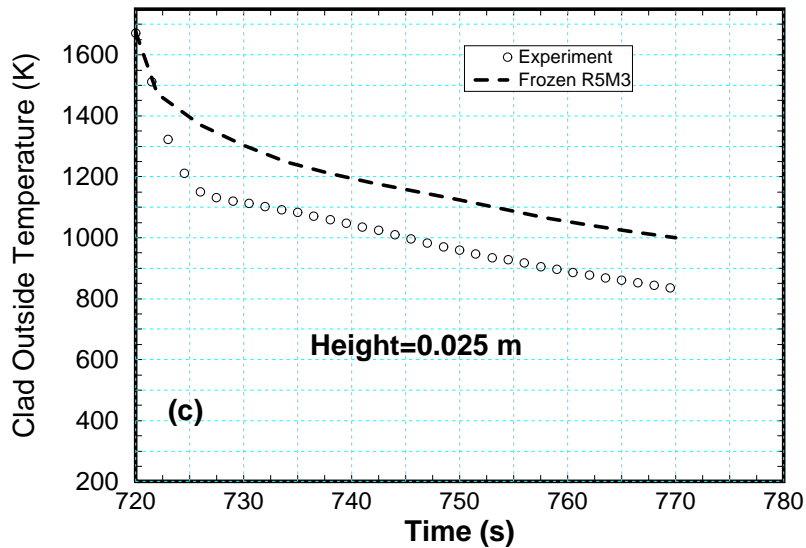
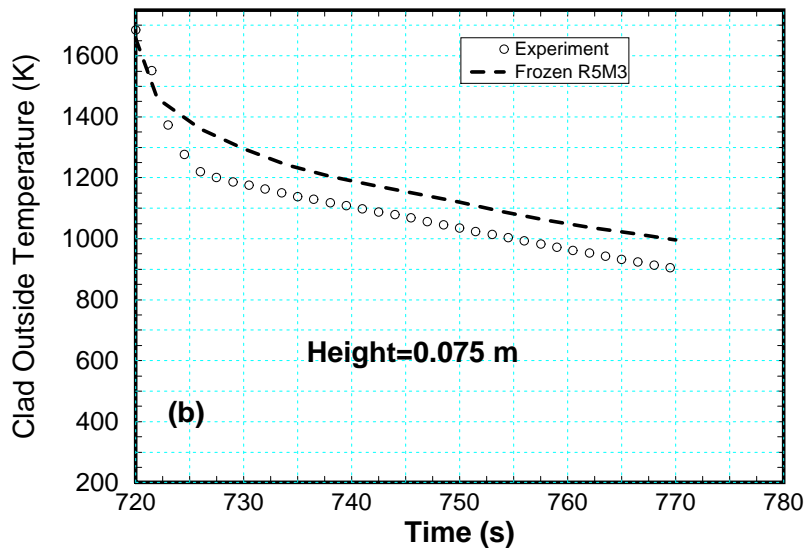
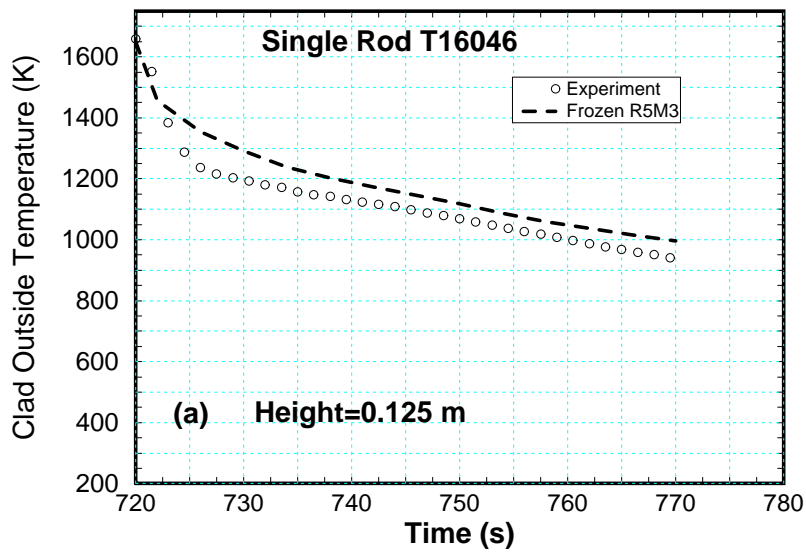


Figure 12: Measured and Predicted Clad Outside Temperatures and Steam Coolant Temperature for the Steam-Cooled FZK Single-Rod Test No.T16046

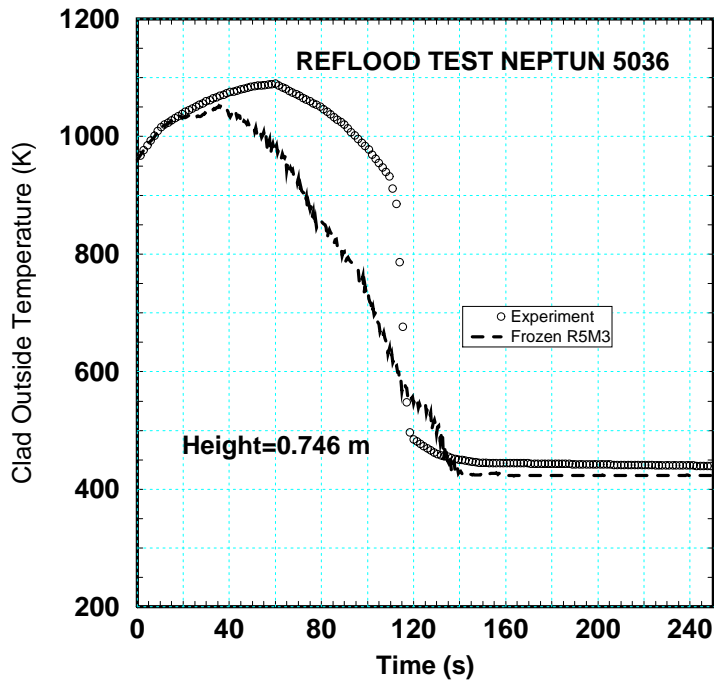


Figure 13: Measured and Predicted Clad Temperature in the NEPTUN Test 3056

Table 4: Test Matrix for Stand-Alone Validation of R5M3-Reflood Model

Reference	Test Type	Main Parameters
Bennett et al.[9]	Heat flux controlled	0.0126 m tube diameter 6.9 Mpa $300 < G < 5500 \text{ kg/m}^2\cdot\text{s}$
Weisman et al. [47]	Temperature controlled heated by Mercury	$0.1 < p < 0.4 \text{ MPa}$ $16 < G < 46 \text{ kg/m}^2\cdot\text{s}$
Johannsen et al. [28]	Temperature controlled	Hollow Cylinder 0.050 m long $od = 0.032 \text{ m}$, $id = 0.010 \text{ m}$ $0.1 < p < 1 \text{ MPa}$ $25 < G < 200 \text{ kg/m}^2\cdot\text{s}$ $3 < \Delta T_{in} < 30 \text{ K}$

The symbols in the Table 4 have the following meaning:

- G mass flux
- od outer diameter
- id inner diameter
- ΔT_{in} inlet subcooling.

6.2 Discussion of Results

The Figure 14 compares the predicted and measured data. Many of the measurements are underpredicted by one or more orders of magnitude. The data shown in Fig. 14 cover a wide range of thermalhydraulic conditions: Bennett et al. [9] report measurement in a vertical electrically heated 12.6 mm inner diameter tube at 6.9 MPa and mass flux of up to 5500 kg/m²·s. Johannsen et al. [28] report measurements of CHF and transition boiling heat flux in a hollow cylinder of 50 mm length with an outer diameter of 32 mm and an inner bore of 10 mm. Data are measured in the pressure range of 0.1 to 1.2 MPa, mass flux of 25 to 200 kg/m²·s and inlet subcooling of 3 to 30 K. An electronic feedback system was applied to control the temperature of the heat transfer surface and thus stabilize the otherwise unstable boiling process. Weisman et al. [47] conducted transition boiling heat transfer tests at low pressure (about 0.2 MPa) using a loop in which the test sections were heated by hot mercury. The inlet linear water velocities were 0.017 to 0.048 m/s which correspond to the lower end of the reflood range of conditions during LOCA.

Careful examination of Fig. 14 shows that the original R5M3 model predicts reasonably well mostly the high quality post CHF data in which the convective heat flux to vapor is the dominant term. Clearly, the introduction of q''_{CHF} instead of the heat flux function, $q''_i(p, \Delta T_s)$, suggested in [11] effectively reduces the contribution of the boiling term in the transition boiling region and causes the R5M3 model to underpredict all the data in the low quality range in which the boiling term is important. This is best demonstrated by a typical case shown in Fig. 15 which compares the measured and predicted heat flux along the pipe wall in run No. 5251 of Bennett et al. [9]. The predicted total heat flux is the sum of a vapor convective term, q''_g , and a boiling term, q''_i . It is seen that the predicted boiling term is negligible throughout the post CHF region. The total heat flux is thus underpredicted.

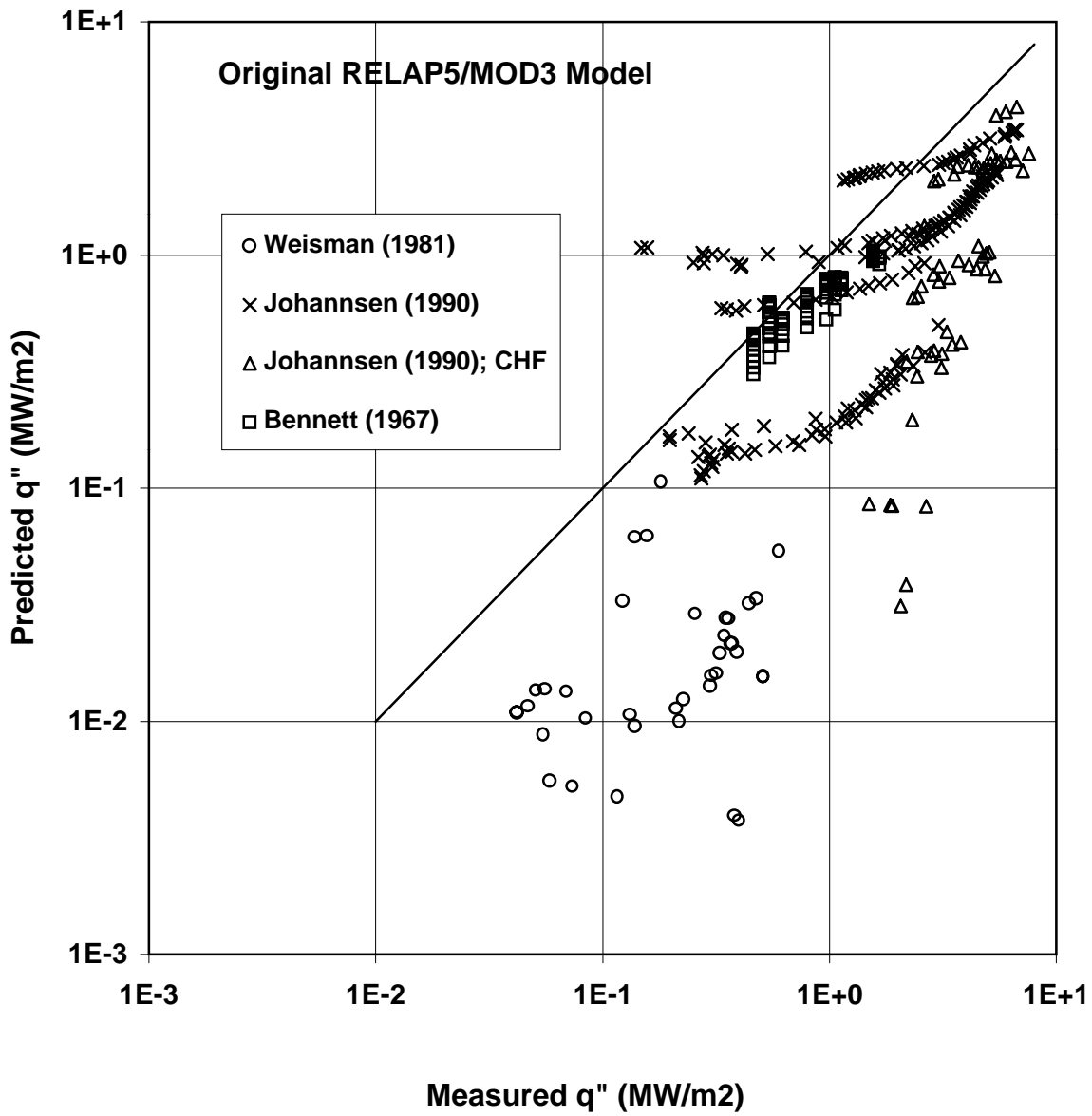


Figure 14: Measured vs Stand-Alone R5M3 Model Predictions of Transition Boiling Data

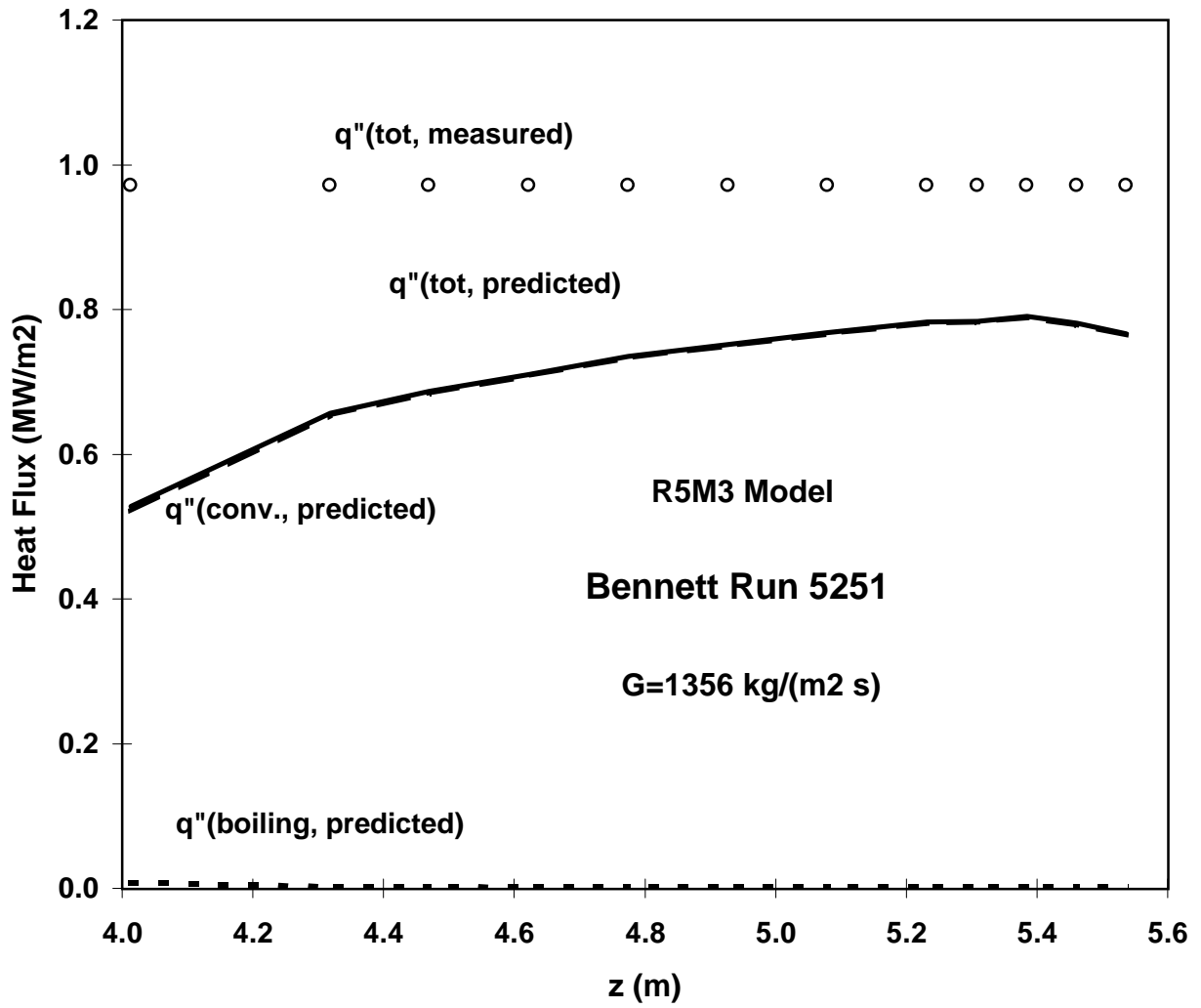


Figure 15: Stand-Alone R5M3 Model Prediction of Run 5251 in Bennett et al. (1967)

7 Limitations of the Current Transition Boiling Model

The calculational results obtained in subsection 5 with the frozen R5M3 version and in subsection 6 with the stand-alone transition boiling model point out the need to improve the reflood prediction capability of the code. The systematic deviations between the predicted and measured quench temperatures outlined above result mainly from the implementation of an inappropriate and physically erroneous interpretation of the Chen transition boiling model in the R5M3 code. In order to better understand the limitation of the current transition boiling model, Table 5 summarizes the main features of the original Chen formulation in comparison with the current R5M3 model. It is noted that some of the constants (0.05 and 0.075 instead of 0.005 and 0.0075) in the correlation of the wetted area fraction, f_l (eq. (9)), are modified in the code in a non-consistent manner. The original Chen correlation with the coefficients 0.005 and 0.0075 was programmed and validated against different tests data obtaining very good results. On the contrary, if the coefficients 0.05 and 0.075 are used, the original Chen graphs cannot be reproduced. As can be seen in the figures 14 and 15, the Bennett data cannot be well predicted, if the R5M3 model with the coefficients 0.05 and 0.075 is used. Therefore the coefficients used in the original Chen model and not the ones used in R5M3 as stated in [22] are correct.

The wall superheat term in f_l is arbitrarily limited in R5M3 to $\sqrt{\Delta T_s} \leq 15$. This limit has a strong effect on the predicted T_q in R5M3. More significantly, the original expression suggested in the Chen model for calculating the wall heat flux is altered by using the critical heat flux to replace the complicated heat flux function, $q_l''(p, \Delta T_s)$, derived by Chen. Since $q_l''(p, \Delta T_s) \gg q_{CHF}''$, the boiling part of the R5M3 transition boiling model is underpredicted. This affects mainly tests at low quality in which boiling is the dominant heat transfer mechanism in the transition boiling regime.

The modifications introduced in R5M3 to the Chen model have resulted in several physically erroneous trends beside the systematic underprediction of T_q . First the predicted dependence of the quenching rate on the coolant inlet mass flux for values higher than 270 kg/m²·s has been shown to be wrong, [2]. Moreover, since $f_l \leq 1$, the heat flux curve in R5M3 exhibits a discontinuity at the CHF point where the heat flux determined by the nucleate boiling model is q_{CHF}'' and that calculated by the transition boiling model is about $f_l q_{CHF}''$. This is clearly demonstrated also in Fig. 11 showing the maximum quench heat flux to be lower than the local q_{CHF}'' . The discontinuity in the heat flux at $q'' \geq q_{CHF}''$ was recently demonstrated by Ruggles et al. [40]. The Figure 16 shows this behavior very clearly [40].

Starting from the extensive validation of the original Chen model reported in [11], it was considered desirable to extend the original Chen model to the range of conditions

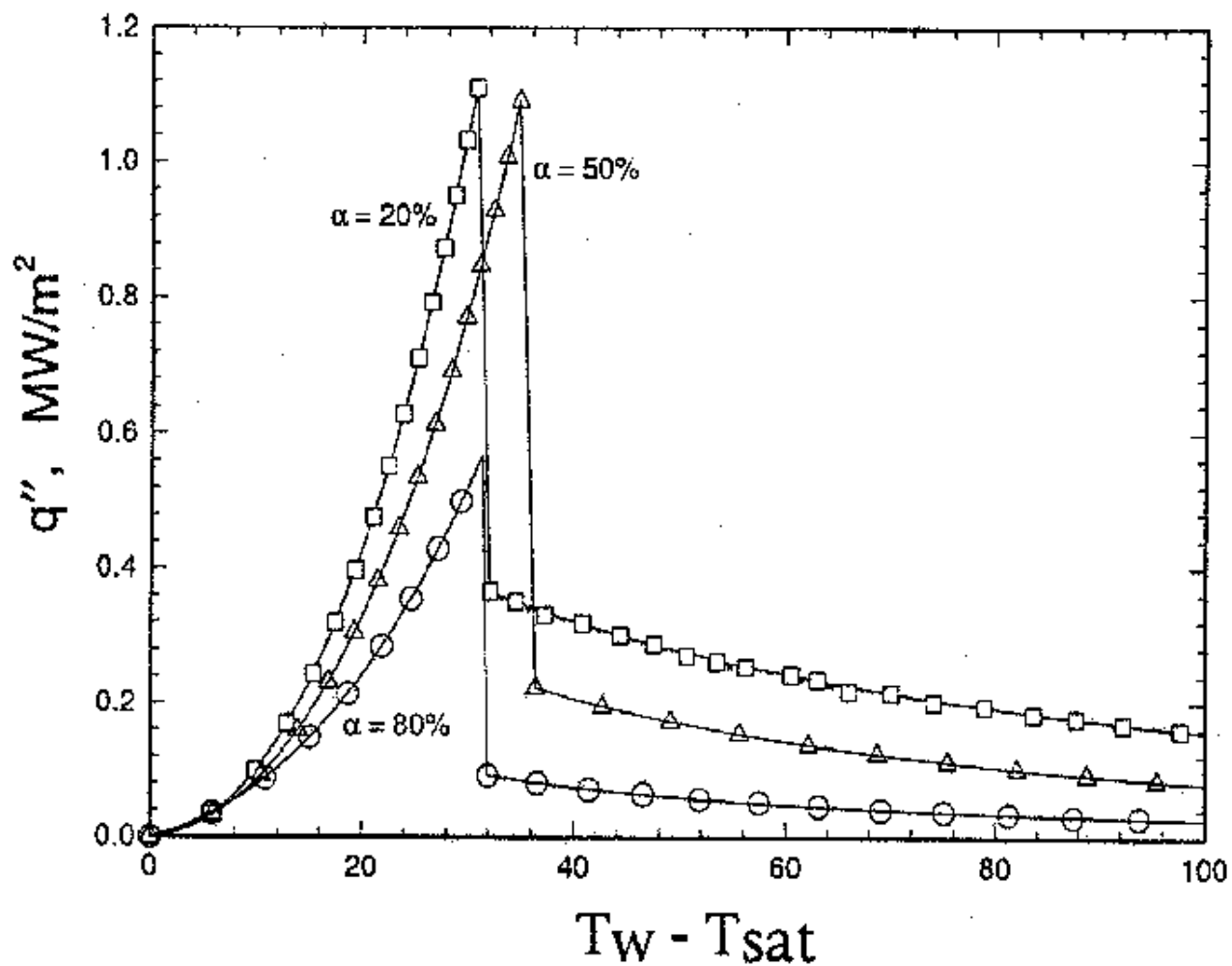


Figure 16: Heat Flux versus Wall Temperature predicted by RELAP5/MOD3 for $G = 20\text{kg/sm}^2$, $p = 0.10\text{MPa}$ and saturated conditions

Table 5: Comparison of RELAP5 and the Original Chen Model for Transition Boiling Heat Transfer

Original Chen T.B. Model	RELAP5/MOD3 Model
$q'' = f_l q_l'' + (1 - f_l) q_g''$	$q'' = f_l M_{stf} q_l'' + (1 - f_l M_{stf}) q_g'' M_\alpha$
$q_l'' = q_l''(p, \Delta T_s) \gg q_{CHF}''$	$q_l'' = q_{CHF}''$
$q_g'' = h_g(T_w - T_g)$	$q_g'' = h_g(T_w - T_g)$
h_g from momentum transfer analogy	h_g from Dittus Boelter correlation
$f_l = \exp \left[-\sqrt{1.8} a(\alpha) f(G) \sqrt{\Delta T_s} \right]$	$f_l = \exp \left[-\sqrt{1.8} a(\alpha) f(G) \min\{15, \sqrt{\Delta T_s}\} \right]$
$a(\alpha) = 0.005/(1 - \alpha^{40}) + 0.0075\alpha$	$a(\alpha) = 0.05/(1 - \alpha^{40}) + 0.075\alpha$
$f(G) = \max(f_1, f_2)$	$f(G) = \max(f_1, f_2)$
$f_1 = 24 - G/135.6$	$f_1 = 2.4 - G/135.6$
$f_2 = 0.2G/135.6$	$f_2 = 0.2G/135.6$
Limits: $x \leq 1$, $f_l q_l'' \leq q_{CHF}''$	No limits applied

applicable for degraded core reflood and to implement it in the R5M3 code instead of the RELAP-transition boiling model. Unlike other models which are based on history parameters such as T_{MFB} or T_{CHF} (which are not readily available at each time step by the R5M3 method of calculation), the suggested model has the additional advantage of utilizing only local channel conditions for predicting the wall heat flux. The new model is fully described in the next section 8. Since several versions of the Chen model have been used by different investigators and since the original report by Chen et al. [11] contains a number of typographical mistakes, the next section 8 is presented in a self-contained manner repeating some of the formulations presented in [11].

8 The Suggested Transition Boiling Model

The mechanistic approach suggested by Chen et al. [11] for predicting q_l'' and f_l in eq. (8) is generally adopted with several modifications to facilitate its implementation in large system codes such as R5M3. The boiling component, q_l'' , is calculated as the average heat flux during the short period of contact between the liquid and the superheated wall. Following the Chen model, a three-step process is postulated to describe the mechanism of heat removal by a film of liquid at the wall: conduction heating of the liquid film, nucleation and bubble growth within the liquid layer and, finally evaporation of a residual liquid film at the wall (see Fig. 17).

8.1 Total Boiling Heat Flux

The total heat flux is then a sum of three terms:

$$q_l'' = \frac{\phi_1 + \phi_{12} + \phi_2}{t_1 + t_{12} + t_2} \psi(p_r, \Delta T_s) \quad (37)$$

where the subscripts 1, 2 and 12 denote the three steps involved, and ϕ_i and t_i are the absorbed heat per unit area and the time associated with each step, respectively. $\psi(p_r, \Delta T_s)$ is an empirical correction function of the reduced pressure, $p_r = p/p_{crit}$, and the wall superheat, ΔT_s . This function is introduced to improve the model predictions at low pressures and low superheat with respect to the original Chen formulation [11].

The first heat transfer mechanism in eq. (37) corresponds to the superheating of a thermal boundary layer in the liquid in contact with the heated wall. In this period heat is transferred from the wall via pure conduction until a layer of liquid equal to the nucleation bubble radius is superheated to the nucleation superheat temperature. This process can be described by solving the transient conduction equation for semi-infinite bodies to determine the heat flux at the heating surface. The solution suggested in [46], [25] and [11] is:

$$\begin{aligned} \phi_1 &= \frac{\Re \sigma \rho_l C_{pl} T_s^2}{0.213 p_l H_{fg}} \\ t_1^{1/2} &= \frac{\Re \sigma T_s^2}{0.24 p_l H_{fg} \sqrt{\alpha_l}} \cdot \frac{\wp_T + 1}{\wp_T} \cdot \frac{1}{\Delta T_s} \end{aligned} \quad (38)$$

where \Re is the ideal gas constant, σ is surface tension, C_p is heat capacity, p is pressure, H_{fg} is the specific latent heat of evaporation and α_l is the thermal diffusivity. The coefficient \wp_T is defined by:

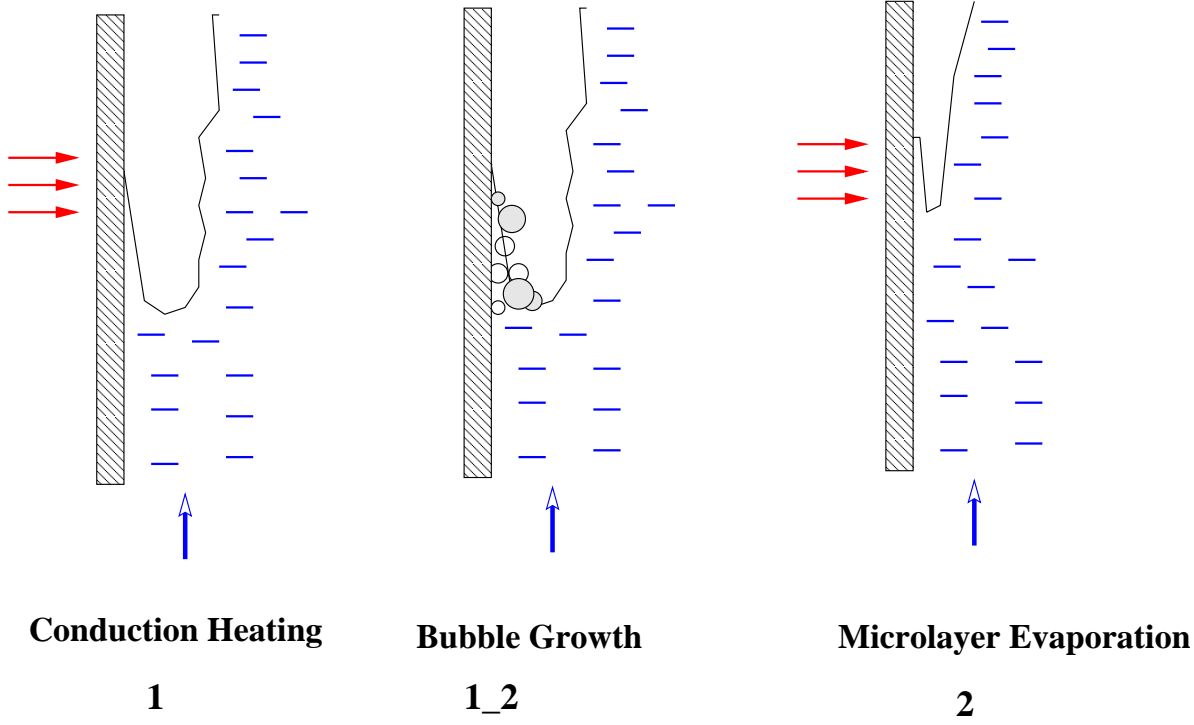


Figure 17: Schematic description of the Suggested Transition Boiling Model

$$\phi_T = \sqrt{\frac{(k \rho C_p)_w}{(k \rho C_p)_l}} \quad (39)$$

The second heat transfer process in eq. (37) refers to the bubble growth period. Following Chen et al. [11] it is assumed that the heat absorbed by the bubbles comes entirely from the superheated liquid layer at the wall, thus:

$$\phi_{12} = 0 \quad (40)$$

The time required for a bubble to grow to its final size can be readily determined by solving the bubble growth equation. However, to avoid the necessary numerical solution of the resulting implicit equation relating the bubble size and time, the period of bubble growth to a maximum size of $15 \mu m$ is correlated as:

$$t_{12} = A \Delta T_s^B \quad (41)$$

where the coefficients A and B are given as functions of the reduced pressure, p_r :

$$\ln(A) = \begin{cases} -12.031 + 72.62p_r - 167.29p_r^2 & p_r \leq 0.136 \\ -8.1724 + 25.14p_r - 26.29p_r^2 & p_r > 0.136 \end{cases} \quad (42)$$

and

$$B = \begin{cases} -0.4379 - 15.52p_r + 49.32p_r^2 & p_r \leq 0.136 \\ -1.3052 - 3.137p_r + 3.827p_r^2 & p_r > 0.136 \end{cases} \quad (43)$$

Subsequent to the bubble growth and escape process a thin superheated liquid micro-layer is formed on the wall, [46]. Heat absorbed from the wall by that layer is given in [11]:

$$\phi_2 = \frac{8 \sigma T_s \rho_l}{\rho_g \Delta T_s} \left(1 - \frac{C_{pl} \Delta T_s}{H_{fg} 2} \right) \quad (44)$$

The time, t_2 , required for this evaporation process may be determined by estimating the thermal conduction from the wall to the evaporating film. Assuming a linear temperature gradient in the liquid film from a value T_w at the wall to T_s at the evaporating interface, we obtain:

$$t_2 = \frac{32 \rho_l \sigma^2 T_s^2}{k_l \rho_g^2 H_{fg} \Delta T_s^3} \left(1 - \frac{C_{pl} \Delta T_s}{H_{fg} 2} \right) \quad (45)$$

The last term in eq. (44) and in eq. (45) accounts for the initial superheat of the liquid layer. At low pressures the film evaporation heat, ϕ_2 , is dominant. The conduction heating process, ϕ_1 is more important at high pressures and larger degrees of superheat.

A correction function, $\psi(p_r, \Delta T_s)$, was introduced in eq. (37) to better fit the data at low pressures and low superheat. An examination of a large amount of experimental results yielded a correlation for ψ in the form:

$$\psi(p_r, \Delta T_s) = 1 + 3 \exp(-0.42p_r^{3/2} \Delta T_s^2) \quad (46)$$

Note that $\psi(p_r, \Delta T_s)$ approaches unity as the wall superheat or the pressure increase.

8.2 Liquid Contact Area Fraction

The model suggested by Chen et al. [11] for estimating the liquid contact area fraction, f_l , is adopted here with some modifications to improve its prediction capabilities at low pressures and low qualities. The present model predicts f_l as an exponential function of the form:

$$f_l = \exp[-a(\alpha)g(G)(1.8\Delta T_s)^n] \quad (47)$$

where $a(\alpha)$ and $g(G)$ are functions of the void fraction, α , and the mass flux, G , given by:

$$a(\alpha) = \frac{0.005}{1 - \alpha^{40}} + 0.0075\alpha \quad (48)$$

and

$$g(G) = \max(g_1, g_2) \quad (49)$$

where

$$\begin{aligned} g_1 &= 20 - 0.6 \frac{G}{135.6} \\ g_2 &= 0.2 \frac{G}{135.6} \end{aligned} \quad (50)$$

The power coefficient, n , in eq. (47) is taken as 0.5 in Chen et al. [11]. Comparison with data at low qualities suggests a quality and pressure dependent function of the form:

$$n = 0.6 + 0.12 \exp(-p/10^5) - 0.24x \quad (51)$$

where x is the local quality and p is the pressure. Equation (51) was found to fit well the available steady-state data on transition boiling. Table 6 compares the present model with the original transition boiling formulation by Chen et al. [11].

Equation (51) concludes the present modified transition boiling model, which can be summarized as follows: knowing the local quality, pressure, void fraction and vapor temperature one can calculate q_l'' , q_g'' , ψ and f_l which, in turn, can be substituted in eq. (8) to yield the total heat flux q_{tot}'' . Recognizing the various approximations involved in the models for q_l'' and f_l , a limit must be applied as follows:

$$f_l q_l'' \leq q_{CHF}'' \quad (52)$$

where q_{CHF}'' is the critical heat flux which can be determined from suitable correlations or from a lookup table as done in the R5M3 code.

8.3 Implementation of the new Transition Boiling Model

The transition boiling model developed in section 8 was implemented in the frozen RELAP5/MOD3.1 code version, getting the new code version RELAP5-MOD3.1-FZK (R5M3-FZK). The implementation affects only the formulation of the subroutine *pstdnb* of the R5M3 code where the post DNB-heat flux and the HTC are calculated. The new model utilizes only local state variables calculated by the R5M3 code like static quality, actual void fraction, mass flux, liquid and vapor temperature, phasic velocities, etc. and does not require other history parameters, such as quench position, critical heat flux, and minimum film boiling temperature, which are not available at each time step.

Table 6: Comparison of the Original and Modified Chen Model for Transition Boiling Heat Transfer

Original Model	Modified Model
$q'' = f_l q_l'' + (1 - f_l) q_g''$	$q'' = f_l M_{stf} q_l'' + (1 - f_l M_{stf}) q_g'' M_\alpha$
$q_l'' = q_l''(p, \Delta T_s)$	$q_l'' = q_l''(p, \Delta T_s)$
$q_g'' = h_g(T_w - T_g)$	$q_g'' = h_g(T_w - T_g)$
$f_l = \exp[-(1.8)^n a(\alpha) g(G) \Delta T_s^n]$ $n = 0.5$	$f_l = \exp[-a(\alpha) g(G) (1.8 \Delta T_s)^n] \psi(p_r, \Delta T_s)$ $n = 0.6 + 0.12 \exp(-221.2 p_r) - 0.24 x$
$a(\alpha) = 0.005 / (1 - \alpha^{40}) + 0.0075 \alpha$	$a(\alpha) = 0.005 / (1 - \alpha^{40}) + 0.0075 \alpha$
$g(G) = \max(g_1, g_2)$	$g(G) = \max(g_1, g_2)$
$g_1 = 24 - G / 135.6$	$g_1 = 20 - 0.6 G / 135.6$
$g_2 = 0.2 G / 135.6$	$g_2 = 0.2 G / 135.6$
Limits: $x \leq 1$, $f_l q_l'' \leq q_{CHF}''$	Limits: $x \leq 1$, $f_l q_l'' \leq q_{CHF}''$

Summarizing, it can be pointed out that the suggested transition boiling model goes back to the original Chen's formulation and extends them for better prediction of reflood situations characterized by low pressure and low quality.

9 Validation of the New Transition Boiling Model

9.1 Stand-Alone Validation

A stand-alone version of the new transition boiling model was formulated for model validation. In this model the same procedure described in section 8 is used to predict the total post critical heat flux for given local conditions. Furthermore, non-equilibrium

effects are also included in the model according to Chen [11] as follows:

$$\frac{x}{x_e} = \frac{H_{fg}(p, T_s)}{H_g(p, T_g) - H_l(p, T_s)} = 1 - B(p_r) \frac{T_g - T_s}{T_w - T_g} \quad (53)$$

where $B(p_r)$ is an empirical function of the reduced pressure, given in [11] as:

$$B(p_r) = \frac{0.26}{1.15 - p_r^{0.65}} \quad (54)$$

Equation (53) is solved iteratively at each point along the test section to yield the quality, x , and the vapor temperature, T_g .

Figure 18 shows the predicted vs measured total heat flux. Considering the wide range of parameters covered by the data (362 data points in the range of up to 7 MPa pressure and mass flux up to 5000 kg/m²·s), the new model is shown to predict the data reasonably well with a standard deviation of about 40%. Additionally, the results in figure 18, where the predicted heat flux for Bennett fits very good the measured data, demonstrates that the coefficients 0.005 and 0.0075 used in the original Chen correlation and not those used in RELAP (0.05 and 0.075) are the right ones.

Figure 19 depicts the new model prediction of run 5251 of Bennett et al. [9]. The boiling component of the heat flux is larger than that shown in Fig. 15 and the agreement with the measured data is significantly improved. The new transition boiling model was implemented in the R5M3 code to predict some of the available reflood data, as described in the next section.

9.2 Validation within RELAP5/MOD3.1-FZK

The FZK single-rod and the NEPTUN bundle tests listed in the Table 3 of section 3.3 were used for extensive model validation. These tests were calculated with both the new and the frozen code version in order to show the improved prediction capability of R5M3-FZK. The most representative results of such calculations are presented and discussed in the following subsections 9.2.1, 9.2.2 and 9.2.3.

9.2.1 Discussion of Results: FZK Single-Rod Tests: Specimen filled with ZrO_2

A.1. Quench Temperature: 1873 K

The tests $T16106$, $T31085$, and $T24066$ were carried out under the same conditions. The Figures 20, 21, and 22 give the specimen temperature at different radial and axial positions, predicted with both the frozen and the modified R5M3 versions, in comparison

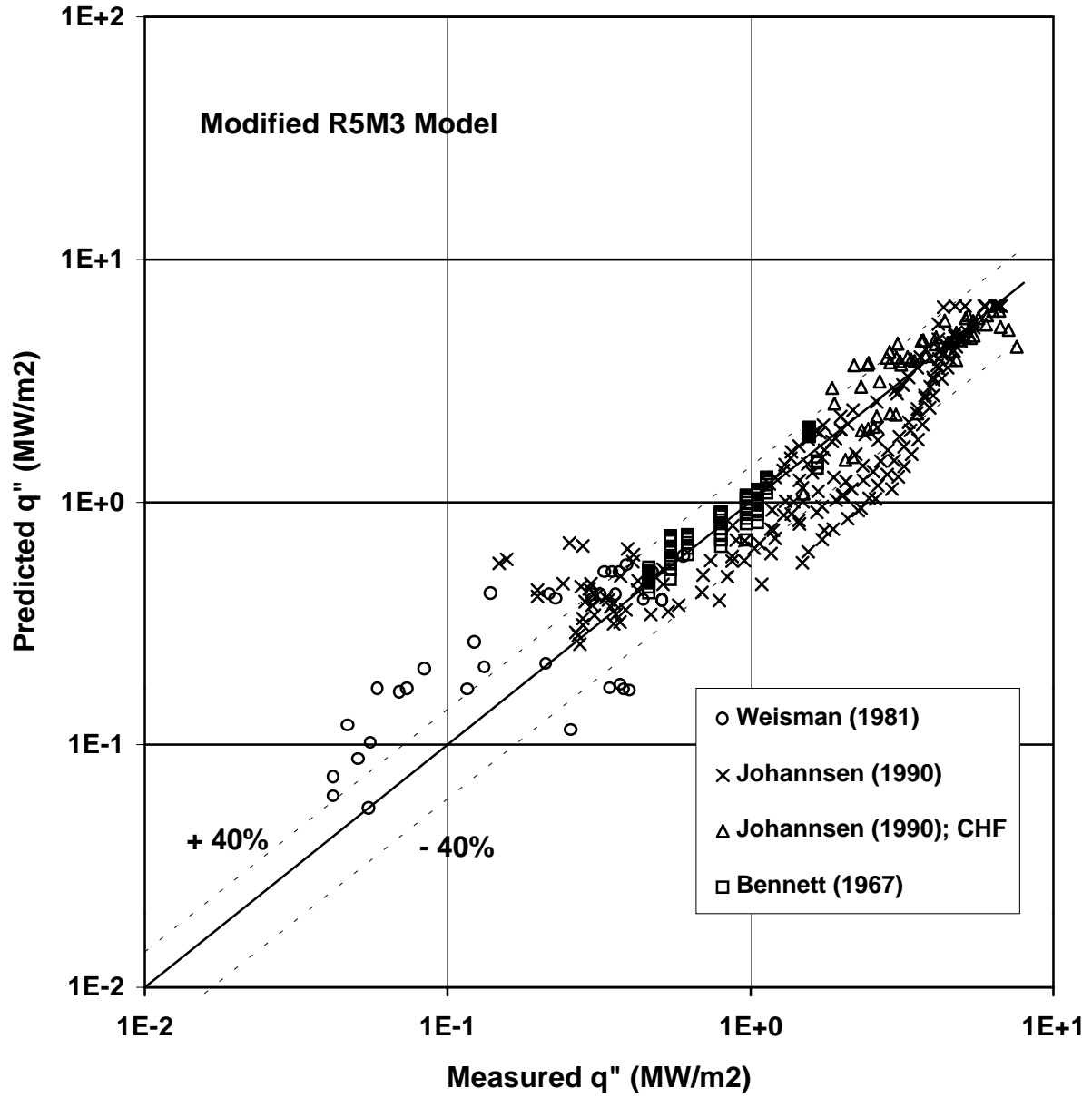


Figure 18: Comparison with Data of a Stand-Alone Formulation of the New Transition Boiling Model

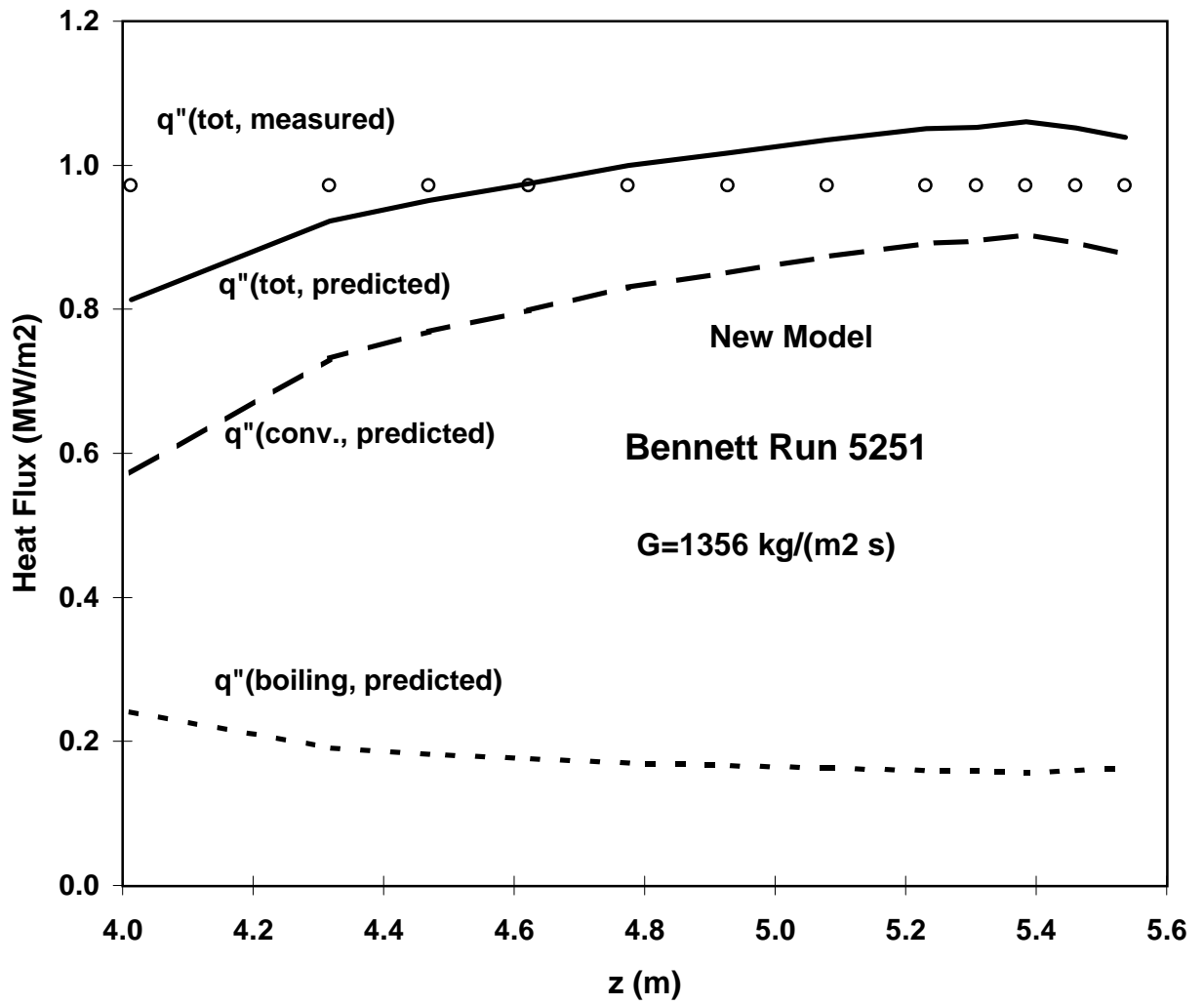


Figure 19: Stand-Alone New Model Prediction of Run in Bennett et al. (1967)

with the measured data. The centerline temperature (picture *a* of Fig. 20) predicted by the modified model is in very good agreement with the measured one. The measured gap temperature (Picture *b* of Fig. 20) coincides with the predicted pellet surface temperature throughout the transient.

The measured clad outside temperature at the middle of the specimen agrees well with the predicted temperature of both code versions for the tests $T31085$, $T24066$, and $T16106$. From the Figures 21 and 22 it can be seen that the measured temperature oscillates very much especially during the transition boiling regime near to the quench front position, where an oscillatory two-phase flow prevails. This and the stochastic nature of the reflood flow makes difficult not only an accurate temperature measurement but also the repeatability of the temperature measurement. The quench time ($770s$) is well predicted by the modified code in the case of the tests $T16106$ and $T24066$. The measured quench time for the test $T31085$ is few seconds later (776). The quench temperature is in good agreement with the measured value (*about* $800K$) for the three tests.

In order to gain a better physical understanding of the complex heat and mass transfer phenomena taking place during quenching, Figs. 23 to 25 present calculated results for various parameters which cannot be readily measured.

Heat transfer data at the mid-section of the specimen are shown in Fig. 23. The rewetting process is shown to coincide with changing heat transfer mode from subcooled film boiling (mode 47) to subcooled transition boiling (mode 45). This change is now earlier than by the frozen version, since the transition boiling heat flux is no more underpredicted. The change from subcooled transition boiling (mode 45) to subcooled nucleate boiling (mode 43) is also initiated earlier when the wall superheat decreases below about 50 K , as expected. The changes in heat transfer mode are accompanied by large variations in the heat flux (see Figure 23a).

The heat flux and the heat transfer coefficient predicted by the modified code version is much higher than the one predicted by the frozen version as a consequence of the model improvements. It nearly reaches the predicted critical heat flux (see Figure 23a), which is in agreement with the known shape of a boiling curve. The deviation of the maximum heat flux from CHF is a result of the fine-mesh scheme used in R5M3 to describe the reflood process. The CHF value is reached in one of the fine-mesh points while values of the average heat flux is plotted in Fig. 23. In Fig. 24 the heat flux as a function of the wall superheat is represented. The maximum heat flux point occurs at $\Delta T_s \approx 40\text{ K}$. The minimum film boiling superheat predicted by the modified model is about 500 K compared to about 200 K in the frozen R5M3 code. This is a result of the modified transition boiling model.

Figure 25 shows the void fraction and vapor velocity at the mid-section of the specimen and the collapsed liquid level in the channel. The rewetting process is shown to be

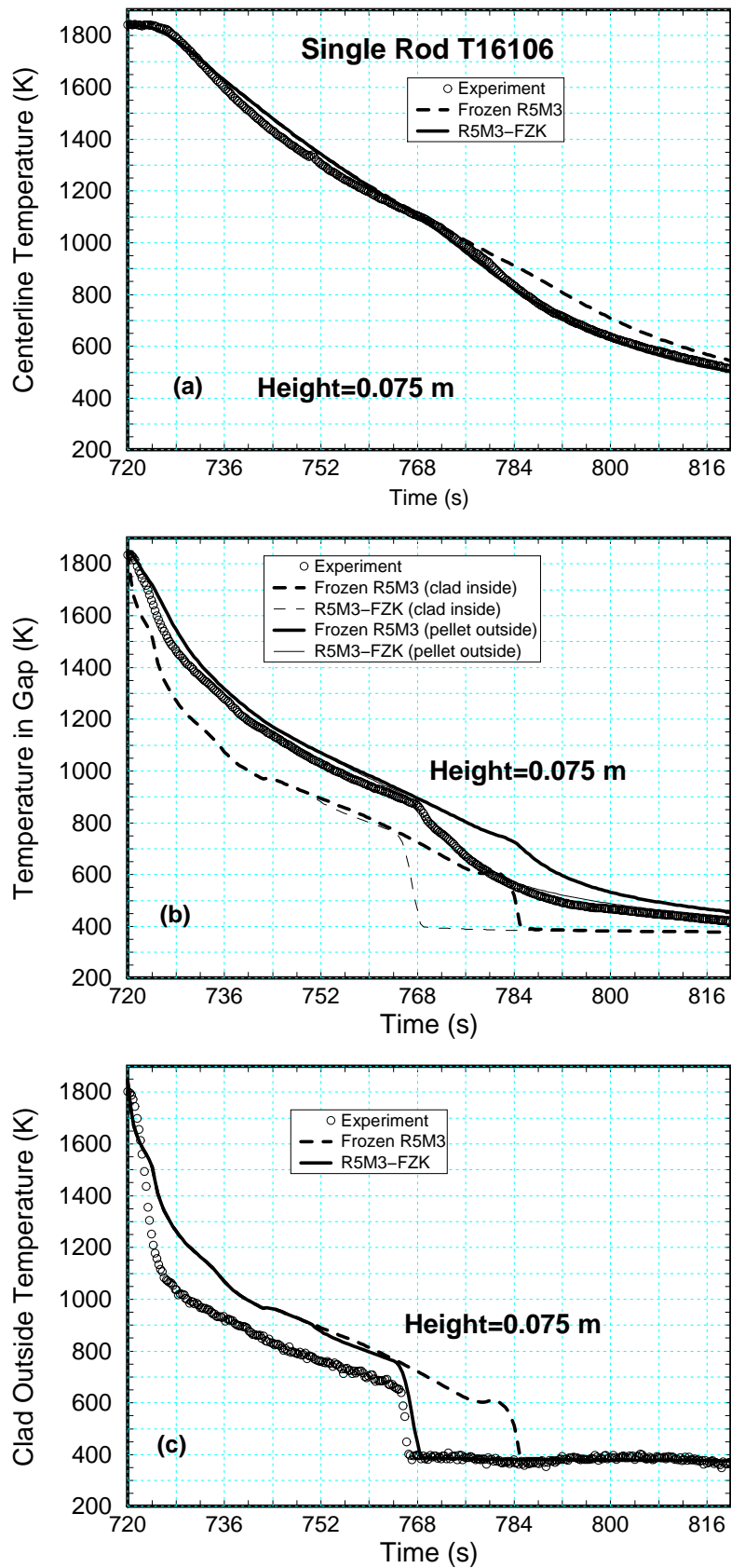


Figure 20: Measured and Predicted Temperatures in the FZK Single-Rod Test No. T16106

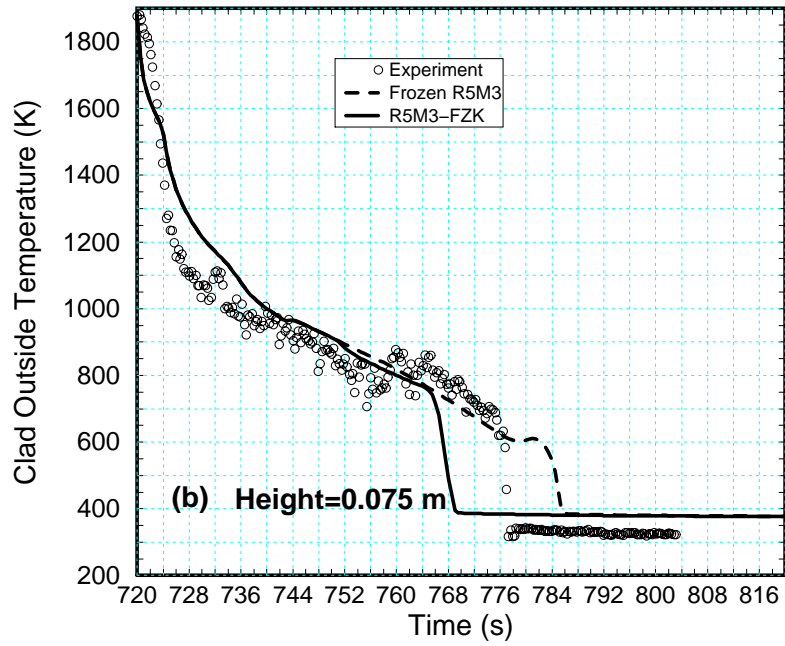
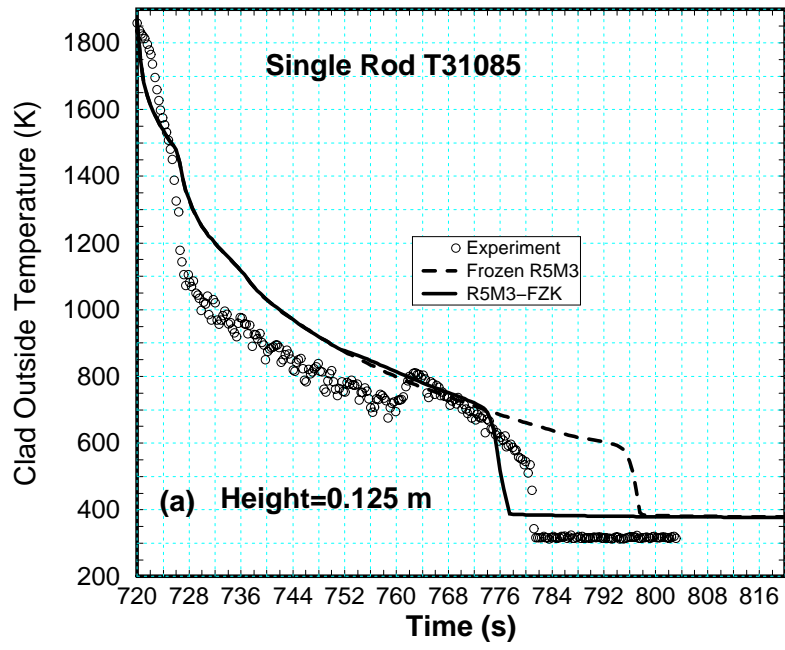


Figure 21: Measured and Predicted Clad Temperatures in the FZK Single-Rod Test No. T31085

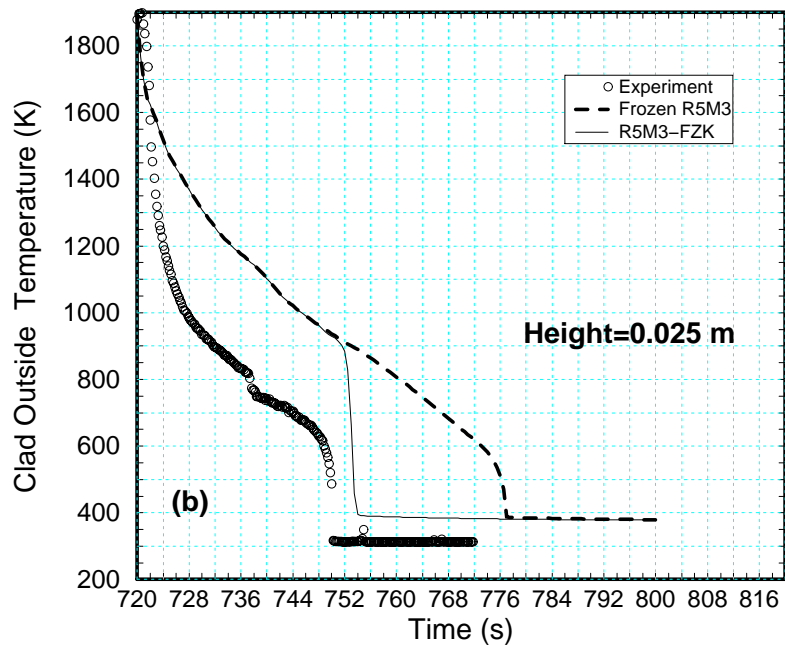
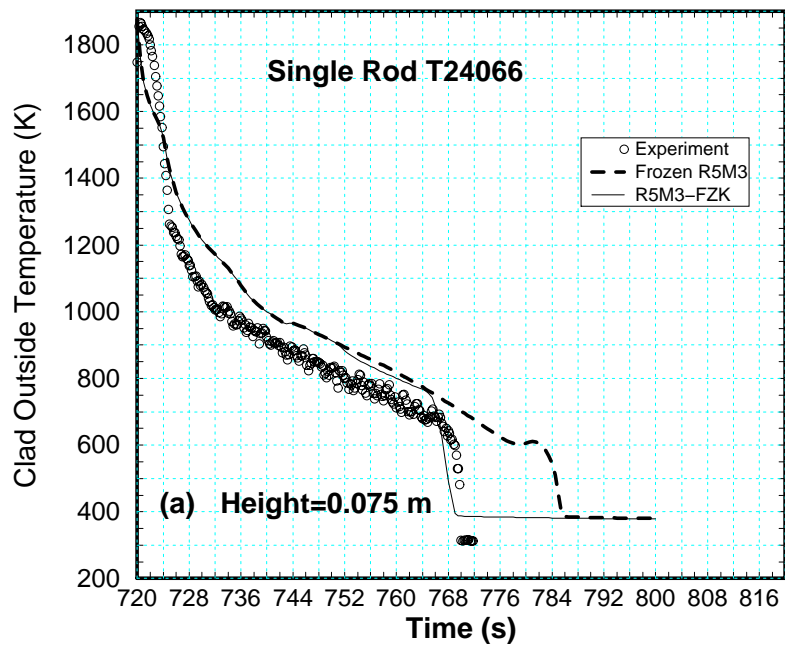


Figure 22: Measured and Predicted Clad Temperatures in the FZK Single-Rod Test No. T24066

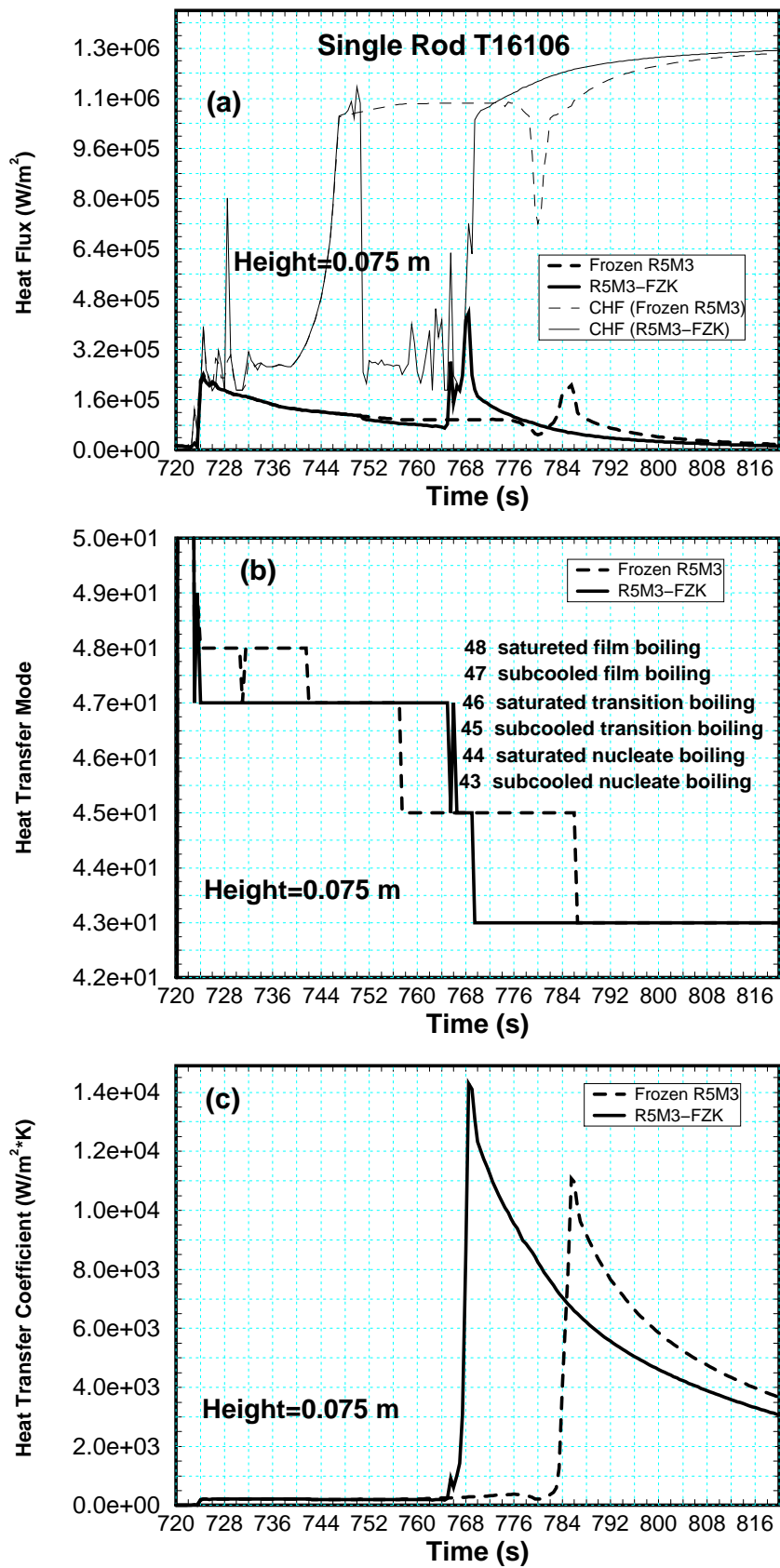


Figure 23: Predicted Heat Flux Parameters at the Mid-Section FZK Single-Rod Test No. T16106

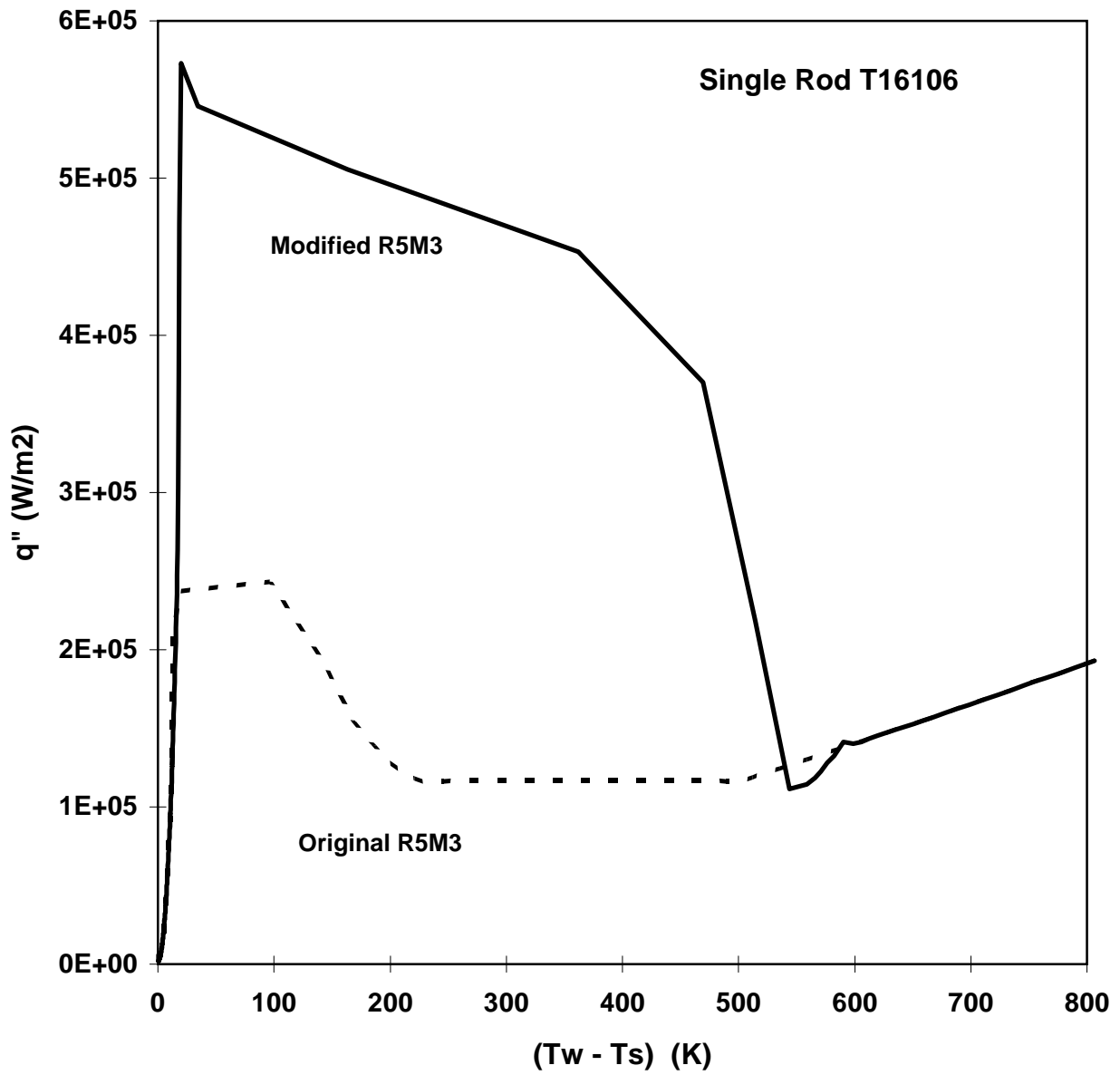


Figure 24: Comparison of Current and Modified R5M3 Predicted Boiling Curves in the FZK Single-Rod Test No. T16106

accompanied by a sharp drop in void fraction and vapor velocity. Since the transition boiling heat flux in the original model is lower, these trends are not as obvious in the results of the frozen R5M3 code. The collapsed liquid level reflects the variations of the average liquid void fraction in the channel. Both void fraction and vapor velocity show an oscillatory behavior near the quench front due to oscillations of the heat flux and therefore of the evaporation rates.

A.2. Quench Temperature: 1673 K

Figure 26 shows the predicted and measured temperatures for run No. T02106 of the FZK single-rod program. This test is similar to the test No. T16106 except for its lower initial temperature which results in a higher quench velocity. In the test T16106 the mid-section quenches in about 50 s while in T02106 quenching occurs after 35 s. The improvements in the results obtained with the modified R5M3 code over the current version of the code are obvious. As expected, the measured gap temperature lies between the predicted inner clad surface temperature and the outer pellet temperature. The test T21066 is similar to the tests T31085 and T24066, where the temperature was measured on the clad outside along the specimen. The predicted clad outside temperatures at the middle and at the upper thermocouple positions agrees much better with the measured values than at the lower part. At the lower part the discrepancy is larger. On the other hand, the quench time predicted with the modified code version is comparable with the measured values.

A.3. Quench Temperature: 1473 K

In this case, the clad outside temperature and the quench time at the middle and at the upper part of the specimen, calculated with the modified code version, is much closer to the experimental results than in most of the other tests (see Figure 28). Merely at the lower part the discrepancy between measured and predicted temperature is larger, but the quench time is close to the measured one. Quenching of the mid-section ($h = 0.075$ m) occurs in this case at $t \approx 755$ s (35 s after reflood initiation). The quench front velocity is decreasing as the initial wall temperature increases.

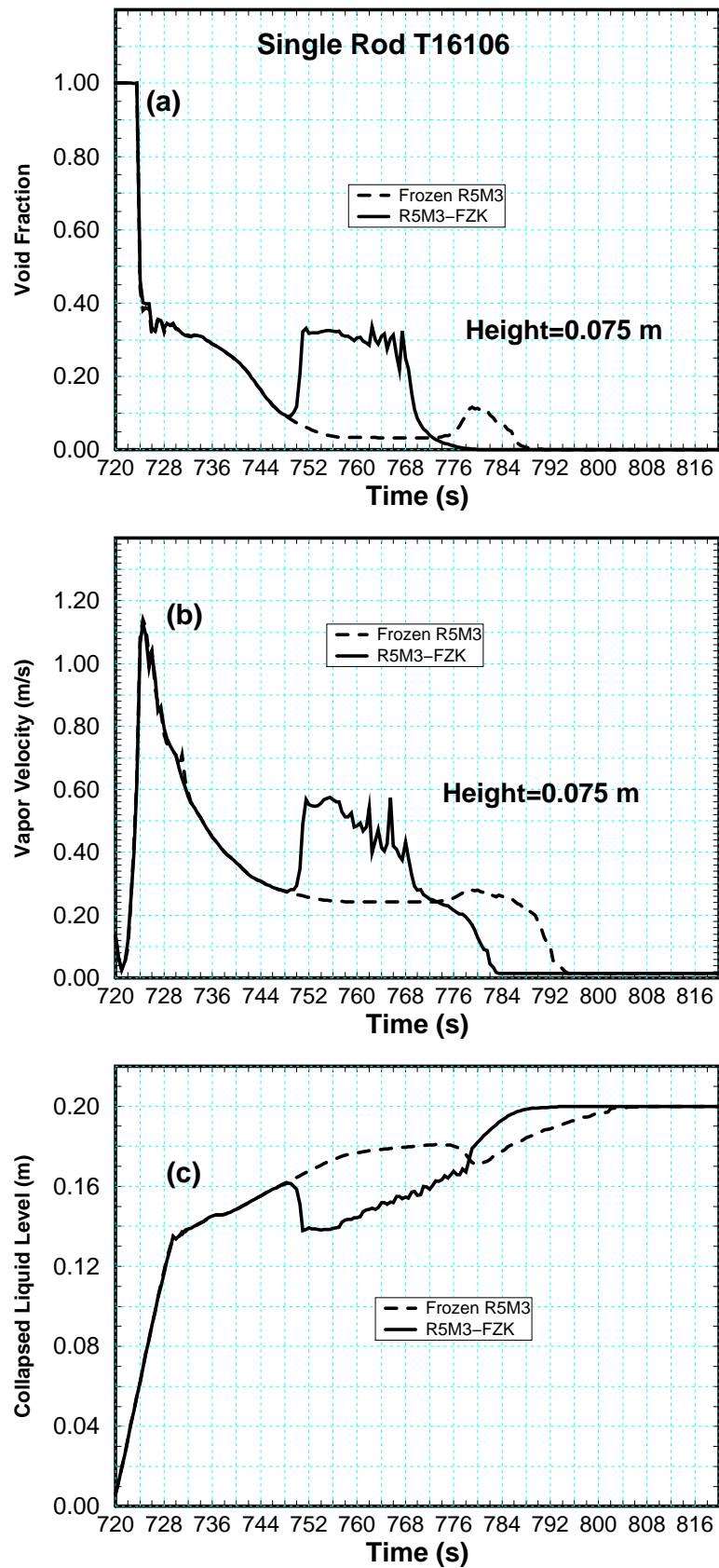


Figure 25: Predicted Flow Parameters in the FZK Single-Rod Test No. T16106

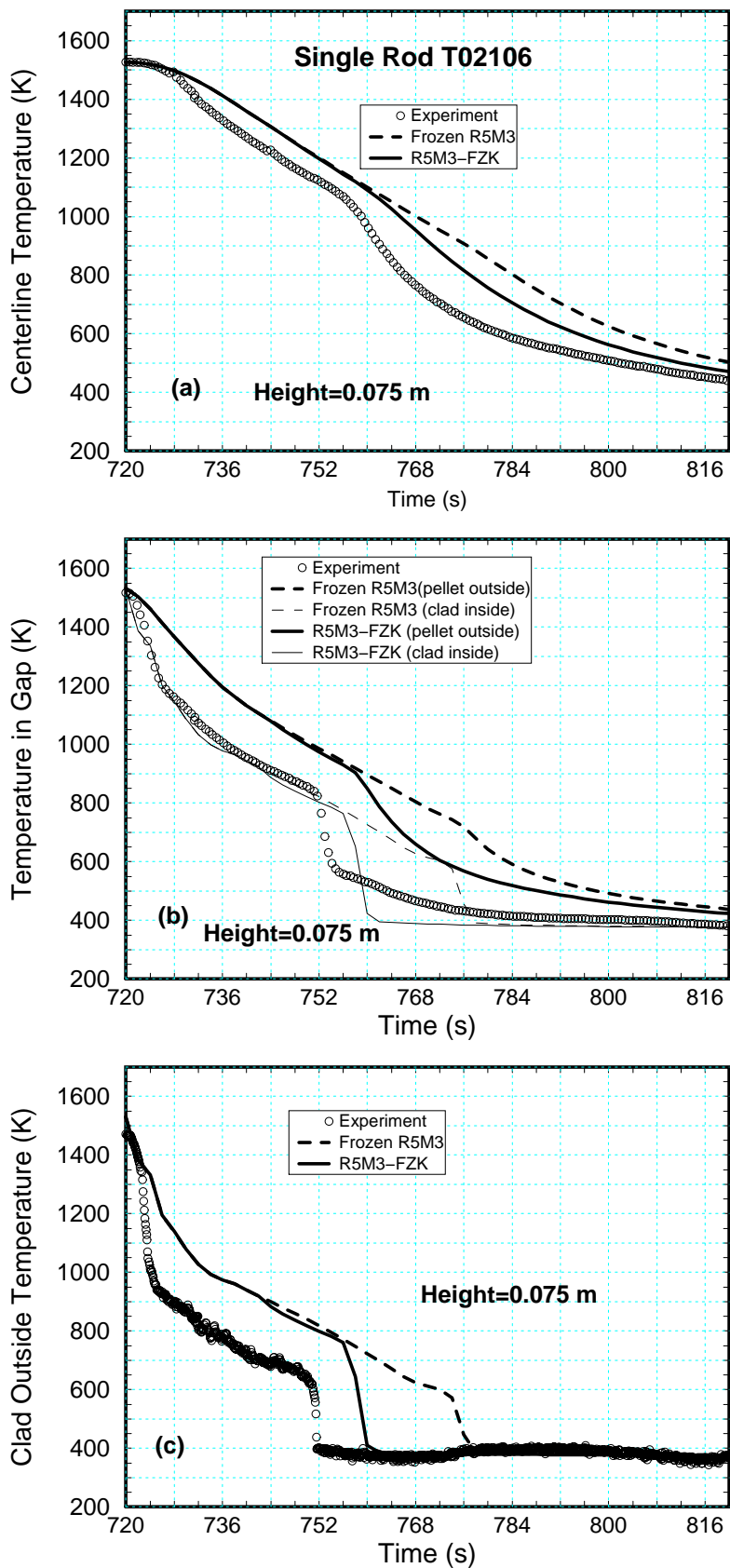


Figure 26: Measured and Predicted Clad and Pellet Temperatures in the FZK Single-Rod Test No. T02106

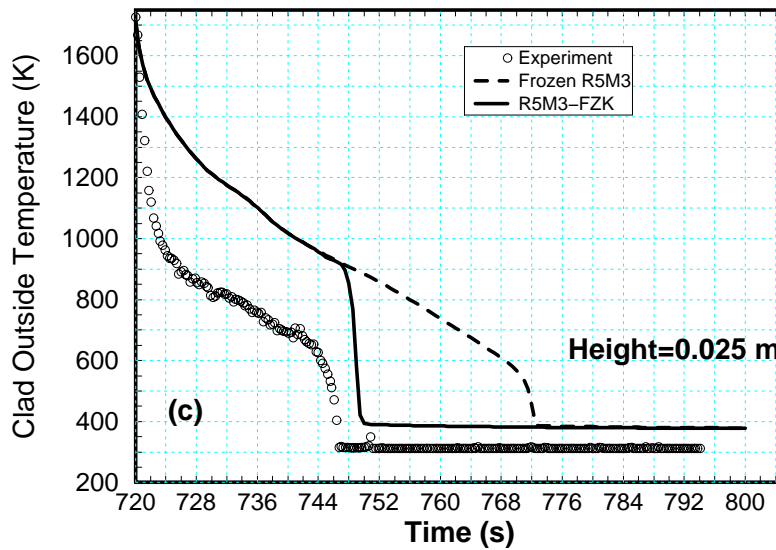
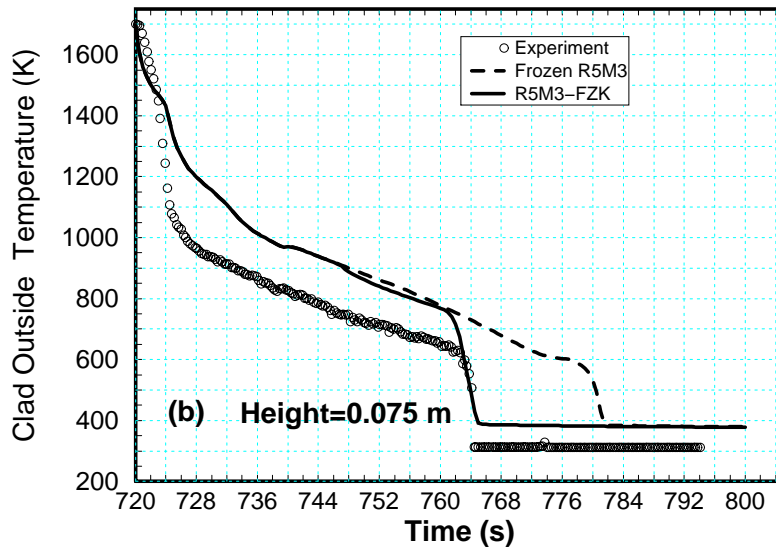
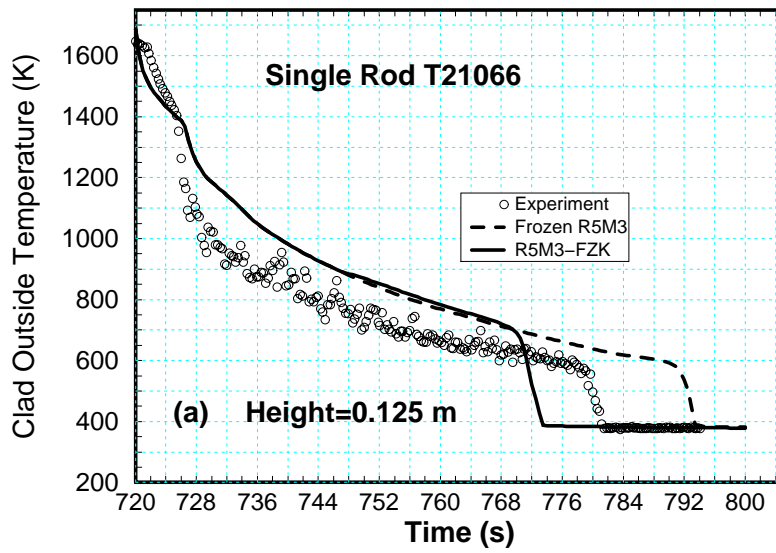


Figure 27: Measured and Predicted Clad Temperatures in the FZK Single-Rod Test No. T21066

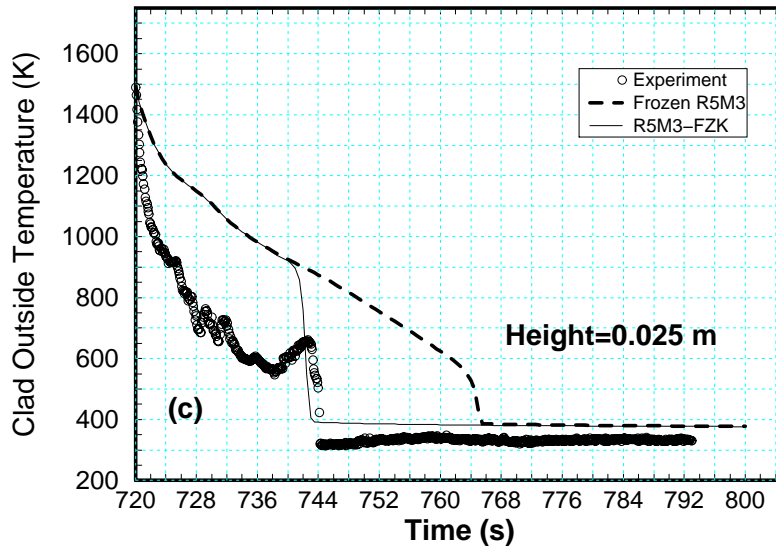
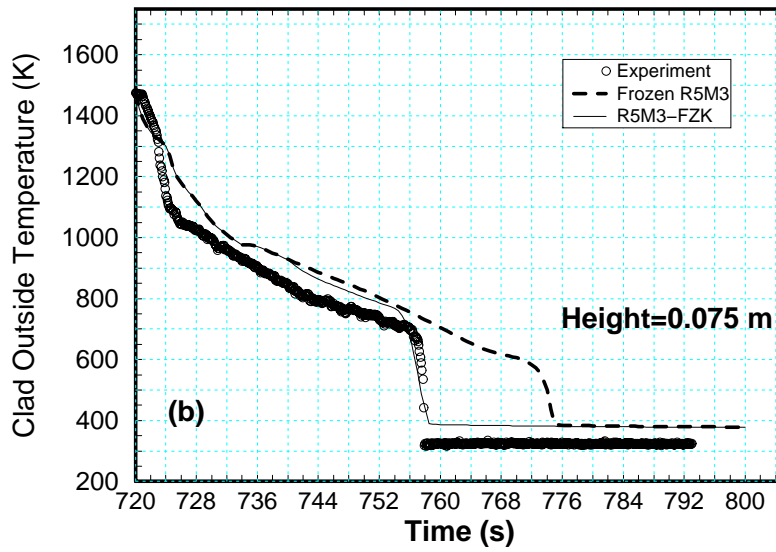
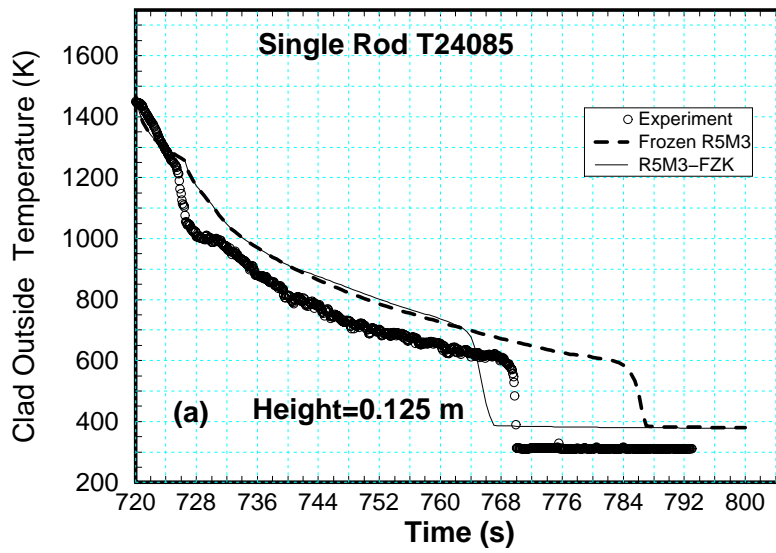


Figure 28: Measured and Predicted Clad Temperatures in the FZK Single-Rod Test No. T24085

9.2.2 Discussion of Results: FZK Single-Rod Tests: Empty Specimen

The calculational results obtained with the frozen and modified R5M3 code for the FZK empty tube tests listed in Table 3 are given in Figs. 29 to 31. These tests differ among each other mainly in their initial temperatures. The predicted inside and outside temperatures at the middle of the specimen are almost identical and. It lies between the measured inside and outside temperature as shown in Figs. 29 to 31. The cladding temperature predicted by the modified model is generally closer to the measured values. The measured clad inside temperature of test 29 exceeds the outside temperature by as much as 400 K. This trend, which persists for a few seconds, is believed to be due to a measurement error. The inner thermocouple is typically mounted on a rhenium foil which is welded to the inner surface. It is believed that the inner thermocouple in this case was disjointed during the test, thus remained at higher temperature for a longer period. In contrast the measured difference between the inner and outer temperatures are small in the two other tests considered in this study (*ITE22115 and ITE29115*). The measured clad outside (tests 29) and clad inside (tests 30 and 31) temperature curves show a clear quench temperature of about 600 – 700K. The measured quench velocity is higher compared to the values obtained by the tests with filled tubes. For the range of initial wall temperatures studied in this program (1300 to 1800 K), the measured quench times for the mid-section of the empty tubes vary between 10 to 18 s while it lies between 52 and 70 s for the filled tubes. Because of the fast transient nature of these tests, temperature measurements are typically scarce and less accurate. The oscillatory behavior of the clad outside temperature can be observed in the Figs. 29 to 31. In addition, the characteristic shape of a temperature curve with a definite ‘knee’ point is not always observed.

In general, the quench times and quench temperatures predicted with the modified code version are closer to the measured data than those obtained by the frozen version. As for the filled tube tests the measured outside surface temperatures are consistently lower than the predicted surface temperatures. As mentioned before, this is mainly caused by the inability to accurately measure the outer surface temperature. The external thermocouples experience an enhanced cooling due to their exposure to the steam flow in the channel. The effect of the thermocouple cooling is, however, smaller at higher elevations where the steam temperature approaches the wall temperature.

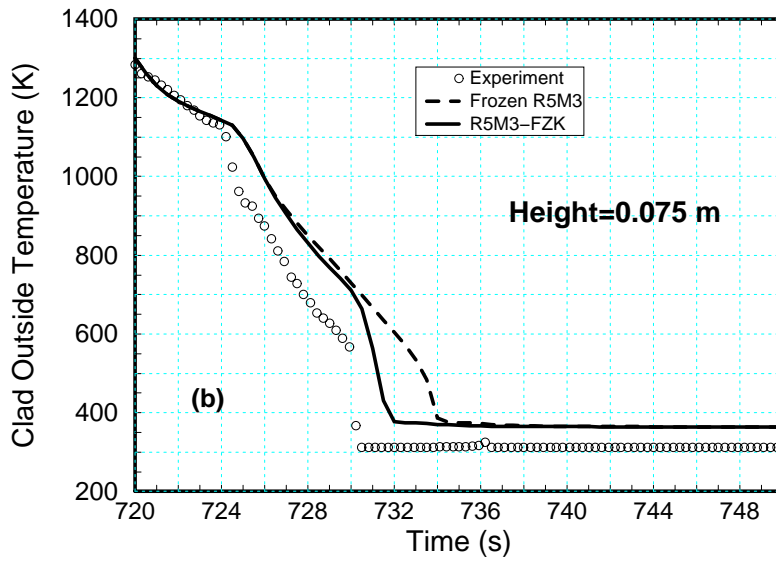
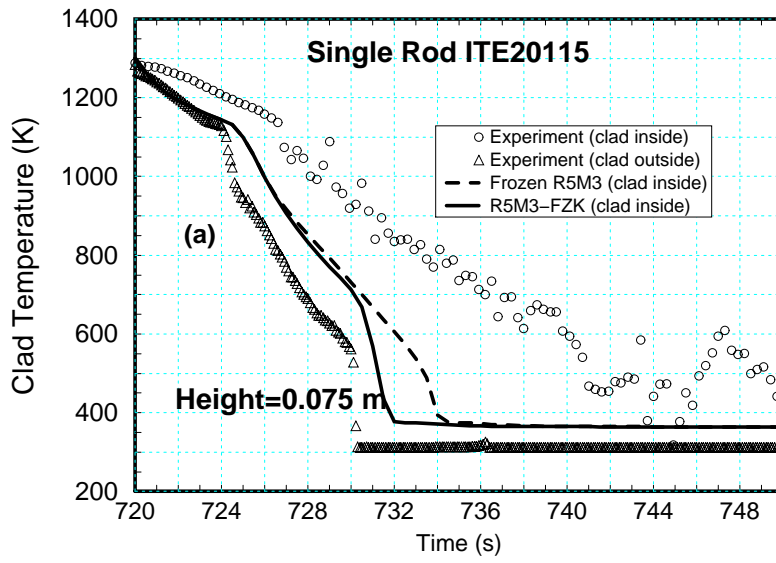


Figure 29: Measured and Predicted Clad Temperatures in the FZK Single-Rod Test No. ITE20115

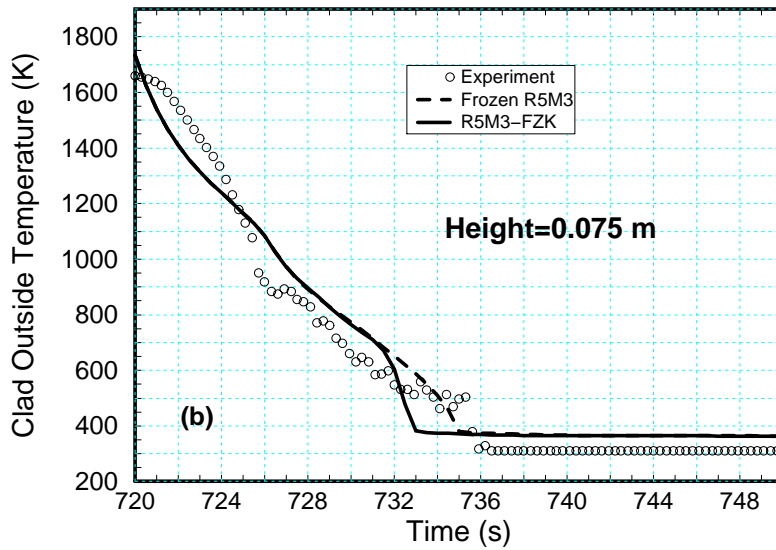
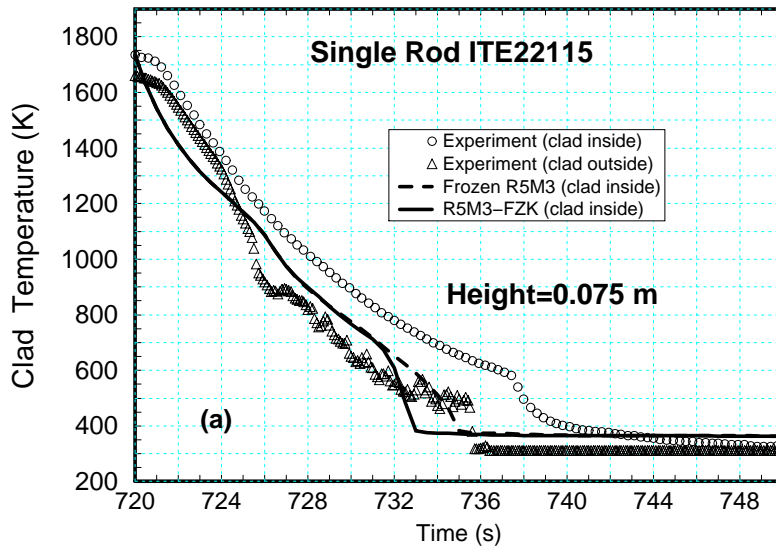


Figure 30: Measured and Predicted Clad Temperatures in the FZK Single-Rod Test No. ITE22115

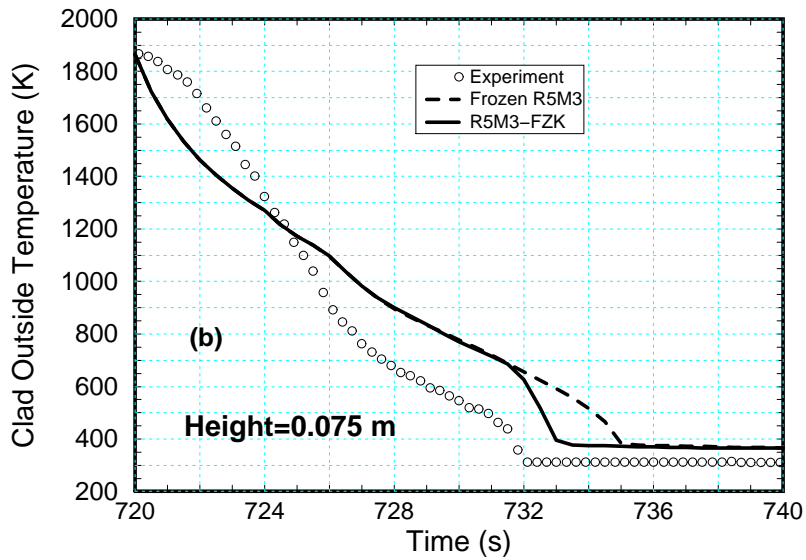
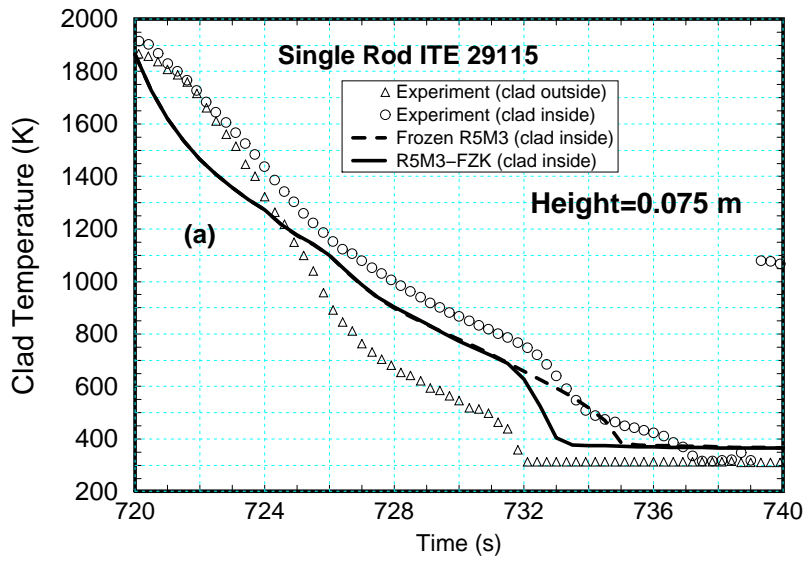


Figure 31: Measured and Predicted Clad Temperatures in the FZK Single-Rod Test No. ITE29115

9.2.3 Discussion of Results: NEPTUN Tests

Figures 32 and 33 present some of the results obtained for the NEPTUN low flooding rate run 5036 along with the measured heater temperature and void fraction. Since a constant electric heating is applied throughout the transient, the temperature at a given axial position rises initially until a turn-around temperature is reached but decreases eventually due to increasing convective heat removal. Results by the frozen version of R5M3 predict early turn-around and show no clear rewetting phenomena. The modified code results agree well with the measurements. Quench times are also well predicted at the two heights plotted in Fig. 32(*b* and *c*). As can be seen from Fig. 32(*a*) the reflow process is accompanied by intense void fraction oscillations. The void fraction drops from its initial value of 1 and, after reaching a minimum value of about 0.5, stabilizes at a level of about 0.8, which is somewhat above the measured value of 0.7. Rewetting at level 0.746 m (at $t \approx 120$ s) occurs at relatively high void fraction. The void fraction oscillations result from oscillations in the heat flux and boiling rate at lower elevations.

Figure 33(*a*) shows frequent variations of the heat transfer mode between transition and film boiling before a transition boiling regime (mode 45) is established at $t \approx 130$ s. This is probably due to the large variations of void fraction experienced between $t = 100$ and $t = 120$ s. The void fraction affects the predicted transition boiling heat flux through its effect on the fractional wetted area (cf. eq. (47)). The rewetting process is accompanied by a significant increase of the HTC at the surface, Fig. 33 (*c*), characteristic to nucleate boiling.

Figures 34 to 37 describe in detail the NEPTUN high flooding rate test (test 5050). Predicted and measured temperatures are shown at three elevations along the heater rod. Unlike the low flooding rate test, the temperature curve in test 5050 does not rise at the beginning of the transient. Enhanced boiling and water entrainment at the bottom of the test section provide ample amount of coolant along the channel to balance the electric power input. The modified R5M3 calculations indicate distinct quench behavior with a clear ‘knee’ temperature. At the 0.746 m elevation, the calculated void fraction at the rewetting time is less than 50 % (Fig. 35), compared to about 80 % void fraction observed in test 5036 at the same elevation (Fig. 32(*a*)). The transient in test 5050 is so fast, that the vapor void fraction histories do not show the distinct oscillations as in the previous case. At lower elevations (up to 0.978 m), the new results are in good agreement with the experimental data. At the higher elevation (1.21 m), the predicted quench velocity is generally overpredicted (early quenching). Although the measured initial temperature at 1.21 m is low, test results show a late quenching, probably due to the relatively high void fraction at that elevation, Fig. 37.

The early quenching predicted by the modified R5M3 code may point out a possible deficiency in the prediction of the void fraction downstream of the quench front. The void

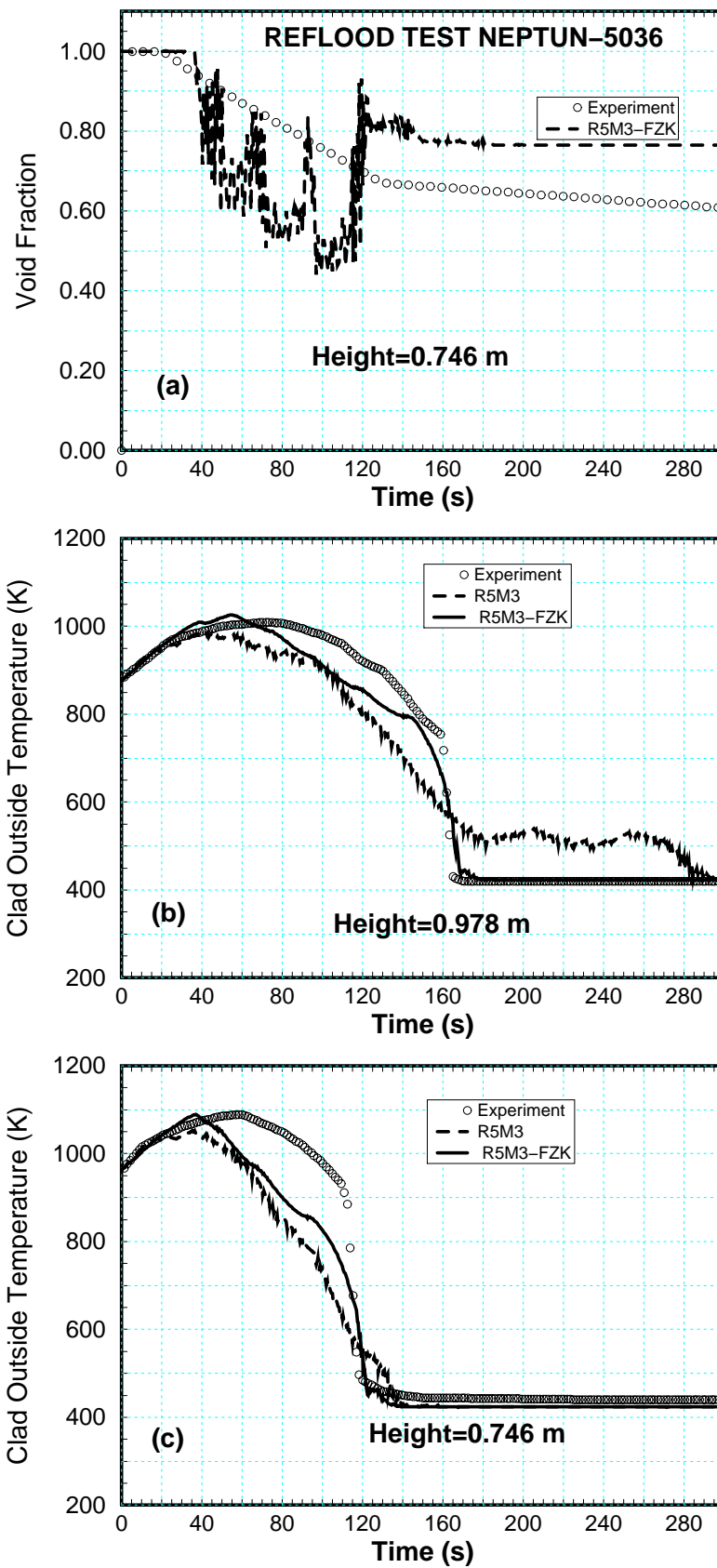


Figure 32: Measured and Predicted Clad Temperatures and Void Fraction in the NEPTUN Test 5036

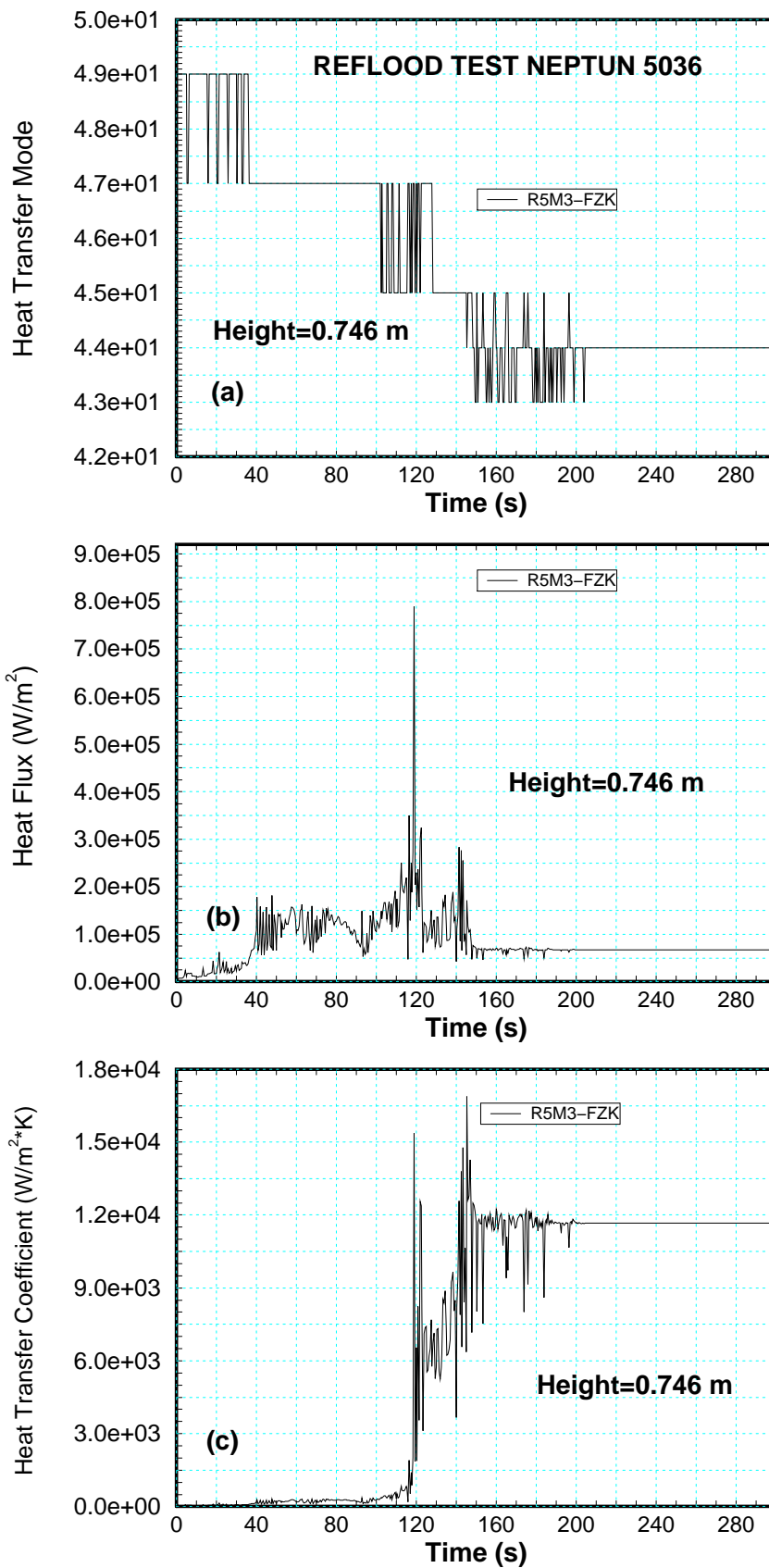


Figure 33: Predicted Heat Transfer Parameters in the NEPTUN Test 5036

fraction calculations are affected mostly by the interfacial momentum transfer and by the vapor generation models of the code. Therefore, further investigation of these models may be necessary before a clear conclusion can be drawn about the disagreement of the quenching rate at high elevation. In addition, refinement of the numerical scheme of the code is recommended in order to account for possible multiple quenching along the fuel rod.

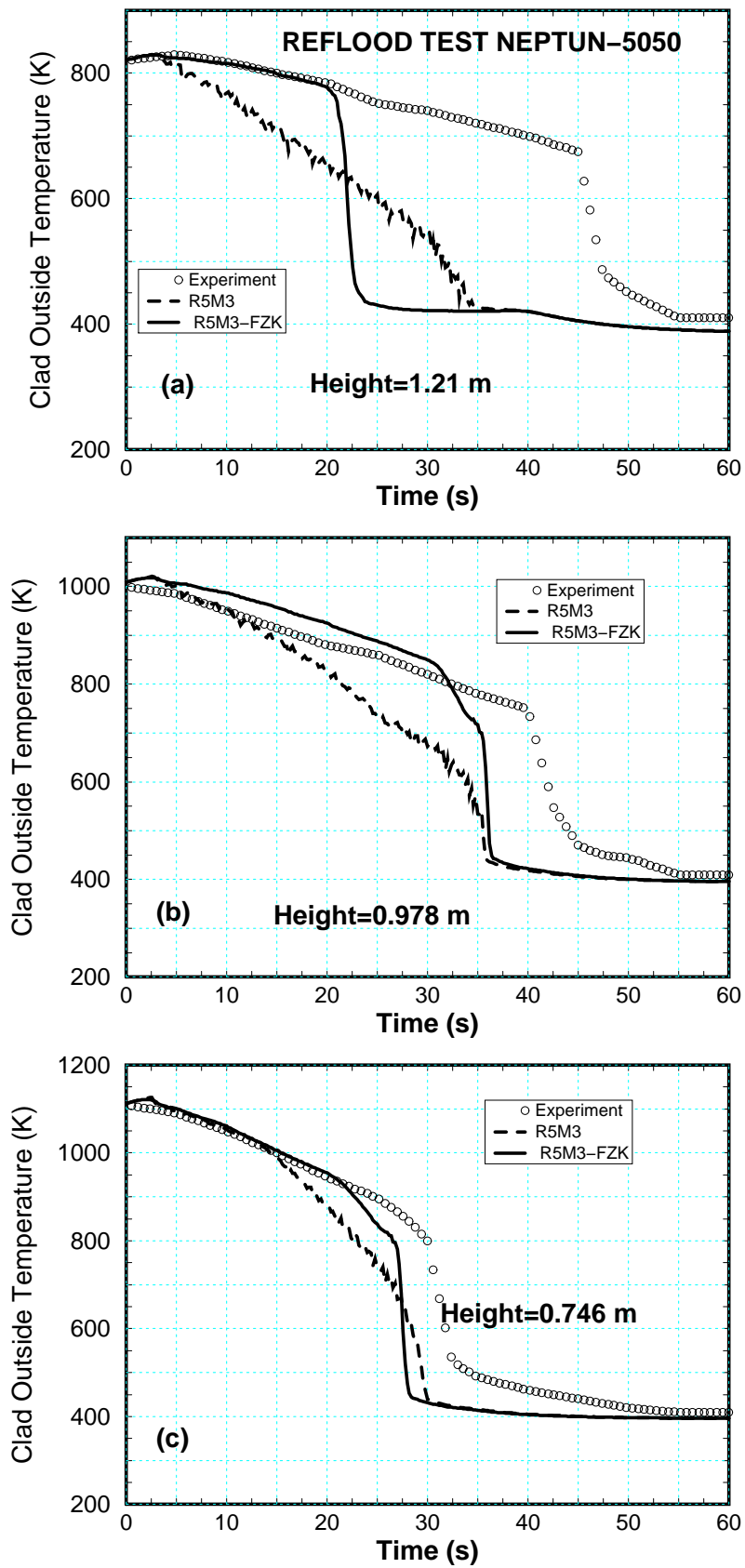


Figure 34: Measured and Predicted Clad Temperatures in the NEPTUN Test 5050

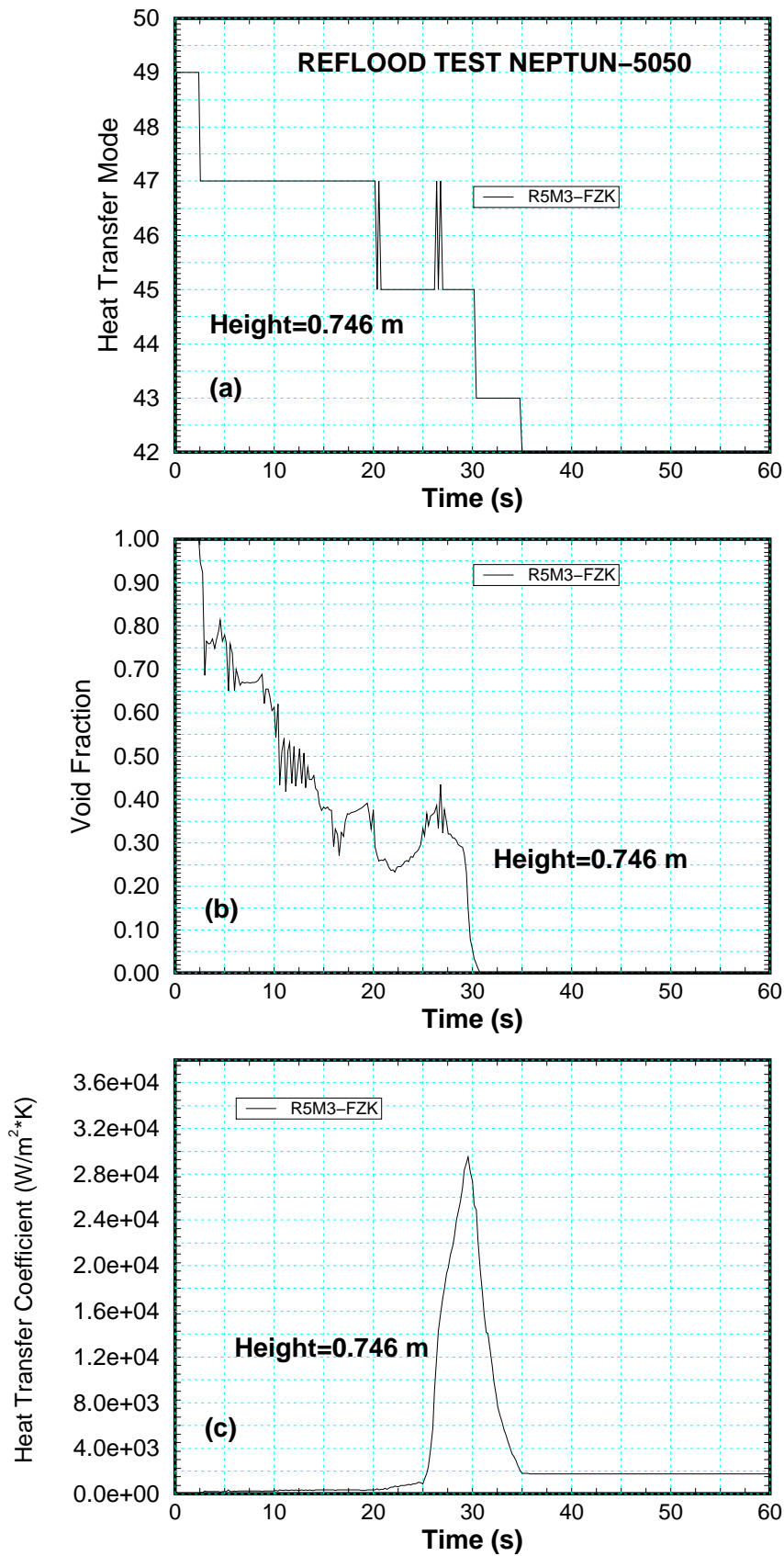


Figure 35: Predicted Heat Transfer Parameters, 0.746 m Elevation in the NEPTUN Test 5050

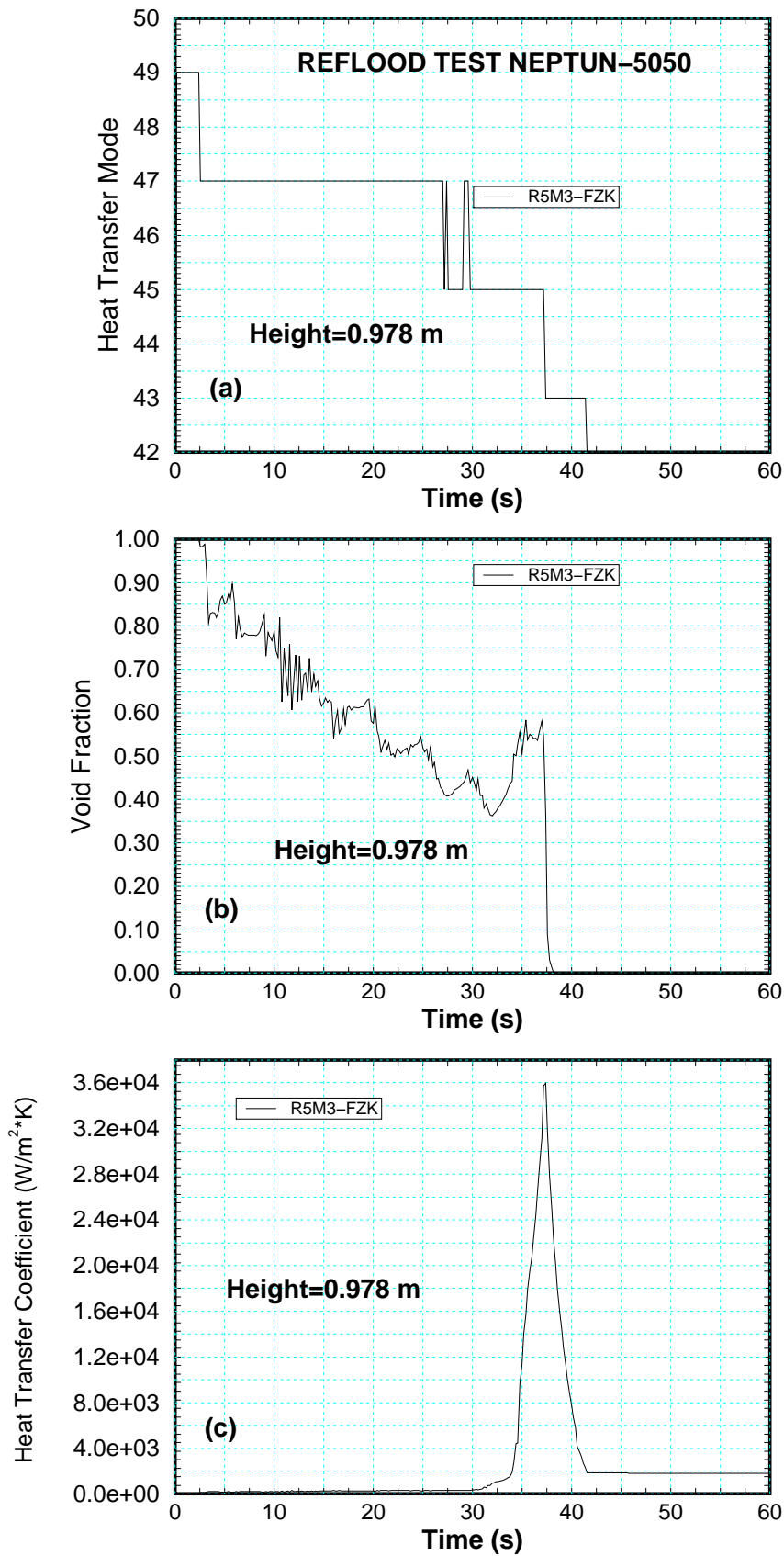


Figure 36: Predicted Heat Transfer Parameters, 0.978 m Elevation in the NEPTUN Test 5050

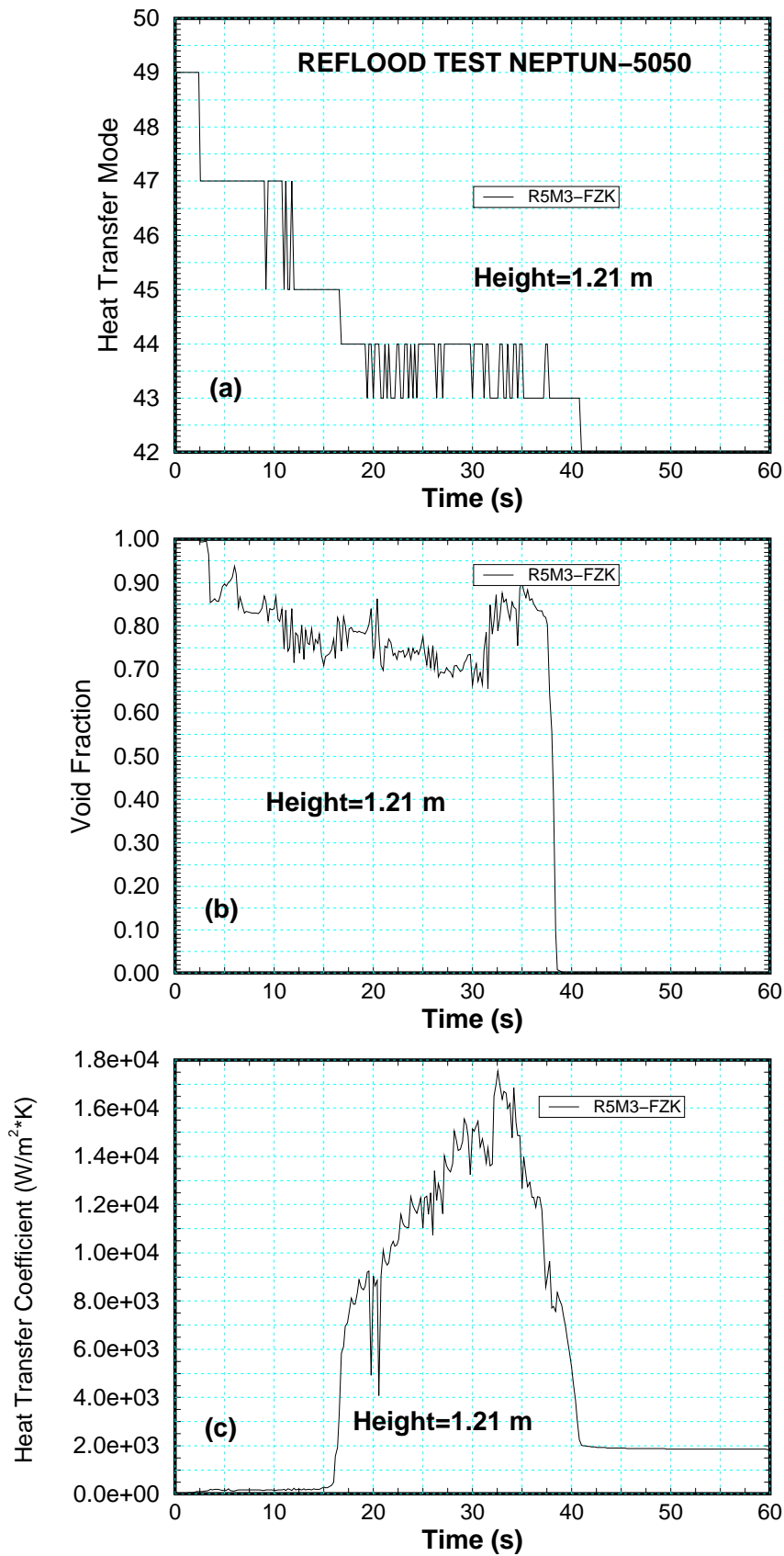


Figure 37: Predicted Heat Transfer Parameters, 1.21 m Elevation in the NEPTUN Test 5050

10 Parametric Studies

In section 2.3 the importance of the heat transfer within the fuel rod was pointed out considering parameters like gap resistance, gap pressure, gap filler gas, etc. during reflood situations. A set of calculations were carried out to study the effect of the gap model in R5M3 on the temperature prediction during reflood. Figure 38 shows different clad outside temperatures predicted under different assumptions. Assuming no gap conductance is equivalent to assuming that there is no interaction between the pellet and the cladding (a gap with infinite heat resistance). Disconnecting the cladding from the pellet results in early quenching as shown in the clad outside and inside temperature curves in Fig. 38. This is in agreement with experimental results [7] which indicate that decreasing the heat conductivity in the radial direction increases the quench front velocity. Neglecting the radiation heat transfer between the pellet and the inner surface of the cladding reduces in principle the gap conductivity and hence, increases the quench velocity (Fig. 38). However the effect of the radiation component on the total gap conductivity is shown to be small. This is better understood by examining Figs. 39 and 40 which show the temperature difference across the gap and the temperatures of the pellet and the inner cladding independently. Significant temperature difference exists during rewetting, but since the clad and pellet temperatures at that time are relatively low, radiation heat transfer does not play an essential role in the total gap conductance.

The gap conductance depends to a large extent on the gap width which is in turn a function of temperature and thermal expansion properties of the clad and pellet materials. Figure 41 is a typical plot of the gap width variations during reflooding. It refers to the predicted results at the mid-section of the specimen in the base case test (FZK single-rod test No. T16106). The gap width drops initially as the cladding is cooled. As the pellet cools down the gap width increases. During the rewetting time the gap width decreases momentarily in reaction to the sudden drop in the cladding temperature.

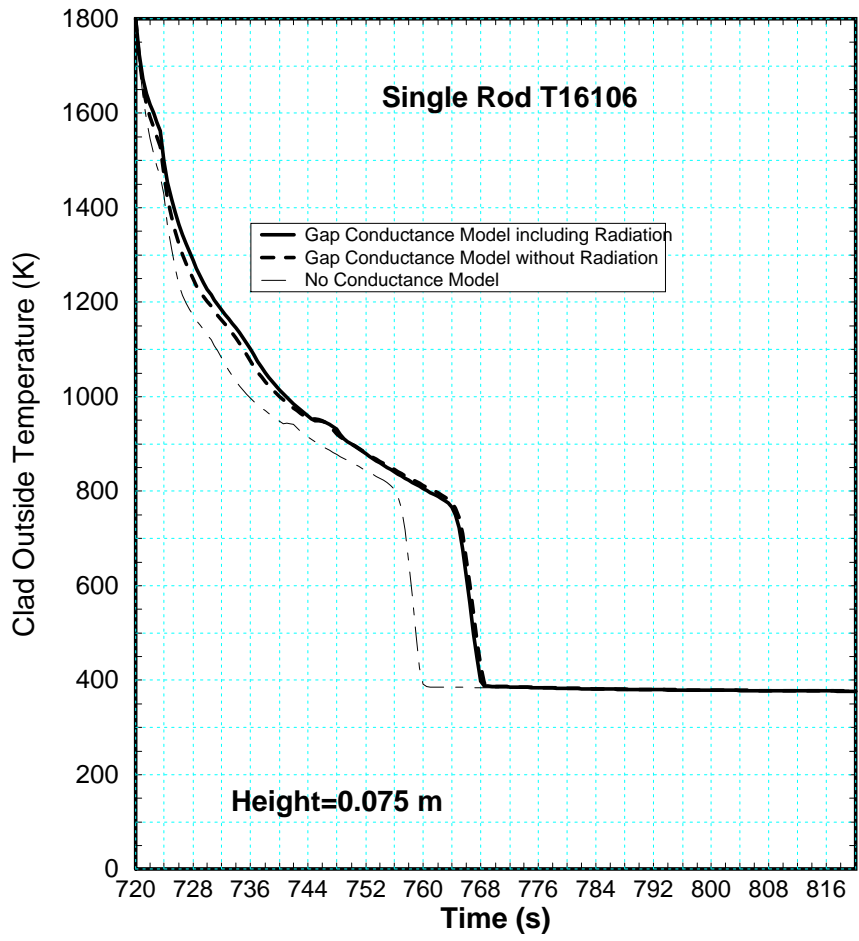


Figure 38: Effect of Gap Conductance on Quench Velocity in the FZK Single-Rod Test No. T16106

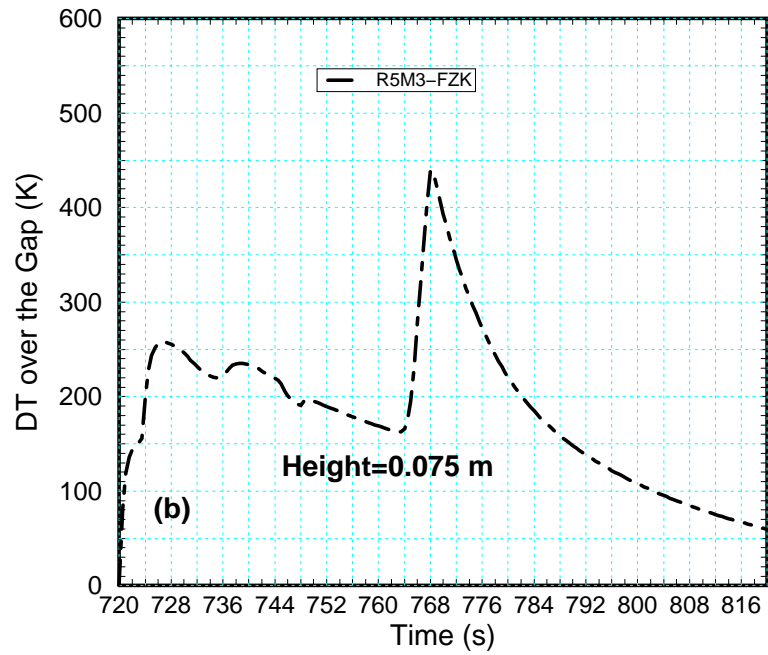
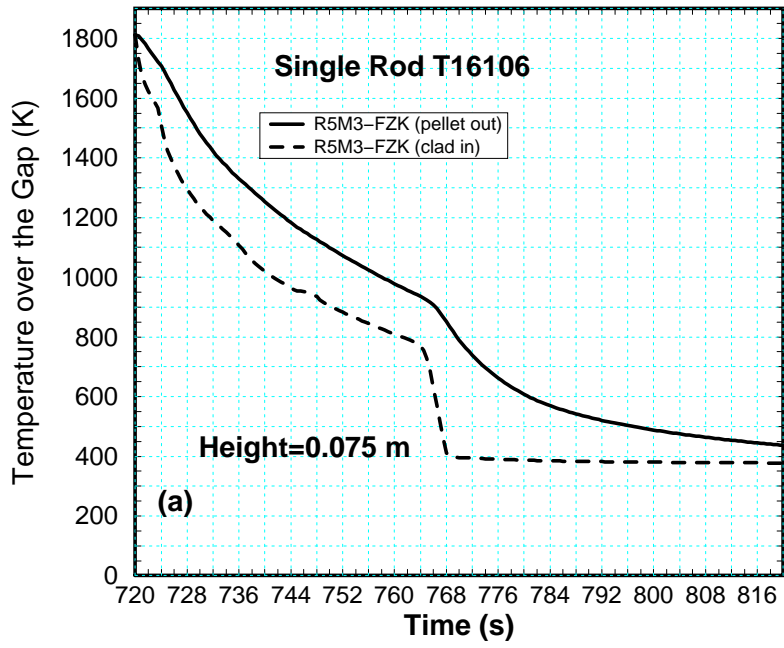


Figure 39: Gap Temperature Curves in the FZK Single-Rod Test No. T16106

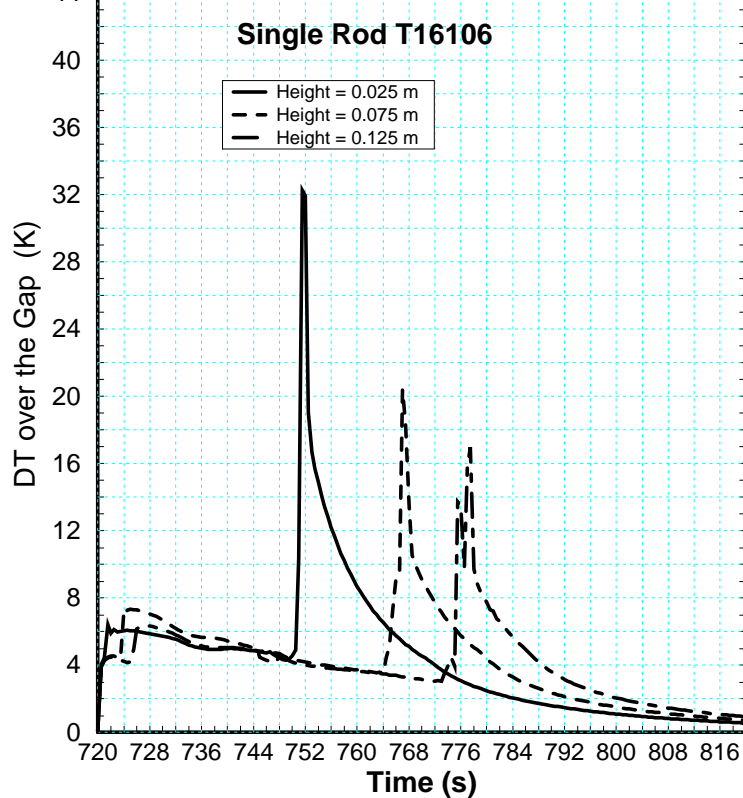


Figure 40: Temperature Difference Across the Gap at Different Heights in the FZK Single-Rod Test No. T16106

11 Run Statistics and Code Performance

The calculations presented in this report were performed on both IBM RS/6000 and parallel IBM RS/6000 SP machines. The discussion is based on the results obtained on the IBM RS/6000 machine.

A. QUENCH Rig

The model used for the QUENCH rig consisted of 19 volumes (15 volumes in the test section, two time dependent volumes, a lower and an upper plenum), 4 junctions and 30 heat structures (see Figure 8). To demonstrate the run statistics and code performance of the modified RELAP5/MOD3.1-FZK in comparison with the frozen version, the test T16106 was chosen. Figure 42 gives the courant time, the CPU time as well as the mass error calculated by both code versions. One can see that both CPU and courant time are similar.

B. NEPTUN Facility

In the case of the NEPTUN tests the facility was modeled by 20 volumes (18 in the test section, a lower and an upper time dependent volume), 2 junctions and 16 heat structures

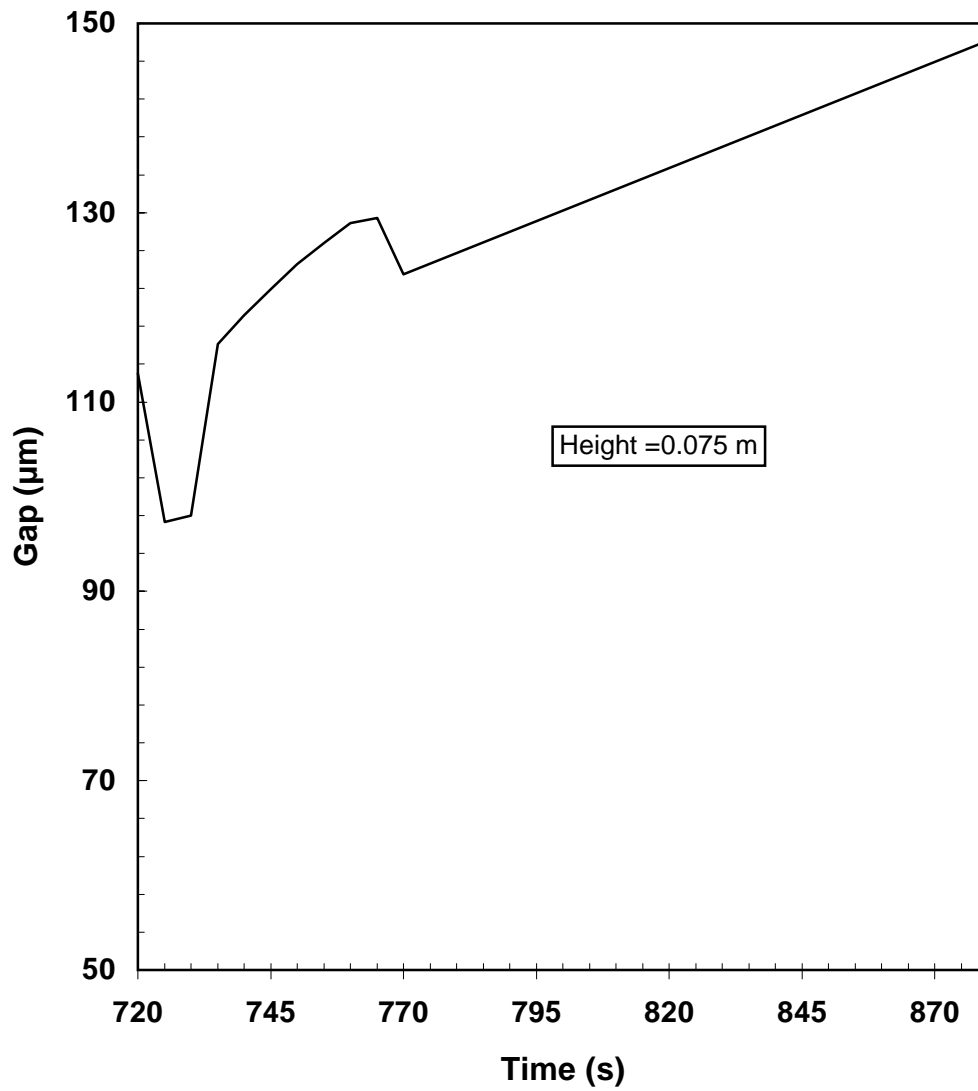


Figure 41: Gap Width Behavior During Reflooding in the FZK Single-Rod Test No. T16106

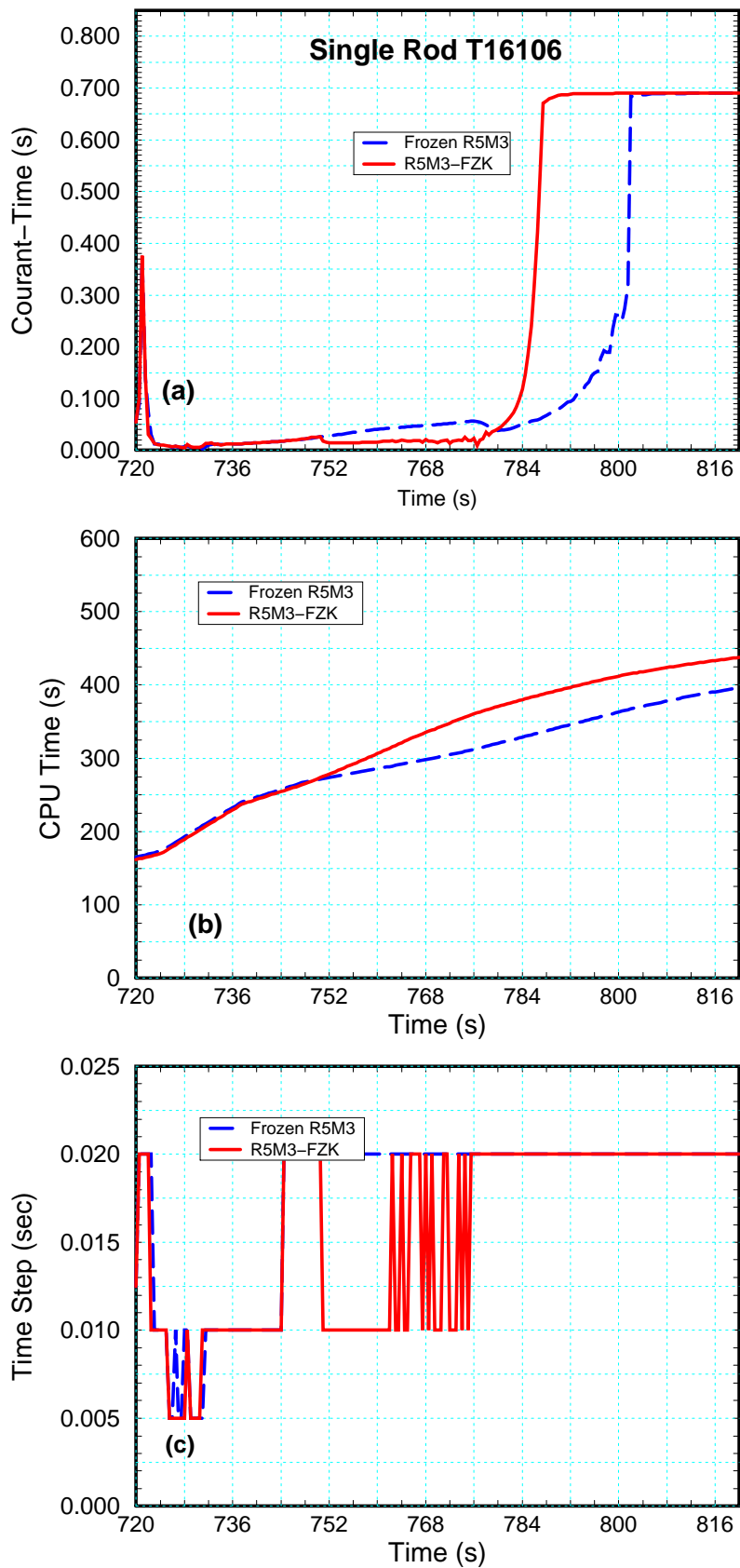


Figure 42: Code Performance: Rod Test No. T16106

(see Figure 9). Figure 43 shows the time step, CPU-time and mass error calculated by both code versions. The time step and mass error predicted by the modified code exhibits much less oscillations than that of the frozen version (see Figure 43 *a,c*). The CPU consumption of the modified version is smaller by about 10 %. Figure 44 depicts the vapor temperature, void fraction and courant time calculated by both code versions. The predictions of the modified code version are in general more stable and oscillate less than that of the frozen code version.

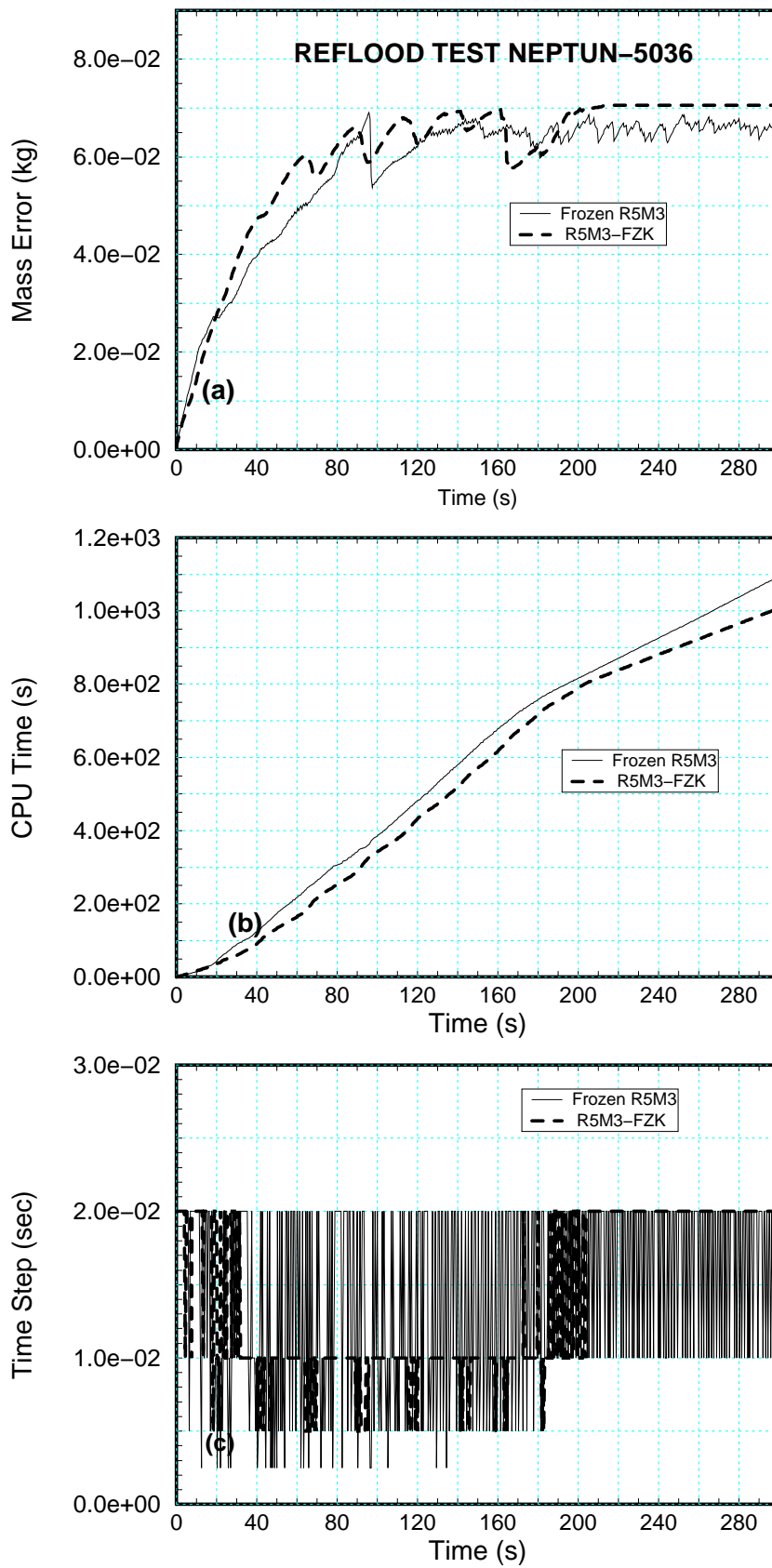


Figure 43: Code Performance: NEPTUN Test 5036

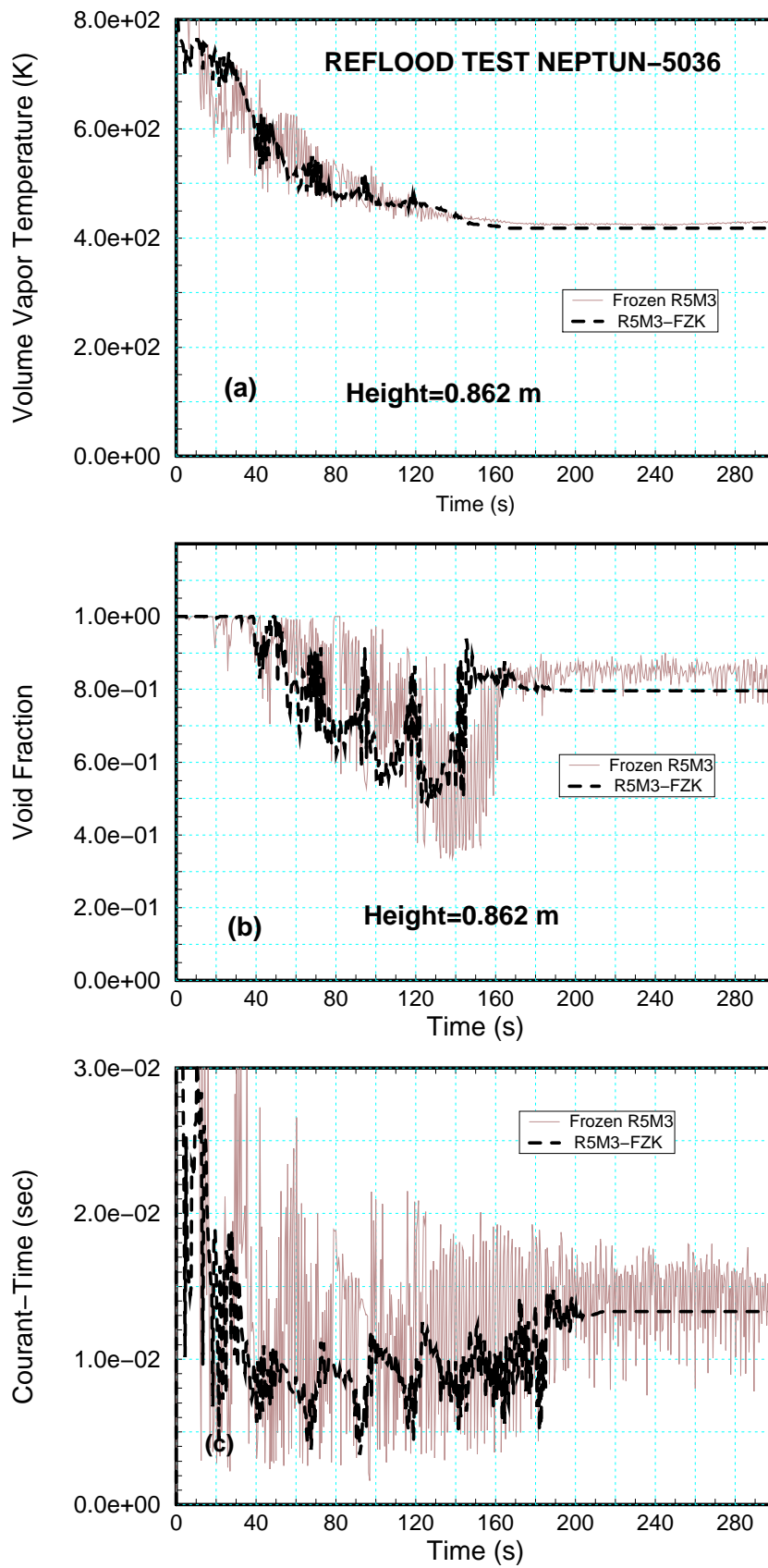


Figure 44: Code Performance: NEPTUN Test 5036

12 General Conclusions and Recommendations

The heat transfer model of the RELAP5/MOD3.1 code was extensively reviewed and assessed. Several reflooding experiments with varying pressure, flooding rate, heating power and initial wall temperature were simulated in order to evaluate the general prediction capability of the code in modeling boil-off and reflow transients. The most important deficiency of the current version of the code was found to result from its treatment of the transition boiling heat transfer regime. In this regime the code significantly underpredicts the heat transfer rate to the liquid. Since at low quality conditions, the liquid boiling component constitutes a major fraction of the total heat transfer, the current model underpredicts the quench temperature and the quenching rate under most conditions relevant to LOCA and degraded core analysis.

In order to further evaluate the transition boiling procedure of the current R5M3 code, a stand-alone model was formulated and tested against the available data-base on steady-state post dryout heat transfer. Analysis of over 360 data points has shown that the R5M3 model consistently underpredicts the measured heat flux in the transition boiling regime. A new model based on an extension of the original Chen model has, therefore, been formulated. The model utilizes only local state variables generally calculated by the R5M3 code and does not require other history parameters such as quench position or CHF and minimum film boiling temperatures, which are not readily available at each time step. Stand-alone validation of the new model has shown acceptable agreement with the data (standard deviation of about 40%). The new model was, therefore, implemented in the R5M3 code and used to simulate a large sample of the FZK Single-Rod and the NEPTUN rod bundle reflow tests. Implementation of the new model in R5M3 is straight-forward and requires modifications in one subroutine only. The model was also implemented in the SCDAP/RELAP5 code and tested against some of the CORA data. The following conclusions can be drawn:

1. The new model yields good predictions of reflow and general heat transfer problems using a single logic of heat transfer selection.
2. High and low flooding rate experiments were predicted relatively well with the modified code. The successful prediction of the high flooding rate tests is particularly important for the analysis of LOCA and degraded core accidents where high flooding rates are to be expected.
3. The unphysical behavior of the current R5M3 code such as continuous cooling of the node without clear turn-around temperature and no quenching phenomena, is eliminated in the modified version of the code.

4. At the NEPTUN high flooding rate test, both the modified and current versions of the code predict early quenching at the upper section of channel. This may be a result of inaccurate modeling of the void fraction downstream of the quench front.
5. The parametric study has shown that an accurate modeling of the gap conductance is important for the analysis of fuel rod or heater rod reflooding. The gap model of the code was found to be adequate.
6. The modifications introduced in R5M3 does not disturb the code performance. On the contrary, the modified code runs faster and more stable with considerable less oscillations of key parameters like void fraction, gas temperature, mass error, and courant–time. Typical CPU-times of the IBM RISC 6000 to run the he tetst *T16016 and NEPTUN5036* are about 400 s and 1000 s, respectively.

Although the suggested model has been validated as a stand–alone program and as a part of the modified R5M3 code, a wider assessment with a large number of different transients is recommended before one can make a definite statement about the capability of the modified code to correctly predict the physical phenomena in the complete range of expected operational and accident conditions. In particular, the model performance at high surface temperatures and oscillating flow conditions far downstream of the quench front, should be studied. For instance, it has been shown [3] that in some of the NEPTUN tests, better agreement between the predicted results and the measured temperature profiles downstream of the quench front can be achieved by limiting the proposed transition boiling model to the range of 0 to 0.2 m from the quench front. Further refinements of the model are, therefore, recommended to improve its performance at high temperatures and high void fractions, characteristic to top-quenching and spray cooling. Several modifications have been introduced in the RELAP5/MOD3.2 version of the code. These are mainly related to heat transfer and to the interface closure laws of the code. It is recommended to implement the present transition boiling model in the R5M3.2 in order to further evaluate its prediction capability for reflood and general heat transfer problems.

Acknowledgements

One of the authors (E. Elias) was privileged to spend six months (from Sept. 1996 to Feb. 1997) on Sabbatical leave at the FZK, Germany. This work was performed within the framework of the FZK–CAMP agreement. We would like to thank S. N. Aksan from PSI for making available to us his NEPTUN 5036 and 5050 input decks.

13 References

- [1] G. T. Analytis. Developmental assessment of RELAP5/MOD3.1 separate effect and integral test experiments: model changes and options. *Nuclear Engineering and Design*, 163, p125-148(1-2), June 1996.
- [2] G. T. Analytis. Developmental assessment of RELAP5/MOD3.1 with separate-effect and integral test experiments: Model changes and options. PSI Ber.96-09, ISSN 1019-0643, Paul Scherrer Institut PSI, CH-5232 Villigen PSI, April 1996.
- [3] G. T. Analytis. *private communication*, May 1997.
- [4] C. Bals, J. Bestele, and K. Trambauer. *Quenchfront modelling in ATHLET-CD*. First International Quench Workshop, Karlsruhe, October 4th-6th 1995.
- [5] C. Bals, J. Bestele, and K. Trambauer. *Modelling of quenching in ATHLET-CD*. Second International Quench Workshop, Karlsruhe, September 17-19 1996.
- [6] Y. Barnea, E. Elias, and I. Shai. Flow and heat transfer regimes during quenching of hot surfaces. *Inter. J. of Heat Mass Transfer*, 37, pp.1441(10), 1994.
- [7] F. Barre. Reflood model of CATHARE2 V1.2E Code:PSCHIT module. STR/LML/EM/91-16, Centre D'Etudes Nucleaires de Grenoble, 1991.
- [8] F. Barre, T. Watanabe, T. Horng, and Y. Yonomoto. Cathare V1.2E Revision 5 - Qualification report, preliminary low pressure reflooding. STR/LML/EM/91-46, Centre D'Etudes Nucleaires de Grenoble, 1991.
- [9] A. W. Bennett, G. F. Hewitt, H. A. Kearsley, and R. K. F. Keays. Heat transfer to steam-water mixtures flowing in uniformly heated tubes in which the critical heat flux has been exceeded. AERE-R-5373, Atomic Energy Research Establishment AERE, Harwell, UK, March 1968.
- [10] J. Chen. Correlation for boiling heat transfer to saturated fluids in convective flow. *Process Design and Development*, 5, pp. 322-329(3), July 1966.
- [11] J. C. Chen, R. K. Sundaram, and F. T. Ozkaynak. A phenomenological correlation for post-CHF heat transfer. NUREG-0237, Lehigh University, Department of Mech. Eng., Bethlehem, PA, June 1977.
- [12] J. G. Collier. *Heat transfer in the post burnout region and during quenching and reflooding*. Handbook of Multiphase Systems. Hemisphere, 1982.
- [13] E. Elias and G. Yadigaroglu. The reflooding phase of the LOCA in PWR's. part 2: Rewetting and liquid entrainment. *Nuclear Safety*, 19(2), March-April 1978.

- [14] E. Farouk. *Thermal-Hydraulics Research Plan of the USNRC*. CAMP-Meeting-Los Alamos National Laboratory, Santa Fe, New Mexico, October, 15-18 1996.
- [15] C. J. Fry and T. Haste. *Examination of Thermocouple Errors in the Single Rod Quench Tests*. Special Meeting on Temperature Measurement at FZK, March, 5th 1997.
- [16] D. C. Groeneveld, P. L. Kirillov, V. P. Bobkov, F. J. Erbacher, and W. Zeggel. *An improved table look-up method for predicting critical heat flux*. NURETH-6, Grenoble, France, October 5-8 1993.
- [17] T. Haste, B. Adroguer, C. M. Allison, S. Hagen, P. Hofmann, and V. Noack. Degraded core quench: A status report. AEA/CS R1047, Draft E, AEA Technology, Winfrith technology Centre, Dorset, DT2 8DH, Dorchester, UK, August 1996.
- [18] P. Hofmann and V. Noack. *Experiments on the quench behavior of fuel rod segments*. Second International Quench Workshop, Karlsruhe, October 4th-6th 1995.
- [19] P. Hofmann and V. Noack. Physico-chemical behavior of zircaloy fuel rod cladding tubes during LWR severe accident reflood. FZKA-5846, Forschungszentrum Karlsruhe FZK, Postfach 3640 D-76021 Karlsruhe, Germany, 1997.
- [20] J. K. Hohorst and C. M. e. a. Allison. *Assessment of SCDAP/RELAP5 using data from the CORA melt progression experiments*. NURETH-5, Salt Lake City, UT, USA, September 1992.
- [21] Y.-Y. Hsu and R. W. Gaham. *Transport processes in boiling and two-phase systems*. Series in Thermal and Fluids Engineering. Hemisphere Publishing Company, first edition edition, 1976.
- [22] Idaho National Engineering Laboratory EG&G Idaho, Inc, Idaho Falls, Idaho, USA. *RELAP5/MOD3.1 Code manual volume I: Code structure, system models, and solution methods*, June 1990.
- [23] Idaho National Engineering Laboratory EG&G Idaho, Inc, Idaho Falls, Idaho, USA. *RELAP5/MOD2.5 Code manual volume I: Code structure, system models, and solution methods*, Aug. 1995.
- [24] Idaho National Engineering Laboratory EG&G Idaho, Inc, Idaho Falls, Idaho, USA. *RELAP5/MOD3.2 Code manual volume I: Code structure, system models, and solution methods*, Aug. 1995.
- [25] O. C. Iloeje, D. Plummer, R. W., and P. Griffith. A study of wall rewet and heat transfer in dispersed vertical flow. MIT 72718-92, MITi-Heat Transfer Lab., 1974.

- [26] G. Jacobs. *Unpublished Report*. D-76021 Karlsruhe, Postfach 3640, 1987.
- [27] G. Jacobs and A. Galvan. *Unpublished Report*. D-76021 Karlsruhe, Postfach 3640, 1987.
- [28] K. Johannsen and Q. Weber, P. an Feng. Experimental investigation of heat transfer in the transition boiling region. EUR-13135, Final Report, Technische Universität Berlin, Marchstr.18, D-10587 Berlin, October 1990.
- [29] P. Kuan, J. L. Anderson, and E. L. Tolman. Thermal interaction during the Three Mile Island Unit 2 2-b Pump Transient. *Nuclear Technology*, 87, pp.977, 1989.
- [30] N. Lee, S. Wong, H. C. Yeh, and H. L.E. PWR FLECHT SEASET unblocked bundle, forced and gravity reflood task data report. NUREG/CR-2256, Electric Power Research Institute, EPRI, 3412 Hillview Avenue, Palo Alto, California 94304, 1981.
- [31] T. J. Liu and T. S. Horng. *Rewetting advances of very hot circular ducts by bottom reflooding*. NURETH-6, Grenoble, France, October 5-8, Grenoble, France 1993.
- [32] M. J. Loftus, L. E. Hochreiter, C. E. Conway, C. E. Dodge, A. Tong, E. R. Rosal, M. M. Valkovic, and S. Wong. PWR FLECHT SEASET unblocked bundle, forced and gravity reflood task data report. NUREG/CR-1532, WCAP-9699, Electric Power Research Institute, EPRI, 3412 Hillview Avenue, Palo Alto, California 94304, 1980.
- [33] Y. Murao. *Discussion on quench models for best estimate codes*. NURETH-5, Salt Lake City, UT, USA, September 1992.
- [34] Y. Murao, K. Fujiki, and H. Akimoto. Evaluation report on CCTF core-1 reflood test CI-19 (RUN 38)- experimental assessment of the evaluation model for the safety analysis on the reflood phase of PWR-LOCA. JAERI-M83- 029, JAERI, Tokai-mura, Ibaraki-ken, 319-11, Japan, 1983.
- [35] V. Noack and Hofmann. *Experiments on the quench behavior of fuel rod segments*. Second International Quench Workshop, Karlsruhe, September 17-19 1996.
- [36] A. Ohnuki, H. Akimoto, Y. Abe, and Y. Murao. Assessment of TRAC-BF1 1D reflood model with CCTF and SCTF data. JAERI-M93- 045, JAERI, Tokai-mura, Ibaraki-ken, 319-11, Japan, 1993.
- [37] T. Okubo, T. Iguchi, H. Akimoto, and Y. Murao. Evaluation report on CCTF CORE-II reflood test C2-15 RUN 75 -investigation of FLECHT-SET coupling test results. JAERI-M91- 227, JAERI, Tokai-mura, Ibaraki-ken, 319-11, Japan, 1992.

- [38] S. Olek. Analytical models for rewetting of hot surfaces. PSI Ber-17, Paul Scherrer Institut PSI, CH-5232 Villigen PSI, Oktober 1988.
- [39] M. Richner, G. Analytis, and S. N. Aksan. Assessment of RELAP5/MOD2, cycle 36.02, using NEPTUN reflooding experimental data. PSI Ber.104 –NUREG/IA–00103, Paul Scherrer Institut PSI, CH-5232 Villigen PSI, Oktober 1991.
- [40] A. E. Ruggles, A. D. Vasil'ev, B. N. W., and W. M. W. The role of heater thermal response in reactor thermal limits during oscillatory two-phase flows. *Nuclear Science and Engineering*, 125, pp.75-83(1), Januar 1997.
- [41] R. A. Seban and S. T. Wang. Heat transfer during quenching and dryout in a vertical tube. EPRI NP-4157, Final Report, Electric Power Research Institute(EPRI), Post Office Box 10412, Palo Alto. CA 94303, 1985.
- [42] M. Sencar and N. Aksan. *Independent Assessment of RELAP5/MOD3/vj7 beta test version with the Lehigh University and PSI-NEPTUN reflooding tests and comparison to RELAP5 /MOD3/v5m5 and RELAP5/MOD2.5*. First CAMP Meeting, PSI, PSI Switzerland, June 24–26 1992. Test Matrix, comparison of calculated with measured results.
- [43] M. Sencar and N. Aksan. *Evaluation and assessment of reflooding models in RELAP5/MOD2.5 and RELAP5/MOD3 codes using Lehigh University and NSI-NEPTUN bundle experimental data*. NURETH-7, New York, USA, September 1995.
- [44] K. H. Sun, J. M. Gonzales-Santalo, and C. L. Tien. Calculations of combined radiation and convection heat transfer in rod bundles under emergency cooling conditions. *Nuclear Engineering and Design*, pp.415-420(8), August 1976.
- [45] C. Unal and R. Nelson. A phenomenological model of the thermal hydraulics of convective boiling during the quenching of hot rod bundles. part ii: Assessment of the model with steady-state and transient post-chf data. *Nuclear Engineering and Design*, 136,p299-318(04), Jan 1992.
- [46] S. van Stralen, M. Sohal, R. Cole, and W. Sluyter. Bubble growth rates in pure and binary systems: Combined effect of relaxation and evaporation microlayers. *Int. J. Heat Mass Transfer*, 18,pp. 453-467, 1975.
- [47] J. Weisman, J. K. Kao, S. Wang, and B. Pei. Studies of transition boiling heat transfer with saturated water at 1-4 bar. EPRI-NP-1899, Cincinnati University, 1981.
- [48] G. Yadigaroglu. The reflooding phase of the LOCA in PWR's. part i: Core heat transfer and fluid flow. *Nuclear Safety*, 19(1), January-February 1978.

- [49] G. Yadigaroglu. *Closure relationships*. Lecture 6: Short course multiphase flow and heat transfer, ETH, Zürich, Switzerland, March 1996.
- [50] G. Yadigaroglu, R. Nelson, V. Teschendorff, Y. Murao, J. Kelly, and D. Bestion. Modelling of reflooding. *Nuclear Engineering and Design*, 145, p1-35, 1993.